CONTROL OF PLANT CELL SHAPE BY IRREGULAR TRICHOME BRANCH GENES IN ARABIDOPSIS

By

XIAOGUO ZHANG

A DISSERTATION PRESENTED TO THE GRADUATE SCHOOL
OF THE UNIVERSITY OF FLORIDA IN PARTIAL FULFILLMENT
OF THE REQUIREMENTS FOR THE DEGREE OF
DOCTOR OF PHILOSOPHY

UNIVERSITY OF FLORIDA

2008

To my great Mom

ACKNOWLEDGMENTS

I offer my sincere gratitude to my advisor and committee chair, Dr. David G. Oppenheimer, for his guidance and encouragement. I especially acknowledge him for improving my knowledge in plant developmental genetics, expanding my thinking on scientific questions, and teaching me English science writing during my doctoral education. I would like also express my great appreciation to our research coordinator, Paris Grey, for her strong support of my research.

I am truly grateful to my supervisory committee, Drs. Alice C. Harmon, Bernard A. Hauser, and Daniel L. Purich, for their valuable advice and inspiring discussions throughout my research. I also thank Drs. Wenyun Song and Xiaodong Ding for training me in yeast two-hybridization in their laboratory. I would also like to thank Drs. Kevin M. Folta and Amit Dhingra for the use of the Gene Gun and help with the transient assays. I also thank the graduate students in the Oppenheimer laboratory, Stacey Jeffries and Meredith Sullivan, for their support and friendship during my education. I want to take this opportunity to thank all the faculty members who taught me classes and all the people in PMCB who helped me during the past three years. Finally I give special thanks to my wife, Qingping Yang, my son, Yuxiang Zhang, and my daughter, Aiwen Zhang, as well as my parents-in-law, Xueren Yang and Dongying Xiong.

TABLE OF CONTENTS

page

LIST OF TABLES

LIST OF FIGURES

Abstract of Dissertation Presented to the Graduate School
of the University of Florida in Partial Fulfillment of the
Requirements for the Degree of Doctor of Philosophy

CONTROL OF PLANT CELL SHAPE BY IRREGULAR TRICHOME BRANCH GENES IN ARABIDOPSIS

By

Xiaoguo Zhang

May 2008

Chair: David G. Oppenheimer
Major: Plant Molecular and Cellular Biology

The control of plant cell shape is fundamentally important not only for the function of individual cells, but also for the morphogenesis of whole plants. The *Arabidopsis* leaf trichome is used as a cell model for genetic screens of mutations, called *irregular trichome branch* (*itb*) and *disproportionate* (*dpp*), which cause changes in trichome shape. Five genes (*ITB1-ITB4* and *DPP*) were cloned through a positional cloning strategy and the functions of these genes were characterized in this study.

ITB1 is a plant homolog of the actin-related protein2/3 complex activator Scar/WAVE, which regulates actin and microtubule organization. Disruption of ITB1 causes disorganization of actin filaments and microtubules, generating distorted trichomes. ITB2 is a putative member of the aminophospholipid translocase (ALA) family. Mutations in this gene result in defective trichomes with reduced branch length. ITB3 is a plant-specific protein that regulates actin organization through interaction with actin depolymerizing factor (ADF). The absence of ITB3 severely changes actin cytoskeleton organization by forming actin rings, but no change was observed in microtubule organization. The trichomes in *itb3* mutants are reduced in size and branch length. ITB4 is the plant homolog of cleavage stimulation factor 64 that influences not only trichome morphogenesis, but also floral development. Compared to wild type, mutations in

ITB4 reduce the trichome branch number and increase sepal and petal numbers. DPP is a keto acyl reductase and is involved in trichome cell expansion. Mutations homozygous for *dpp* are lethal. At the restrictive temperature (22˚ C), heterozygous plants of the *dpp* mutants display trichomes with reduced branch length and increased stalk length. Although the five gene products described above have different functions in plant cells, their mutations all cause changes in *Arabidopsis* leaf trichome shape. These results indicate that plant cell shape can be controlled by different genes with a wide range of functions on multiple dynamic cell processes such as cytoskeleton dynamics and endomembrane dynamics.

CHAPTER 1
LITERATURE REVIEW: PLANT CELL EXPANSION

Introduction

Significance of Cell Expansion

The intricate coordination of cell division and expansion allows plants to achieve a unique developmental plasticity that reduces the constraints of various adverse environments for plant survival. Plants need continued availability of light, water, and nutrients throughout their life cycle. However, plants are stationary and plant cells are surrounded by rigid cell walls, which make plants unable to escape resource-depleted environments. Therefore, plants adjust the rate and direction of cell division and expansion. Rigid cell walls offer structural and mechanical support for plant bodies, and ultimately are responsible for the plant architectural design and morphology. Thus, plant cell expansion is the basis for both the whole plant morphogenesis and plant flexibility to adapt environmental conditions (Thompson, 1917).

General Characterization of Cell Expansion

An expanding plant cell is similar to an inflating balloon in direction determination, force requirement, and wall alteration. Balloons can form diverse shapes, if specific locations of the balloon surface are forced by counter-pressure to change conformation. So can plant cells, too, expanding in directions that follow their functional requirement. The driving force of cell expansion comes from the internal turgor pressure, generated by the water content of the protoplast. During cell expansion, water needs to enter into the protoplast across the semi-permeable plasma membrane to keep a constant turgor pressure (Steudle and Zimmermann, 1977). Second, the direction of cell expansion is spatially determined by the orientation of cellulose microfibrils, which in turn is controlled by the plant cytoskeleton. The plant cytoskeleton is composed of microtubules and microfilaments. It is generally believed that

microtubules orient the deposition of cellulose microfibrils in cell walls, and microfilaments serve as tracks for transporting vesicles to specific sites of the wall that are loosened by lytic enzymes or wall-remodeling proteins. Through exocytosis, dynamic vesicles, which contain polysaccharides and proteins from endomembrane compartments, are fused with the plasma membrane, and their contents are discharged into the extracellular matrix space for building cell walls (Murphy et al., 2005; Samaj et al., 2005; Johansen et al., 2006). Even though the volume of an expanding cell increases to a thousand times the original volume, the walls maintain a relatively constant thickness. All cell expansion is mechanistically divided into two basic types of growth: tip growth and diffuse growth. For tip growth, a spatially focused cell expansion, cells grow exclusively at the extreme tip of the cell. Pollen tube and and root hairs are cell types that expand using tip growth. For diffuse growth, expansion can occur at multiple locations and encompass larger regions than occurs during tip growth (Baskin, 2005).

Cell Wall Dynamics and Cell Expansion

The plant cell wall may seem to be a paradoxical entity because it serves to both maintain cell shape through constraint of cell expansion, yet it promotes development of cell morphology by extension of itself. The wall provides rigidity to a plant cell, strength, and protection against various mechanical stresses. It also limits the entry of large molecules and pathogens into cells. The wall further creates a stable osmotic environment by preventing osmotic lysis and retaining water. Finally, the wall determines plant cells myriad shapes. All these functions of the wall underlie its action as a physical barrier, which constrains cell expansion. To solve the paradox, plants have evolved a dynamic cell wall. Thereby, this wall is not only suited to flexible cell expansion, but also participates in cell to cell and cell to nucleus communication through signaling molecules and receptors in the wall (Darley et al., 2001).

Cell Wall Components

As mentioned above, cell walls allow plants to form various shapes. Thus, cell expansion appears to be its wall extension. To understand cell expansion it is first necessary to know the chemical composition of the wall. Because only primary walls can be remodeled for cell expansion, my focus here is on those aspects that are germane to understanding cell expansion. Secondary walls, which are formed after the cessation of cell expansion, are not covered in this literature review.

Plant cell expansion requires coordination between maintenance of osmotic potential and changes in wall properties, which are determined by wall components. Plant cell walls are highly organized; the diverse components include cellulose, glycans, pectins, proteins, and aromatic substances, as well as metal ions. Cellulose, a major component of plant cell walls, plays the most important role in the wall architecture. Approximately 36 chains of 1,4 linked, β-D-glucose associate through intermolecular hydrogen bonds to form a microfibril, which serves as a structural scaffold to support other wall components, and forms a fundamental framework of the wall architecture. The microfibrils in walls are paracrystalline and resistant to hydrolysis by acids, bases and enzymes (Reiter, 2002; Somerville, 2006).

Glycans, a mixture of branched polysaccharides, form molecular backbones through the linkage of β-D-hexosyl residues with the same bond as in cellulose. Distinct glycans interlock microfibrils by hydrogen bonding. Glycans and pectins form the secondary network, which strengthens the wall architecture. Xyloglucan (XyG), glucuronoarabinoxylans (GAX), mixed linkage glucans (MLG), and (gluco) mannans are found to be the four main glycans in primary cell walls. Because glycans have a property of random arrays and amorphous structures in the wall they are readily hydrolyzed by dilute acids, bases, or myriad enzymes (Reiter, 2002).

Pectins are a family of heterogeneous polysaccharides that all contain 1,4-linked α-D-galacturonic acid. Because of this residue, pectins provide cell walls a hydrated and charged surface. Additionally, a pectin polymer has a multitude of branches, which makes cell walls porous. These componential and structural features of pectins also allow cell walls to modulate pH and ion balance. Homogalacturonan (HG) and rhamnogalacturonans (RG-I and RG-II) are fundamental constituents of pectins in primary cell walls (Willats et al., 2001).

The majority of proteins in cell walls are glycoproteins that have oligosaccharide chains covalently attach to particular moieties of polypeptides. Hydroxyproline-rich glycoproteins (HRGPs, also called extensins), the arabinogalactan proteins (AGPs), and the proline-rich proteins (PRPs) are the most abundant glycoproteins in plant cells. Although proteins are not a major component of cell walls, they display a wide variety of structures and functions. These proteins make the wall a dynamic entity throughout the cell's life. For example, expansin induces the pH-dependent wall extension and stress relaxation in a characteristically unique manner (Cosgrove et al., 2002). Wall-associated kinases (WAKs), which are covalently bound to pectin, have the potential to provide a physical and signaling continuum between the cell wall and the cytoplasm (Wagner and Kohorn, 2001). The absence of AGPs in cell walls causes aberrant cell expansion, which forms numerous bulges in root epidermal cells (Willats and Knox, 1996; Ding and Zhu, 1997).

Minerals appear in micro amounts in cell walls, but they also play a role in the wall structure. If plants lack them, normal cell wall formation is disrupted. For example, Ca^{2+} links distinct pectin polymers (RG-I) through an ionic bond (Catoire et al., 1998). Another example is boron, which is predominantly associated with rhamnogalacturonan II (RG-II). Disruption of the

linkage between borate and RG-II affects plant growth, and borate deficiency compromises plant cell expansion in growing tissues (O'Neill et al., 2004).

Cell Wall Synthesis and Cell Expansion

Biosynthesis of plant cell walls is intimately connected with cell expansion. While a cell is increasing its volume, its wall becomes thinner and thinner. Finally, if the cell wall fails to incorporate new materials, it bursts. Thus, wall biosynthesis is required for cell expansion. In recent years, the study of the biosynthesis of wall components has made substantial progress through biochemical, genetic, and genomic approaches. Here, the emphasis is on the genes that are involved in primary wall synthesis and their mutations that cause disruption of cell expansion and generate aberrant cell shape.

Cellulose is synthesized by cellulose synthase (CESA), which has been identified in most plant species. In the *Arabidopsis* genome, ten genes code for CESA; in rice there are at least nine genes (Keegstra and Walton, 2006), and poplar has 18 (Djerbi et al., 2005). All CESAs share common structural features: eight transmembrane domains, two glycosyltransferase domains, and several microtubule-interaction domains. Six hexamers of CESA form a symmetric rosette on the plasma membrane plane; rosette movement is guided by cortical microtubules. Each subunit of CESA in the rosette synthesizes one 1,4 β-D-glucose chain (Somerville, 2006).

Glycan synthesis includes backbone synthesis and side chain addition. Compared to CESA, glycan synthesis is not well understood, although there is a structural similarity between cellulose and glycans. Basing on this similarity, the CSL hypothesis has been established. It was hypothesized that *CELLULOSE SYNTHESIS LIKE (CSL)* genes encode Golgi-localized glycan synthases. This hypothesis is supported by recent discoveries of several glycan synthase genes (Lerouxel et al., 2006). For example, mannan synthase, MLG synthase, XyG glucan synthase, and galactomannan galactosyltransferase are all encoded by members of the *CSL* gene family.

Additionally, these enzymes are all responsible for the backbone synthesis of glycans. XyG fucosyltransferase and XyG xylosyltransferase (XT1) were found to add side chains to the backbone of glycans (Reiter, 2002; Lerouxel et al., 2006).

Pectin biosynthesis is much more complicated than cellulose and glycan synthesis because it is difficult to investigate pectin synthases using traditional biochemical purification techniques and forward genetics. Through reverse genetics and genomics approaches, more than 50 glycosyltransferases (GTs) are predicted to be required for pectin synthesis (Ridley et al., 2001). At present, only a few genes for pectin biosynthetic GTs have been identified, and for some of their products, the activity of the pectin synthesis is not clear (Bacic, 2006). HG galacturonosyltransferase (GAUT1) is the first functional identification of GTs using biochemical and functional genomic approaches in *Arabidopsis* (Sterling et al., 2006). Other putative GTs include *QUA1* (Bouton et al., 2002), *NpGUT1* (Iwai et al., 2002), and *PARVUS/GLZ1* (Lao et al., 2003).

During cell expansion, polysaccharides are deposited into existing walls. If polysaccharide synthesis is disrupted, old wall reinforcement and new wall assembly cannot take place. Thus, normal cell expansion is disrupted, resulting in aberrant cell shapes. For example, mutations in *CESA* cause alterations of cell shape in diverse cell types because cellulose forms a fundamental framework of the wall architecture. *RSW1* encodes CESA1. The *rsw1* mutation causes disassembly of CESA complexes on the apoplastic side plane of the plasma membrane and reduction of cellulose accumulation in cell walls (Arioli et al., 1998). The *rsw1* mutants display shorter roots with radial swellings (*rsw*), smaller leaf blades with shorter petioles, and aberrant trichomes at the 31°C restriction temperature. All these defects are indicative of abnormal cell expansion owing to the *rsw1* mutation (Williamson et al., 2001). The root radial swellings of the

rsw1 mutants exactly mimic phenotypic responses of wild-type roots to cellulose synthesis inhibitors such as dichlorobenzonitrile. This observation suggests that the abnormal cell expansion is due to reduction of cellulose synthesis. Further evidence for this view comes from down-expression of *CESA1* and *CESA3*, using transformation with antisense constructs. The antisense phenotypes of *CESA1* or *CESA3* display shorter inflorescent shoots and stamen filaments, a result of reductions in cell length rather than cell number. In addition, the severity of the manifestation of both genes of interest is closely similar and intimately correlated to their reduced expression (Burn et al., 2002). *PROCUSTE1* (*PRC1*) is another gene, coding for CESA6. Mutations in this gene also exhibit similar defects as *rsw1*, including decreased cell elongation, especially in roots and dark-grown hypocotyls. The cell elongation reduction is correlated to a cellulose deficiency (Fagard et al., 2000). These observations indicate that the reduction of cellulose in walls generally causes suppression of cell expansion.

Glycans form the cell wall matrix, which enhances the wall strength. Probably because of this role, mutations in glycan synthase genes often cause only a slight alteration of cell expansion and shapes. In addition, a specific mutation in one glycan synthase gene fails to cause a visible phenotype. For example, *MUR2* encodes XyG fucosyltransferase (AtFUT1). The cell walls of *mur2* contain less than 2% of the wild-type amount of fucosylated XyG. The *mur2* plants show a normal growth habit and wall strength. On the other hand, *MUR1* codes for a 4,6-dehydratase, responsible for the de novo synthesis of l-fucose. Mutations in *MUR1* cause structural changes in several cell wall polysaccharides (Bonin et al., 1997). Thus, *mur1* mutants exhibit a dwarfed growth habit and decreased wall strength, probably indicating aberrant cell expansion (Reiter et al., 1993; Bonin et al., 1997). *MUR3* encodes XyG galactosyltransferase, which specifically catalyzes formation of the α-L-Fuc-β-D-Gal- side group. Although the XyG in the *mur3* cell walls

completely loses the fucosylated disaccharide side chain, *mur3* plants are visibly indistinguishable from wild-type plants except for a collapse of trichome papillae (Madson et al., 2003). However, later investigators found that the galactose residues of XyG are essential to maintain wall mechanical strength during rapid cell expansion. The *mur3* mutations result in reduced wall strength. Through studies using a scanning electron microscope, the defects in the *mur3* hypocotyl cells were observed. In addition, these defects are similar to the phenotype of mutations in *rsw1*, generating swollen cells of larger size (Pena et al., 2004). These defects indicate abnormal cell expansion can be caused by a reduction of cell wall strength.

Pectins combine with glycans to form the secondary network of cell wall architecture. Thus, mutations in the pectin synthesis genes share similar phenotypes to the phenotypes seen in plants with defective GT genes. *QUASIMODO1* (*QUA1*) codes for a putative membrane-bound GT. When the *qua1* mutants were grown in light, the plants showed reduced height because of the pectin deficiency in cell walls; similarly, the *qua1* seedlings grown in the dark had shorter hypocotyls, compared with the wild type. These defects are likely due to suppressed cell expansion (Bouton et al., 2002). The dwarfism phenotype was also observed in the *parvus* mutants because of both reduction in RG-I branching and alterations in the abundance of xyloglucan linkages. PARVUS encodes another putative GT (Lao et al., 2003). Pectins play a crucial role in pollen tube elongation because they are the only kind of molecule that makes a single layer of wall at the growing tip (Stepka et al., 2000). *VANGUARD1 (VGD1)* encodes a pectin methylesterase (PME), which, depending on ambient pH, by enzymatic activity can lead either to stiffening or to loosening of cell walls (Catoire et al., 1998; Denes et al., 2000). Mutations in *vgd1* cause a rupture of elongating pollen tubes in vitro and retarded growth in vivo (Jiang et al., 2005). Moreover, when PME is exogenously added to growing pollen tubes, the

apical wall is thickened, resulting in inhibition of pollen tube elongation (Bosch et al., 2005). PME activity that promotes cell wall loosening will be described below.

After cell division, through anisotropic expansion plant cells generally reach their final sizes. At this time, polysaccharides have been almost equally deposited into primary cell walls. A majority of the cells further differentially form specific shapes through further anisotropic expansion. Before this process occurs, the cell wall at specific sites is biochemically "loosened" for turgor-driven cell expansion (Cosgrove, 2000a). Additionally, the wall is loosened without compromising the tensile strength of the pliant wall (Cosgrove, 2000b). The reason plant cells have the capacity for this complex event is that the walls contain such unique proteins as expansins, PME, and XyG endotransglucosylase (XET). PME de-esterifies highly methylesterified pectins, converting the methoxyl groups into carboxyl groups on the polygalacturonic acid chain, and releasing both methanol and protons. This conversion promotes pectin gelation accompanying wall stiffening, due to the formation of the cooperative Ca^{2+} cross-bridges between free carboxyl groups of adjacent pectin chains (Catoire et al., 1998). In addition, the de-esterification reduces the local pH, which promotes activity of several other cell wall-loosening hydrolases, such as expansins, polygalacturonases, and pectate lyases (Cosgrove et al., 2002). Under-expression of *PME* by antisense RNA in transgenic pea reduced root hair elongation. Moreover, the root length reduction was correlated with an increase in extracellular pH (Wen et al., 1999). The activation of wall hydrolases by acidification of cell walls was also supported by the functional analysis of DET3, which is a vacuolar H+-ATPase (V-ATPase). Mutations in DET3 lead to defects in hypocotyl cell elongation. It was suggested that V-ATPases contribute to maintaining the internal turgor pressure of plant cells through modulation of solute uptake to vacuole (Schumacher et al., 1999). Subsequently, another kind of vacuolar H+-pump

called H+-PPase AVP1 (AVP1) was found to be implicated in this transport process. AVP1 adjusted the distribution and abundance of H+-ATPases in the plasma membrane by controlling its trafficking through the endocytic secretory pathways. Over-expression of AVP1 increased the accumulation and polar distribution of the H+-ATPase in the plasma membrane. Consequentially, more H+ was pumped to the apoplast and the cell wall was acidified. Thus, cell elongation occurred. In the *avp1-1* null mutant, root cell elongation was severely disrupted (Li et al., 2005).

Expansin, another cell wall protein, induces pH-dependent wall extension and stress relaxation in a characteristically unique manner (Cosgrove et al., 2002). Expansin has been proven to cause isolated wall extension in vitro under constant mechanical stress (McQueen-Mason et al., 1992). Application of exogenous expansin from cucumber in excised *Arabidopsis* hypocotyls stimulates cell elongation. At a high concentration of applied expansin, the tips of growing root hairs burst; at a lower level, exogenous expansin caused radial swelling at the tip (Cosgrove et al., 2002). Over-expression of *Arabidopsis EXP10* results in transgenic plants with longer petioles and larger leaf blades because of increased cell size (Cho and Cosgrove, 2000). Over-expression of *EXP1* in tomato fruit enhances fruit softening and cell wall breakdown (Brummell et al., 1999).

The enzymatic activity of XET breaks the existing linkages in the XyG-cellulose network and rejoins the resultant ends with new partners at different positions. XET loosens the wall during cell expansion through cooperation with expansin (Nishitani and Tominaga, 1992). XET activity is intimately correlated to the cell growth rate and epidermal lengthening in the growing zone of maize leaves (Rose et al., 2002). XET also is specifically localized at the site of

trichoblast walls, where the future bulge is formed during root hair initiation. A locally high level of XET activity stimulates trichoblasts to initiate root hairs (Vissenberg et al., 2001).

Plasma Membrane Dynamics and Cell Expansion

The plasma membrane abuts cell walls and participates in cell wall synthesis. As mentioned above, the plasma membrane protein CESA synthesizes cellulose for direct wall synthesis. The plasma membrane also actively performs exocytosis for indirect wall synthesis during cell expansion. In addition, the structural asymmetry of the plasma membrane provides cell polarity for anisotropic expansion (Fischer et al., 2004). To understand the roles of the plasma membrane in cell expansion, I briefly describe its components, highlighting its structural asymmetry. After this, the assembly of the plasma membrane and its relation to cell expansion are described.

Components of the Plasma Membrane

The plasma membrane of plant cells is composed of lipids, proteins, and carbohydrates in a molecular ratio of approximately 2 : 2 : 1. The membrane lipids include phospholipids, sphingolipids, and sterols (Moreau et al., 1998; Jaillais and Gaude, 2008). Some phospholipids such as phosphatidylcholine (PC) and phosphatidylethanolamine (PE) have head groups with positive charges; whereas others are negative or neutral, depending on pH. More importantly, the ratio of lipid classes in plant plasma membranes shows a wide range of variation among the different organs in a given plant or identical organs in distinct plants (Jouhet et al., 2007). The majority of carbohydrates in plant plasma membranes are present in the form of oligosaccharides that are covalently linked to proteins to generate glycoproteins (Bacic et al., 1996; Classen et al., 2005).

Asymmetry of Plant Plasma Membranes

Lipids, proteins, and carbohydrates of plant plasma membranes are regularly arranged in an asymmetric bilayer structure. The lipid amphipathy allows for spontaneous assembly of bilayers. The hydrophilic heads maximize their interactions with water, whereas the hydrophobic tails interact with each other, minimizing their exposure in the exoplasmic leaflet (Holthuis and Levine, 2005; Pomorski and Menon, 2006). Sphingolipids and sterols are abundant in microdomains (lipid rafts), in which signaling proteins accumulate. Other proteins are also localized at particular sites in the plasma membrane. For example, auxin carriers are positioned at the apical or basal plasma membrane of root epidermal cells (Muller et al., 1998; Swarup et al., 2001), whereas glycosylphosphatidylinositol (GPI)-anchored proteins (GAPs) such as COBRA (COB) preferentially localizes to lateral membrane in root cells (Schindelman et al., 2001). This asymmetric distribution establishes and maintains cell polarity, which is required for longitudinal expansion at the elongation zone (Fischer et al., 2004; Kramer and Bennett, 2006).

Plasma Membrane Assembly and Cell Expansion

Plasma membranes of plant cells are assembled using various lipids and diverse proteins. In addition, different lipids interact with distinct proteins, and specific proteins have particular positions in lipid bilayers. During isotropic cell expansion, the plasma membrane evenly enlarges its area, whereas in polar expansion it is assembled only at the growing sites. For any cell expansion, the plasma membrane maintains the dynamic stability of chemical composition and distribution of protein components. In addition, it has the capacity for flexible changes in these features in response to intracellular and extracellular signalings for anisotropic expansion. Perturbations of membrane stability cause abnormal cell expansion (Schrick et al., 2000; Souter et al., 2002; Jaillais and Gaude, 2008).

Changes of lipid composition in the plasma membrane cause disruption of normal cell expansion (Jaillais and Gaude, 2008). *COTYLEDON VASCULAR PATTERN 1* (*CVP1*) and the *ORC* gene encode a sterol methytransferase for sterol biosynthesis. Mutations in either *CVP1* or *ORC* alter the membrane sterol composition, which raises the level of cholesterol and campesterol at the expense of sitosterol. The $smt1^{orc}$ and $smt2^{cvp1}$ double mutants display defects in polar cell expansion that result in the perturbed alignment of cells into parallel vascular cell files in cotyledons because abnormal cell expansion leads to aberrant cell shapes (Carland et al., 2002; Willemsen et al., 2003). Sterols are enriched in lipid crafts, which provide platforms that anchor polar proteins to the plasma membrane. Thus, the influence of sterol composition on the localization of polar proteins has been widely reported in yeasts and animals (Simons and Ikonen, 1997; Bagnat et al., 2000; Bagnat and Simons, 2002; Danielsen and Hansen, 2006). These events are also likely to occur in plants. For example, it has been found that, in *Arabidopsis,* $smt1^{orc}$ root cells mislocalized auxin carriers on the plasma membrane (Willemsen et al., 2003).

Changes in anchored proteins of the plasma membrane also cause disruption of normal cell expansion. In eukaryotic cells, glycosylphosphatidylinositol (GPI) anchored proteins (GAPs) have been extensively reported to be plasma membrane bound proteins (Oxley and Bacic, 1999; Sherrier et al., 1999; Zhao et al., 2002). *Salt-overly-sensitive 5* (*SOS5*) encodes a plant GAP. Mutations in *SOS5* cause strong radial expansion of the cells in the elongation zone of roots, instead of the longitudinal expansion seen in wild type. Thus, the epidermal, cortical, and endodermal cells in *sos5* roots display a swelling phenotype (Shi et al., 2003). COB, another plant GAP, is anchored on the extracellular side of the plasma membrane and also released into the wall. It is required for highly anisotropic expansion of all plant cells. The *cob-4* null allele

shows greatly reduced growth of all organs in seedlings. However, because the *cob-4* root cells expanded radially in the elongation zone, the root diameter ultimately reaches nearly twice that of the wild type. The root epidermal cells displayed a severe bulging phenotype. In addition, their cell walls were occasionally broken. COB plays a crucial role in the oriented deposition of cellulose microfibrils during rapid anisotropic expansion (Roudier et al., 2005). SKU5 has the same cell localization as COB, which is in the cell wall and on the plasma membrane anchored by GPI. *SKU5* is expressed most strongly in expanding cells. Mutations in *SKU5* cause skewed roots and shortened hypocotyls because of abnormal cell expansion (Sedbrook et al., 2002). Although PNT1 is not a GAP, it encodes a mannosyltransferase for the GPI synthesis. All five *pnt* mutants strongly reduce accumulation of GAPs. In the *pnt1* mutants, the cell walls had decreased crystalline cellulose; embryos showed delayed morphogenesis; apical meristems were defective; and seedlings did not survive. All phenotypes were due to aberrant cell expansion (Gillmor et al., 2005). ETH1 and SETH2 also are involved in GPI biosynthesis. The *seth1* and *seth2* mutations specifically block or reduce pollen tube elongation because of abnormal callose deposition. In addition, another 47 genes, which all encode potential GPI-anchored proteins, are likely to play important roles in the establishment and maintenance of polarized pollen tube expansion (Lalanne et al., 2004).

Normal cell expansion is disrupted by changes in the position of polar proteins. *Arabidopsis* phospholipase Dζ1 (AtPLDζ1) is preferentially localized at the tip of growing root hairs. Ectopic over-expression of *AtPLDζ1* disrupts its distribution in specific tissues and induces non-root cells to form ectopic root hairs in cotyledons and hypocotyls. The raised level of AtPLDζ1 in root cells generates swollen or branched root hairs (Ohashi et al., 2003). It is likely that the intrinsic polarized distribution of AtPLDζ1 is perturbed, thus losing capacity for tip

growth. Recently, AtPLDζ2 was also found to be involved in cell expansion. Mutations in this gene reduced the hypocotyls cell elongation (Li and Xue, 2007). More recently, it was found that ROOT HAIR DEFECTIVE 2 (RHD2) is located at the growing tip of root hair cells. Mutations in *RHD2* causes defective root hairs (Takeda et al., 2008). AGC2 is a member of the cAMP/cGMP-dependent kinase or protein kinase C family kinase (AGC kinase). It localizes to the root hair tip. The *agc2-1* mutants have short root hairs because of reduced cell elongation (Anthony et al., 2004). Other polar proteins of plant plasma membranes that play a role in cell expansion in response to phospholipid signaling are transported by oriented vesicle trafficking involving such proteins as PIP5K3 (Kusano et al., 2008) and RHD4 (Thole et al., 2008). These proteins are described below in the endomembrane dynamics and cell expansion section.

In recent years, numerous observations of transcytosis of the plasma membrane in plant cells were reported as a result of the application of fluorescent styryl dyes, such as FM1-43 and FM4-64, particularly in expanding root hairs and pollen tubes (Samaj et al., 2006). Through exocytosis, secretory vesicles containing the cell wall cargo molecule fuse with the plasma membrane, releasing their contents into the extracellular space for wall loosening, strengthening, or assembling during cell expansion, whereas, through endocytosis, the extra plasma membrane proteins and lipids are transferred into the cytosol for recycling at the growing sites (Samaj et al., 2005; Johansen et al., 2006). Increasing evidence shows that blocking exocytosis with brefeldin A (BFA) inhibits pollen germination and pollen tube elongation (Wang et al., 2005b). Because transcytosis is tightly coupled with the endomembrane trafficking network, details of this topic are described below.

Endomembrane Dynamics and Cell Expansion

Endomembrane trafficking is essential for cell expansion, especially for polar expansion (Samaj et al., 2006). Except for cellulose, almost all cell wall components are synthesized in the

Golgi apparatus (GA) and endoplasmic reticulum (ER), further packaged into vesicles, and finally transported to the wall space (Reiter, 2002; Dhugga, 2005; Lerouxel et al., 2006). The oriented trafficking of vesicles serves to establish and maintain cell polarity, which initiates polar expansion. In this part, I introduce general endomembrane pathways first, focusing on their characteristics in plant cells. After that, I highlight the influence of the disruption of endomembrane trafficking on plant cell expansion.

Endomembrane Trafficking Pathways

The endomembrane system is composed of all intracellular membranous compartments. These compartments communicate with each other through exchanging molecules using ubiquitous vesicles as carriers. The vesicles containing cargo molecules secrete from donor compartments, and fuse with target compartments. During vesicle trafficking, the GA plays a leading role. It lies at the heart of the membrane trafficking pathway, serving as the crossroad in various trafficking events (Hawes and Satiat-Jeunemaitre, 2005a). At its *cis*-face, the GA receives the vesicles from the ER (anterograde transport) and sends their vesicles back (retrograde transport). At its *trans*-face, the GA sends its vesicles to endosomes, storage vacuoles, lytic vacuoles, and the plasma membrane. The vesicles, from the plasma membrane through endocytosis, are recycled in the GA. The vesicles exported from the ER can also bypass the GA pathway and go directly to a vacuole or the plasma membrane (Hawes, 2005).

The GA is the sum of numerous polarized stacks of membrane-bounded cisternae. Within the GA, cargo molecules are processed, concentrated, and packaged into vesicles (Hawes, 2005). The mature cargo molecules in the vesicles are intracellularly routed to specific cellular destinations within cells. For plant cells, the GA is an important organelle that specializes in the synthesis and processing of complex components of cell walls, such as glycans and glycoproteins (Hawes and Satiat-Jeunemaitre, 2005b). Probably to this end, the GA organization in plant cells

is different from its counterpart in animal cells, in which the GA is composed of many stacks that are generally arranged side-by-side in a ribbon structure around the nucleus. In plants, the GA is divided into individual Golgi stacks that are distributed through the cytoplasm (Latijnhouwers et al., 2005). The number of Golgi stacks per cell and the number of cisternae per stack varies with cell developmental stages and cell types (Neumann et al., 2003). Mammalian GA is a rather static organelle, but plant GA is a highly mobile biosynthetic factory that moves over the ER on an actin network at the speed of 2 μm per second (Boevink et al., 1998; Nebenfuhr et al., 1999). This characteristic of the plant GA enables cargo molecules to be efficiently transported to the extra-cellular matrix.

Vesicle Dynamics

In eukaryotic cells, the vesicle is a ubiquitous vector for endomembrane trafficking. The highly dynamic vesicles are generated through membrane fission of donor compartments, and disappear by membrane fusion at destination compartments. The processing of both the fission and the fusion elements involves close contact between lipid bilayers and the final combination of bilayer leaflets at specific sites (Markvoort et al., 2007). Fission begins with bending of membranes at the export site. The bent membrane invaginates to an extreme curvature to form a highly constricted neck. The neck further elongates and narrows until the two membranes merge, which leads to the separation of the vesicles from the donor compartment. Membrane fusion begins with docking of vesicles at acceptor compartments. The lipid bilayer of the docked vesicle gradually unites with the membrane of the acceptor compartment (Sollner and Rothman, 1996; Atilgan and Sun, 2007). Membrane fission and fusion are completed by the vesicle assembly machinery. In mammalian and yeast cells, the components of this machinery are well known. Generally they include the coat proteins, adaptor proteins, cargo receptors, and small GTPase proteins (Marks et al., 2001).

Vesicle Fission Machinery

During vesicle assembly, numerous proteins are recruited at the exit site. On the internal surface of membranes, cargo receptors such as v-SNARES specifically bind outgoing molecules from the lumen. On their external surface, the ADP-ribosylation factors (ARFs) are recruited from the cytosol to bind tightly to the membrane. The ARFs further interact with their effectors and regulators. A regulator such as GAP, contributes to hydrolysis of the active GTP-bound ARF form to the inactive GDP-bound ARF form with opposite conversion catalyzed by GEF. The change of the ARF conformation during GTP hydrolysis leads to structural alterations of both the lipid and the effectors attaching with the membrane. This alteration promotes vesicle budding and delivery from the donor compartment. The ARF effectors mainly include coat proteins (Donaldson and Jackson, 2000; Donaldson et al., 2005). Three types of coat proteins have been found: clathrin, COPI, and COPII. Clathrin coats the transport vesicle that shuttles between the GA and the plasma membrane, the GA and endosomes, and the plasma membrane and endosomes; COPs wrap the vesicles that shuttle between the GA and the ER. COPI coats vesicles from the GA to the ER, while COPII coats the vesicles from the ER to the GA. Recent research has shown that COPI interacts with Brefeldin-A ADP-ribosylated substrate (BARS) (Yang et al., 2005; Yang et al., 2006) and the actin cytoskeleton provides force both for membrane deformation during vesicle formation and for vesicle trafficking to the correct destination (Goley and Welch, 2006; Kaksonen et al., 2006; Co et al., 2007).

Vesicle Fusion Machinery

After the vesicles detach from the donor membrane, the coat proteins release from the vesicle surface into the cytosol for recycling. Thus, the vesicle surface marker v-SNAREs (soluble N-ethylmaleimide-sensitive-factor attachment protein receptors) is exposed, as well as their complementary SNAREs, termed t-SNAREs, on the target compartment. The interaction

between these two SNAREs causes fusion of the vesicle with the target membrane (Chen and Scheller, 2001; Bonifacino and Glick, 2004). More than 30 members in the SNARE superfamily were found in mammalian cells (Chen and Scheller, 2001). A large number of SNAREs were also found in the *Arabidopsis* genome and other plants (Sanderfoot and Raikhel, 1999; Sanderfoot et al., 2000; Sanderfoot, 2007).The regulatory protein Rab participates in specific junctions of v-SNAREs with t-SNARSEs. Rab is a GTP-binding protein. It also provides energy for driving membrane fusion through GTP hydrolysis, while binding with the t-SNAREs (Segev, 2001; Zerial and McBride, 2001)

Vesicle Trafficking and Cell Expansion

Identifying the molecular machinery of the plant membrane trafficking pathway reveals significant homology with that of mammalian and yeast counterparts. Coat proteins (COPI, COPII, and clathrin), small GTPases (Rabs, Arf, Sar1, and Rac), and fusion proteins (SNAREs) appear to be well conserved throughout eukaryotic cells. In plant cells, the majority of the COPI and COPII machinery and their associated effectors, such as Arf and Sar1, have been cloned, and their functions are now being determined. More and more data have indicated that vesicle trafficking contributes to establishment of the structural and molecular asymmetry at the cell surface, which is the beginning of cell polar expansion (Xu and Scheres, 2005a; Friml et al., 2006).

Brefeldin A (BFA) is a fungal toxin that has been widely used as a reversible inhibitor of vesicle trafficking in yeast, mammalian, and plant cells. BFA blocks the detachment of vesicles at the exit site of the GA membrane to form aggregates, which disrupts the normal flow of the vesicles within cells. BFA has been shown to alter the distribution of such plasma membrane-localized proteins as PIN1, AUX1, PM-ATPase, and pectins in plant root cells. In addition, the epidermal cells of *Arabidopsis* roots treated with BFA lost their polarity, displaying a decrease in

cell length and increase in the apical-basal initiation ratio, as well as formation of double root hairs, in which two root hairs are derived from one trichoblast (Grebe et al., 2002). The molecular mechanism of BFA inhibition of vesicle trafficking is due to the binding of BFA with the ARF1-GDP/ARF-GEF complex, which prevents ARF1 activation necessary for vesicle budding and cargo molecule selection (Robineau et al., 2000). In mammalian cells, ARF1 is a core component of the vesicle assembly machinery, recruiting COPI and clathrin coat proteins to membranes for vesicle assembly in mammalian cells (Boman, 2001; Rein et al., 2002; Spang, 2002; Song et al., 2006). In *Arabidopsis*, ARF1 rescued the ARF1/ARF2 lethal yeast double mutant, which suggest that plant ARF1 has similar functions to its yeast and mammalian counterparts (Takeuchi et al., 2002). Moreover, *Arabidopsis* ARF1 is also located to the GA and endocytic organelles. The over-expression of the engineered ARF1 with dominant activation and inactivated formats that are targeted to interfere with the endogenous ARF1 function in trichoblasts significantly inhibited polarized tip expansion, which produced shorter roots. After strong heat shock induction, the trichoblasts and epidermal cells in the transgenic lines displayed many more severe defects, such as apical-shifted root hairs, double root hairs, and bulged epidermal cells. All these phenotypes show that the cells lost their polarity and capacity for polar expansion (Xu and Scheres, 2005b). The ARF GTPase activating protein, ROOT AND POLLEN ARFGAP (RPA), activates ARF1 and plays a role in the elongation of root hairs and pollen tubes in *Arabidopsis*. RPA is specifically expressed in roots and pollen; its product is located in the GA. Additionally, RPA complements the *glo3 gcs* double mutants in yeast (Song et al., 2006). GLO3 and GCS1 are two yeast ARFGAPs that function efficient retrograde trafficking of vesicles from the GA to the ER (Poon et al., 1999; Robinson et al., 2006). ARFGAP1 promotes both vesicle formation and cargo sorting by functioning as a component of the COPI coat (Yang

et al., 2002; Lee et al., 2005). The loss-of-function mutant, *rpa*, causes root cells to isotropically expand to generate short and branched root hairs, as well as a slowing of pollen tube elongation (Song et al., 2006). Over-expression of the rice *OsARFGAP* also interfered with vesicle trafficking, which influenced on the root hair formation and elongation. Transgenic plants of *Arabidopsis* and rice had a reduced number of lateral roots and reduced root length. The ratio of length and width of epidermal cells at the elongation region also decreased compared to wild-type plants. Additionally, abnormal vesicle aggregates (the BFA compartment, a typical defect of disrupted vesicle trafficking) were observed in the transgenic cells (Zhuang et al., 2005; Zhuang et al., 2006). The ARF guanine-nucleotide exchange factor (ARF-GEF), GNOM, functions in the establishment of apical-basal cell polarity by mediation of specific endosomal trafficking pathway in *Arabidopsis* embryos and roots. GNOM localizes to endosomes. The loss-of-function mutant of *gnom* lacked an apical-basal polar axis and embryonic root in early embryos (Geldner et al., 2003). This phenotype is probably a result of defective cells that are unable to expand or anisotropically expand.

Arabidopsis Rab GTPase RabA4b was found to function in cell directional expansion through the regulation of vesicle trafficking involved in the polarized deposition of cell wall components in tip-growing root hair cells (Preuss et al., 2004). Mammalian Rab11 has a high degree of homology to RabA4b, as does *Arabidopsis* Ara4, which was localized to Golgi-derived vesicles, Golgi cisternae, and the trans-Golgi network (Ueda et al., 1996). Vesicles with the EYFP-RabA4b labeling marker accumulated in the actively expanding zone in the growing root hair. Such accumulation is necessary for root hair initiation and elongation. In the *rhd1-1* mutant, and the *rhd2-1* mutant, their defective cells did not show accumulation of the vesicles with Rab4A (Preuss et al., 2004). Plant Rab11 also plays a role in pollen tube tip growth.

Tobacco Rab11b was localized to the pollen tube tip. Interference of endogenous Rab11b activity in its mutated variants gave rise to a reduction of pollen tube growth rate and change of pollen tube morphology (de Graaf et al., 2005). Tobacco Rab2 also functions in cell polar expansion of pollen tubes through a vesicle trafficking pathway at the GA. NtRab2 localizes to the GA. The mutated NtRab2 blocks vesicle release from the GA so that the normal delivery of Golgi cargo to their destinations, such as the cell surface, was disrupted, inhibiting pollen tube expansion (Cheung et al., 2002).

Cytoskeleton Dynamics and Cell Expansion

The plant cytoskeleton includes microtubules and microfilaments that spatially control cell expansion (Smith and Oppenheimer, 2005). It is generally believed that microtubules serve as a scaffold for cells and are important for establishing and maintaining cell expansion direction, whereas microfilaments function as a track for vesicles to specific sites to deliver cargo required for expansion (Mathur and Hulskamp, 2002). Although many observations have shown that cytoskeletal dynamics and proper organization are essential for cell expansion, much remains to be learned, including the precise roles of microtubules and microfilaments in spatial control of cell expansion. There is evidence, however, that shows that the direction of the wall's main structural component, cellulose, is determined by microtubules. The arrangement of cellulose microfibrils in the wall is a key determinant of the cell expansion pattern and is clearly related to the arrangement of cortical microtubules in expanding cells (Smith and Oppenheimer, 2005). A rapidly growing body of knowledge has accumulated about how the dynamics and organization of both classes of filaments are controlled in expanding cells (Baskin, 2005). Here, however, we emphasize recent work explaining regulation of the cytoskeleton and its contributions to patterning of plant cell expansion.

The Microtubule Cytoskeleton and Cell Expansion

Microtubules orient the deposition of microfibrils in walls, which determines the cell expansion direction. The direction of cell expansion is determined by the organizational pattern of cortical microtubules because it was found that the latter normally mirrors the arrangement of cellulose microfibrils, the key structural element of the wall, in growing cells. Based on this observation, the co-alignment hypothesis was established. It was hypothesized that movement of cellulose synthase enzyme complexes in the plasma membrane is constrained by interactions with the cortical microtubules (Giddings and Staehelin, 1991). To accommodate later, conflicting, observations, this hypothesis has further evolved into several distinct versions, such as the template incorporation model (Baskin, 2001) and the microfibril length regulation hypothesis (Wasteneys, 2004). Here I will describe the evidence that support these hypotheses, with an emphasis on major advances in recent years.

Early observation showed that the deposition of cellulose microfibrils in elongating cells was typically perpendicular to the axis of cellular expansion. In addition, disruption of these fibrils with colchicine caused an isodiametric expansion. These characteristics led to the prediction that cytoplasmic elements exist in the cell periphery, orient the deposition of cellulose microfibrils, and constrain the pattern of cell expansion (Green, 1962). Only one year later, electron microscopy showed slender tubules (microtubules) at the cell cortex. More importantly, the orientation of these tubules mirrored that of the cellulose microfibrils in the adjacent cell walls (Ledbetter and Porter, 1963). Thereafter, cortical microtubules were often observed to lie parallel to the cellulose microfibrils (Hepler and Palevitz, 1974).

Microinjection of rhodamine-conjugated tubulin into the epidermal cells of pea internodes showed the array shift of the cortical microtubules between the transverse organization pattern and longitudinal one after application of gibberellic acid for induction of cell growth. This shift

is likely to be involved in a range of responses that alter the direction of cell expansion (Yuan et al., 1994).

Disruption of the dynamics and organization of endogenous microtubules with microtubule-modifying drugs gives rise to aberrant cell expansion. For instance, oryzalin is a compound that causes microtubule depolymerization, whereas taxol has an opposite effect; it promotes microtubule assembly. *Arabidopsis* seedlings treated with either oryzalin or taxol display an identical defective phenotype, the radial expansion of root cells. This result indicates the importance of microtubule dynamics in cell expansion. Additionally, the defective severity of the cortical microtubules in the swelling root cells increases with drug concentration. At low concentrations of oryzalin, microtubule arrays are disorganized; at medium concentrations they are fragmented, and at high concentrations they are totally depleted. However, in the taxol-treated root cells, the cortical microtubules at the elongation zone display disorganization in directionality compared with the control cells. At 10 micromolar concentration, many stele cells have more longitudinal microtubules, whereas many cortical cells appear to have more transversely aligned microtubules (Baskin et al., 1994). These experiments were repeated later (Sugimoto et al., 2003). The same results were obtained from an experiment with maize roots treated with oryzalin or taxol (Hasenstein et al., 1999).

Microtubules are polymers of tubulin. Mutations in the genes for tubulin also cause aberrant cell expansion, such as helical elongation. Dominant negative mutations in the α-tubulin genes cause left-handed helical growth and clockwise twisting in elongating organs of *Arabidopsis* because the mutant tubulins are incorporated into microtubules, producing right-handed obliquely oriented cortical arrays in the root epidermal cells. Additionally, the cortical microtubules in the mutants had increased sensitivity to microtubule-specific drugs, indicating

that the reduced microtubule stability can produce left-handed helical cell expansion (Thitamadee et al., 2002). The same defective cell expansion was exhibited in transgenic plants with the same mutated version of the α-tubulin gene (Abe and Hashimoto, 2005). This result further confirms that disturbance of endogenous microtubules influences cell expansion.

During cell expansion, the dynamic and well organized microtubules are mediated by the regulators, the majority of which are microtubule-associated proteins (MAPs). Thus, mutations in the MAP genes suppress the dynamics of microtubules, block their reorganization, and affect cell expansion. *MICROTUBULE ORGANIZATION 1 (MOR1)* encodes a member of an ancient family of MAPs. The amino acid sequence of MOR1 is similar to Xenopus MAP215. In *Arabidopsis* MOR1 regulates cortical microtubule organization, likely through stabilization of microtubules. Mutations in *MOR1* generate unstable microtubules. At the 29°C restrictive temperature, the cortical microtubules in leaf epidermal cells of *mor1* mutants break into fragments, but at the 21°C permissive temperature, the microtubules revert to their normal appearance. At the restrictive temperature, the *mor1* plants are severely stunted, producing radially swollen and short organs indicative of aberrant cell expansion (Whittington et al., 2001).

FRA2, another microtubule regulator, was found to have the activity of severing microtubules in vitro. Through confocal microscopy and immunofluorescence, it was found that the cortical microtubules are disorganized in *fra2* mutants. Meanwhile, using field emission scanning electron microscopy for studies on the walls, the *fra2* mutation alters the normal orientation of cellulose microfibrils in walls of expanding cells. The *fra2* mutants show reduced cell elongation. These findings strongly support the co-alignment hypothesis that microtubules orient cell expansion through the control of directional deposition of cellulose microfibrils in the

wall (Burk and Ye, 2002). Using the same methods for the *cob* mutations, strong evidence supporting this hypothesis was also obtained (Roudier et al., 2005).

COB is not a MAP, but an anchor to GAP, which is involved in regulation of cell polarity (Fischer et al., 2004). As mentioned above, COB is polarly targeted to both the plasma membrane and the longitudinal cell walls. Additionally it is distributed in a banding pattern perpendicular to the longitudinal axis via a microtubule-dependent mechanism. The elongating root cells in *cob* mutants lose capacity for anisotropic expansion and display a swelling phenotype. The defective cells are accompanied by disorganization of the orientation of cellulose microfibrils (Roudier et al., 2005).

The direct evidence supporting the microfibril and microtubule co-alignment hypothesis was recently gained using spinning disk confocal microscopy. The process of cellulose deposition was visualized in living cells by fluorescently-tagged CESA. The CESA complexes in the plasma membrane moved at a constant rate in a linear track that was aligned and coincident with cortical microtubules. Inhibition of microtubule polymerization changed the fine-scale distribution and pattern of moving CESA complexes in the membrane, indicating a direct mechanism for the guidance of cellulose deposition by microtubules (Paredez et al., 2006).

Signaling pathways of phospholipids and GTPases are involved in the regulation of the microtubule organization for cell expansion. In recent years, rapid advances have been made on understanding microtubule regulation by distinct signaling pathways, which are intimately related to anisotropic cell expansion, particularly by phospholipids and Rho of plants (ROPs). A wealth of mutations in the genes encoding components of these pathways causes aberrant cell expansion.

Phospholipase D (PLD) is a key component of the phospholipid signaling pathway. It was found that PLD decorates microtubules in plant cells (Marc et al., 1996) and is localized to the plasma membrane (Marc et al., 1996; Gardiner et al., 2001). PLDs are enzymes that hydrolyze structural phospholipids such as phosphatidylcholine to produce free choline and phosphatidic acid (PA), which function as a second messenger in cell signaling. Biotic and abiotic stresses such as wounding and pathogen infection rapidly stimulate PLD activity (Laxalt and Munnik, 2002; Wang et al., 2002; Meijer and Munnik, 2003). PLD activation triggers reorganization of plant microtubules (Dhonukshe et al., 2003). Changes of PLD levels disrupt the phospholipid signaling transmission, resulting in aberrant cell expansion likely because of the microtubule disorganization. Thus, raised levels of AtPLDζ1 generate either swollen or branched root hairs (Ohashi et al., 2003). AtPLDζ2 absence reduced the hypocotyl cell elongation (Li and Xue, 2007).

ROP GTPases are plant-specific signaling molecules. They potentially interact with cell surface-associated signal perception apparatus for such extracellular stimuli as hormones, pathogen elicitors and abiotic stress. ROP GTPases mediate diverse cellular processes, including microtubule dynamics and organization (Nibau et al., 2006). It was found that ROP2 inactivates ROP-interactive CRIB motif-containing protein1 (RIC1) in *Arabidopsis* epidermal leaf pavement cells. RIC1 activity promotes well-ordered cortical microtubules. The RIC1-dependent microtubule organization not only locally inhibits outgrowth, but also in turn suppresses ROP2 activation in indentation zones. RIC1 over-expression suppresses lobe formation, and *ric1* mutants exhibit wide neck regions (Fu et al., 2005).

Actin Cytoskeleton Dynamics and Cell Expansion

The mammalian actin cytoskeleton not only mechanically supports cells for formation of various shapes, but also generates a driving force for such diverse cellular or intracellular events

as cell migration, vesicle trafficking, exocytosis, and endocytosis (Kaksonen et al., 2006). As these events occur, actin cytoskeleton dynamics are essential for re-assembly of actin filaments at distinct subcellular locations (Goley and Welch, 2006). The dendritic nucleation model of actin polymerization is used for interpretation of the molecular mechanism of these events (Mullins et al., 1998; Pollard and Borisy, 2003). A leading hypothesis for force generation is through actoclampin, the ATP hydrolysis-dependent, affinity-modulated motor unit (Dickinson and Purich, 2002; Dickinson et al., 2004; Zeile et al., 2005). However, the role of the plant actin cytoskeleton is just coming of age. In recent years, increasing evidence has shown that the plant actin cytoskeleton is important for cell expansion during cell morphogenesis, particularly for tip growth and anisotropic expansion (Hussey et al., 2006). The role of the actin cytoskeleton is generally believed to be the delivery of specific vesicles containing cell wall materials to specified sites for local growth. The majority of investigations were done using cell-specific models, such as pollen tubes, root hairs, trichomes, and leaf pavement cells (Mathur and Hulskamp, 2002; Schellmann and Hulskamp, 2005; Smith and Oppenheimer, 2005; Cole and Fowler, 2006).

Polarized organization of the actin cytoskeleton is required for tip growth. Both pollen tubes and root hairs offer suitable models to study the roles of F-actin organization and dynamics in tip growth. In these cells, it has been observed that at least two forms of F-actin exist. One is the actin cables arranged along the elongation axis; and other is the dynamic fine F-actin localized to the tip (Hepler et al., 2001; Cole and Fowler, 2006). A wealth of observations shows chemical and genetic disruption of F-actin dynamics and polarized organization in tip-growing cells arrests tip growth.

For investigation of the roles of actin cytoskeleton in tip growth, LatB is the first chemical agent used to inhibit actin polymerization. LatB-treated maize pollen tubes display a dose-dependent depolymerization of F-actin. The elongation of the LatB-treated pollen tubes is arrested because of F-actin depolymerization (Gibbon et al., 1999). The same result was obtained in LatB-treated pollen tubes of *Picea meyeri* (Chen et al., 2007). The pollen tubes treated with 15 nM LatB for 20 hours show severe disruption of actin filaments. The polarized actin cables become short fragments throughout the tubes. In addition, some actin fragments tend to aggregate into clusters in the sub-apical region of the tube. The tip of LatB-treated pollen tubes swelled because of its loss of polarity (Chen et al., 2007).

Genetic disruption of the actin cytoskeleton also causes aberrant tip growth. Formins are actin-nucleating proteins that stimulate the de novo polymerization of actin filaments in mammalian cells (Kovar, 2006). It has been found that plant formins appear to have the same function as that in mammalian cells. Thus, changed levels of formin expression in pollen tubes affect the dynamics of F-actin and disrupt tip growth. Over-expression of *Arabidopsis* formin AFH1 in pollen tubes induces the formation of arrays of actin cables, resulting in depolarization of tip growth and generation of a broadening tube. Moreover, severe membrane deformation was observed in the apical region (Cheung and Wu, 2004).

Longitudinal actin cables serve as tracks for motor proteins that transport vesicles to the tips of growing pollen tubes and root hairs. Active vesicle transport was observed in root hairs, particularly at the growing tips. This cellular process is based on F-actin, which, when disrupted, arrests vesicle trafficking (Voigt et al., 2005).

Precise organization of the actin cytoskeleton is important for cell morphogenesis. The *Arabidopsis* trichome provides an excellent model for studies on cell morphogenesis. The

trichome is a large, single cell that develops on the epidermal surface. Its morphogenesis is a complex process, in which an approximately round, epidermal cell develops into a stellate symmetrical trichome (Schellmann and Hulskamp, 2005). Using this model cell, investigators found indirect evidence supporting the importance of precise actin cytoskeleton organization for trichome morphogenesis in pharmacological experiments with drugs that affect actin dynamics. When developing trichomes were treated with microfilament destabilizing antagonists (cytochalasin D and latrunculin B) or filamentous actin (F-actin) stabilizing inhibitors (phalloidin and jasplakinolide), both observations shows stage-specific requirements for the actin cytoskeletal array. Although the establishment of trichome cell polarity seems not to need precise actin organization, the rapid expansion of trichome cells after branching is sensitive to the inhibitors, causing an aborted, swollen stub or a highly elongated and distorted structure because of their disorganized F-actin arrangement (Mathur et al., 1999; Szymanski et al., 1999).

The direct evidence supporting the necessity of a precise actin organization for trichome morphogenesis comes from the discovery of the genes that encode the subunits of Arp2/3 and the WAVE complexes in the *Arabidopsis* genome. The Arp2/3 complex by itself is inactive and needs the WAVE complex to activate it. These two complexes coordinately regulate actin polymerization, and influence F-actin reorganization in both mammalian (Goley and Welch, 2006) and plant cells (Schellmann and Hulskamp, 2005; Szymanski, 2005; Uhrig and Hulskamp, 2006). Recent work has indicated that mutations in the components of the Arp2/3 and WAVE complexes cause a common trichome defect, resulting in distorted trichomes. In addition, the F-actin is disorganized in the defective trichomes (Mathur et al., 2003; Basu et al., 2005; Zhang et al., 2005b; Uhrig et al., 2007). The characterizations of the defective trichome phenotype and the F-actin disorganization in the *dis* mutants are reminiscent of trichomes treated with anti actin

drugs. These uniform results strongly support a crucial role of a precise actin cytoskeleton in trichome morphogenesis.

The *Arabidopsis* epidermal leaf pavement cells are another ideal model for cell morphogenesis. These cells have a unique structure, which produces a jigsaw-like appearance. They exhibit an interlocked arrangement that results from the interdigitation of adjacent cells through the formation of complementary lobes and indentations. Working on these cells, researchers discovered additional evidence supporting the critical role that the actin reorganization plays in cell morphogenesis. ROP2, a small GTPase, is redundantly required for normal pavement cell morphogenesis. Genetic disruption of ROP2 results in a severe decrease in the lobe elongation of pavement cells. Additionally, fine F-actin is also reduced at the lobes of the defective cells (Fu et al., 2002). ROP2 promotes F-actin assembly through interaction with RIC4, which is also expressed in leaves, and localizes preferentially at the cortical sites of incipient lobe formation Moreover, *RIC4* over-expression promotes the accumulation of fine F-actin and generates deep lobes. On the other hand, *ric4* mutants display pavement cells with shallow lobes. Thus, the fine cortical F-actin at specific sites promotes outgrowth for lobe formation (Fu et al., 2002; Fu et al., 2005).

Although the role of the actin cytoskeleton in the control of plant cell morphology is well established, all these results do not yet offer an explanation of its molecular mechanism. Many questions have yet to be answered. For example, why are abundant actin filaments observed in defective trichomes of *dis* mutants? Why does the difference between distorted trichomes and normal ones exist only at the late stage of trichome development? Also, tip-growing cells, such as root hairs and pollen tubes, have a strict requirement for actin cytoskeleton. Why do they

display no defective phenotype in the *dis* mutants? More information is needed to put together the elegant interdigitating mechanism of this jigsaw puzzle.

CHAPTER 2
IRREGULAR TRICHOME BRANCH 3 (ITB3) IS A NOVEL REGULATOR OF ACTIN ORGANIZATION

Introduction

The actin cytoskeleton not only mechanically supports mammalian cells for the formation of various shapes, but also generates a driving force for motility of diverse cellular or intracellular events such as cell migration, vesicle trafficking, exocytosis, and endocytosis (Kaksonen et al., 2006). As these events occur, actin cytoskeleton remodeling is active in the assembly of actin filaments at specific subcellular locations (Goley and Welch, 2006). End tracking motors (actoclampins) at the barbed end of growing actin filaments generate the propulsive force for motile events (Dickinson and Purich, 2002; Dickinson et al., 2004).

The dendritic nucleation model of actin polymerization is well established for interpretation of the molecular mechanisms of cell migration (Mullins et al., 1998). Human epithelial fibroblasts and fish epithelial keratocytes are rapidly moving cells. They both form a protrusion called a lamellipodium with a thin layer of cytoplasm containing a dense meshwork of actin filaments. While the keratocyte migrates along the substrate surface, actin and its regulators accumulate in lamellipodia. Actin depolymerizing factor (ADF) at the rear of the leading edge severs and depolymerizes actin filaments and creates new plus ends for the growth of new actin filaments at the front, where the actin nucleator ARP2/3 and its activator WASP/Scar/WAVE polymerize actin filaments (Svitkina and Borisy, 1999). Actoclampin hydrolyzes ATP for free energy and pushes the plasma membrane, propeling the cells forward (Dickinson and Purich, 2002; Dickinson et al., 2004). In mammalian cells, the actin tail, a comet-shaped structure of actin filaments at the rear of rocketing cells, is responsible for driving the pathogenic bacteria *Listeria* and *Shigella* across the host cell cytoplasm using the same molecular mechanism as the dendritic nucleation model (Cameron et al., 2000). Besides these moving cells, vesicle

trafficking also is dependent on the force generated from dynamic actin filaments. For example, endocytic vesicles that budded from the yeast plasma membrane were observed to use a comet tail for rapid trafficking deeper into the cytoplasm (Engqvist-Goldstein et al., 2004). Vesicle formation also needs actin filaments, which participate in coated pit formation, vesicle constriction, and vesicle scission (Yarar et al., 2005). During vesicle formation, the actin filaments assembling at endocytic sites bind to dynamin through cortactin (Merrifield et al., 2002; Merrifield et al., 2005). Dynamin and cortactin are important components of the vesicle scission machinery. Cooperating with dynamin, dendritic actin filaments generate a strong tension at the vesicle neck for vesicle budding (Roux et al., 2006). Cortactin may rearrange actin filaments in specific directions (Kessels and Qualmann, 2005).

Unlike a mammalian cell, the plant cell is surrounded by a rigid cell wall, thus precluding migration. The actin cytoskeleton is implicated in intracellular organelle motility and vesicle trafficking, particular the Golgi apparatus (GA) movement. In mammalian cells, the GA is located close to and around nuclei, but in plant cells, the Golgi carried by myosin, rapidly moves along actin cable tracks throughout the whole cell (Brandizzi et al., 2003; Hawes and Satiat-Jeunemaitre, 2005b; Latijnhouwers et al., 2005). In the tip growing cells of pollen tubes and root hairs, a polarized actin cytoskeleton enables tip-directed organelle and vesicle trafficking. Although pollen tubes and root hairs are two distinct cell types, they share a common morphological form, consisting of a shank, a sub-apical zone, and an apical zone. The gradient of actin filaments are regularly organized in these zones (Cole and Fowler, 2006; Samaj et al., 2006). During pollen tube elongation, thick actin cables are arranged in parallel to the shank and serve as tracks for myosin motors carrying organelles or vesicles to the growing site. In the sub-apical zone, there is a dense fringe of actin filaments, which may promote vesicle formation from

endomembrane organelles (Cole and Fowler, 2006). In the apical zone, abundant vesicles are embedded in the actin filament meshwork, which appears to propel vesicles to the plasma membrane at the growing tip like the comet tail in animal cells (Hepler et al., 2001; Cole and Fowler, 2006; Samaj et al., 2006). Root hairs demonstrate polarized characteristics similar to pollen tubes. Abundant and highly motile endosomes were found in root hairs, and their intracellular motility relied fully on the actin cytoskeleton. At the tip of root hairs, motile F-actin patches have been presumed to propel endosomes to the plasma membrane (Voigt et al., 2005; Samaj et al., 2006).

Although trichome cell expansion is not tip growth, it is a typical anisotropic diffuse growth. It also was found that the actin cytoskeleton plays an important role in trichome morphogenesis (Szymanski et al., 1999; Smith and Oppenheimer, 2005; Hussey et al., 2006). Based on evidence from experiments with actin inhibitor-treated trichomes (Mathur et al., 1999; Szymanski et al., 1999) and characterization of the actin cytoskeleton in distorted trichome mutants (Mathur et al., 2003; Szymanski, 2005; Zhang et al., 2005b), the current hypothesis is that the actin cytoskeleton maintains and coordinates the growth pattern established by microtubules. Microfilaments are expected to play the same role in trichome morphogenesis as in tip growth, which is to deliver specific vesicles containing cargoes, such as cell wall materials to specific sites for local growth (Mathur et al., 2002; Smith and Oppenheimer, 2005). However, during trichome morphogenesis, a gradient of actin filaments was not found. Additionally, microtubules were observed to act as tracks for GA transport. Mutations in *KINESIN-13A* cause defects in the GA transport and result in misshaped trichomes (Lu et al., 2005). Therefore, the precise role of the actin cytoskeleton in anisotropic cell expansion is still not known. In this study, ITB3 was found to be a novel regulator of actin organization in *Arabidopsis* trichome

morphogenesis. Mutations of the *ITB3* gene caused a change in trichome shape. The actin cytoskeleton was aberrantly disorganized in *itb3* mutants. Abundant rings formed by actin cables were observed in the *itb3* mutant, but never in the wild type. ITB3 was found to directly bind to actin depolymerizing factor and inhibits it activity. These results indicated that the actin cytoskeleton plays a crucial role trichome morphogenesis, which provides insight into the role of the actin cytoskeleton in anisotropic cell expansion.

Materials and Methods

Plant Materials and Growth Conditions

The fast neutron induced mutant, *itb3-27,* was isolated in the Rschew (RLD) genetic background (Zhang et al., 2005). The mutants, *itb3-1* (SalK_073071) and *itb3-2* (Salk_015997) are T-DNA insertion mutant alleles in the Columbia (Col) genetic background from the SALK T-DNA Insertion Database (http://signal.salk.edu/cgibin/tdnaexpress). The wild type used for construction of the mapping population is the Landsberg *erecta* (Ler) ecotype.

Seeds were sown on a soilless potting medium, Fafard 2 Mix (Conrad Fafard, Inc., Agawam, MA). Seedlings were grown at 24°C under constant light, provided by 40W cool white fluorescent tubes. Plants were watered with PGP nutrient solution (Pollock and Oppenheimer, 1999) every two weeks.

Positional Cloning of *ITB3*

The mapping population for cloning the *ITB3* gene was generated as described by Zhang et al. (2005). Phenotypically *itb3* mutant plants were selected from the F2 population. From each selected plant, one of the cotyledons was removed for DNA extraction using the RED Extract-N-Amp Plant PCR Kit (Sigma-Aldrich, St. Louis, MO). The isolated DNA was used to map the *itb3* mutation relative to simple sequence length polymorphisms (SSLPs) (Bell and Ecker, 1994).

After the *itb3* mutation was mapped to a narrow region, the expected large deletion was detected by PCR.

Plasmid Construction

For expression of *ITB3*, the *ITB3* gene, which covers the 113-bp 5' UTR, the 501-bp coding sequence and the 277-bp 3' UTR was amplified using genomic DNA from RLD wild type plants as the template using the appropriate primer pair (Table 2-1). The 891-bp PCR product was cloned into pENTR1A (Invitrogen, Carlsbad, CA) using the *BamH*I and *EcoR*I sites, and transferred into either pAM-PAT-GW (Bekir Ulker, Max Planck Institute for Plant Breeding, Cologne, Germany) for expression from the 35S promoter or pCK86 (Arp Schnittger, Max Planck Institute for Plant Breeding) for expression from the GL2 promoter through an LR recombination. To localize ITB3, a *35S:ITB3-GFP* construct was made. The 498-bp *ITB3* open reading frame was amplified using primer pairs that introduced *Nco*I sites at both ends of the PCR product. The digested PCR product was cloned into the *Nco*I site of the GFP fusion vector, pAVA319 (von Arnim et al., 1998). The resulting gene fusion was liberated by digestion with *EcoR*I and *Not*I and transferred to pENTR1A through the same cut sites. Finally it was transferred into the destination vectors, either pAM-PAT-GW or pCK86 as in the previous constructs. Through the same strategy, for FRET assays, the *35S:ITB3CFP*, *35S:ITB3L4CFP*, and *35S:ADF3YFP* were constructed with pAVA574 containing CFP and pAVA 554 containing YFP. To produce the ITB3 protein, the 501-bp coding sequence of *ITB3* was cloned into pET41 Ek/LIC, pET15b through *Nde*I and *BamH*I or pET41a through *Mfe*I depending on the specific tag needed (Novagen, Madison, WI). For pET41a-ITB3-GFP, the PCR products were amplified using primers containing *EcoR*I sites at both ends of ITB3-GFP.

To construct pDBLeu-ITB3, used as bait for the yeast two-hybrid screen, the 501 bp coding sequence of *ITB3* was cloned into pDBLeu with kanamycin resistance (provided by Wen-

Yuan Song at the University of Florida) through *Not*I and *Sal*I sites. All PCR products were sequenced by the Interdisciplinary Center for Biotechnology Research (ICBR) at the University of Florida to ensure no mutations were introduced.

RNA Extraction and RT-PCR

Total RNA was extracted from six-week-old Col wild-type plants using the RNeasy Plant Mini Kit (Qiagen Inc. Valencia, CA) according to the manufacturer's instructions. The full length *ITB3* cDNA was amplified, following instructions for the cMaster RT plus PCR System (Eppendorf AG, Hamburg, Germany). First-strand DNA synthesis was primed using oligo $(dT)_{20}$. The cDNA was amplified using the specific primers for *ITB3* (see Table 1). The PCR products were sequenced by ICBR at the University of Florida.

Plant Transformation

For ITB3 subcellular localization, the *35S:ITB3-GFP* constructs were transferred into onion epidermal cells by particle bombardment, using the Biolistic PDS-1000/He Particle Delivery System (Bio-Rad, Richmond, CA), and the transformation protocol supplied by the manufacturer was followed. A total of 5 μL of DNA (1μg/μL) was precipitated on 3 mg gold microcarriers 0.6 μm in diameter (Bio-Rad), by adding 50 μL of 2.5 M $CaCl_2$ and 20 μL 0.1 M of spermidine. After the precipitated DNA was washed once with 140 μL 70% and once with 100% ethanol, it was resuspended in 50 μL of 100% ethanol. 10 μL of this solution was spread on one rupture disk labeled with a burst pressure of 1,100 psi. Square tissue sections approximately 2 x 2 cm were cut from onions and placed on Murashige and Skoog (MS) solid medium for bombardment. Fluorescence was visualized after 36 hours incubation at room temperature in darkness.

The constructs of *35S:ITB3*, *GL2:ITB3*, *35S:ITB3-GFP*, *GL2:ITB3-GFP*, and *35S:ITB3-CFP* were transferred into *itb3-27* mutants by the floral dip method (Clough and Bent, 1998).

35S:ITB3L4CFP was transferred into the *itb3l-4* mutant, *35S:ADF3YFP* was transferred into *adf3* mutants. The transgenic plants were selected using a 1000X dilution of Finale (Farnam Companies Inc, Phoenix, AZ) with 5.78% glufosinate-ammonium.

Yeast Two-hybrid Assays

The protocol for the yeast two-hybrid assay was described by (Ding et al., 2004). The bait construct pDBLeu-ITB3 was transferred into the yeast strain CG1945 through the Leu selection marker using the Yeast Transformation Kit (Sigma, St. Louis, MO) according to the manufacturer's instructions. The prey, pPC86-cDNA, was a rice cDNA library, (provided by Wen-Yuan Song at the University of Florida) with Trp as the selection marker in yeast strain Y187. The mated cells of CG1945 and Y187 were spread on the YPD medium without Trp, Leu, and His for positive selection. The plasmids were isolated from the grown yeast colonies with Zymoprep Yeast Plasmid Miniprep (Zymoprep, Orange, CA 92867) and transferred into XL2-Blue Ultracompetent Cells (Stratagene, LaJolla, CA). The genes of interest were sequenced using plasmid DNA from individual bacterial colonies.

Protein Isolation

The constructs, pET41 EK/LIC-ITB3, pET15b-ITB3, and pET41a-ITB3, were transferred into the host cell BL21 (DE3) (Novagen, Madison, WI) through chemical transformation for ITB3 expression. The single colony with the target construct was inoculated into 500 ml Overnight Express Instant TB Medium (Novagen, Madison, WI) for overnight culture. The harvested host cells were lysed by 1x FasBreak Cell Lysis Reagent (Promega, Madison, WI). For pET15b-ITB3 with the 6xHis-tag, HisLink Protein Purification Resin (Promega) was used for His-tagged ITB3 binding. For pGEX-profilin, pGEX-ADF1 (provided by C. Staiger at Purdue University) and pET41-ITB3, which the proteins of interest were tagged with GST, the GST Binding Resin was used for the protein purification following the manufacturer's instructions for

the BugBuster GST·Bind Purification Kit (Novagen). The 6xHis-tag was removed from the fusion ITB3 with a Thrombin Cleavage Capture Kit (Novagen) and the GST tag was removed using an Enterokinase Cleavage Capture Kit (Novagen) following the manufacturer's instructions. The concentration of the purified proteins was measured using a DC Protein Assay Kit (Bio-Rad) following the manufacturer's instructions.

Pull-down Assay

The purified proteins in 1x PBS were diluted to a 1µg/µl concentration with 1x PBS. The binding reaction was done in 100 µl of binding buffer, which contained 5 mM Tris-HCl, 100 mM KCl, 1 mM MgCl, 1 mM $CaCl_2$, 50 ng/µl 6xHis-ITB3, and 100 ng/µl ADF1 or profilin or BSA, pH 7.5. The reaction was allowed to proceed at room temperature for 80 minutes. After the binding was completed, 12.0 µl of 10x nickel resin binding buffer containing 1 M HEPES and 100 mM imidazole (pH 7.5) and 8.0 µl of 50% HisLink Protein Purification Resin (Promega) were added to the binding buffer. The reaction tubes were rotated at 12 rpm at room temperature for 60 min. The resin was spun down and washed three times for 10 minutes, with washing buffer containing 100 mM HEPES, 10 mM imidazole, and 0.1% NP-40. 3.0 µl NuPAGE LDS Sample Buffer (4x) (Invitrogen, Carlsbad, CA) was added to the pellet resin suspension (~10.0 µl). After a 5 minute heating at 95ºC, the samples were loaded into NuPAGE 12% Bis-Tris Gel (Invitrogen, Carlsbad, CA) for protein separation.

Morphological Analysis

SALK lines (SALK_073071, 015997, 019320, 008148, 001114, 001117, and 019328), which were ordered from *Arabidopsis* Biological Resource Center (The Ohio State University, Columbus, OH) were examined under a dissecting microscope, and lines SALK_073071 and 015997 showed segregation of plants with the *itb3* trichome phenotype.

Immunostaining of the Actin and Microtubule Cytoskeletons

The immunostaining protocol for actin filaments and microtubules, using specific antibodies against tubulin or actin, were described in our previous studies (Zhang and Oppenheimer, 2004; Zhang et al., 2005b)

Microscopy

Fluorescent images were collected with a Zeiss Axiocam HRm camera mounted on a Zeiss Axioplan 2 Imaging microscope (Jena, Germany). The following filter sets were used to collect fluorescent images: red fluorescence was obtained with Zeiss filter set 20 (excitation, 546/12; dichroic, 560 LP; emission, 575 to 640), green fluorescence was obtained with Zeiss filter set 10 (excitation, 450 to 490; dichroic, 510 LP; emission, 515 to 565). Optical sections were collected using the Zeiss Apotome and Axiovision 4.1 software. Light micrographs were collected with a Zeiss Axiocam MRc5 camera mounted on a Zeiss Stemi SV11 dissecting microscope. For scanning electron microscopy (SEM), previously described methods were used (Luo and Oppenheimer, 1999).

Double Mutant Construction

The double mutants were selected from individual F2 plants. The *itb3-27* mutant was crossed with the T-DNA insertion lines, *itb3l-4* and *adf3*. The selected putative double mutants were self pollinated. These F3 individuals were crossed with their original parents to check for mutations through exhibition of their specific mutant phenotypes.

Results

Cloning of the *ITB3* Gene

The mutation in the *itb3-27* mutant was mapped between the markers s2 (to BAC clone T5A14) and s3 (to BAC clone T30E16) on chromosome I (Zhang et al., 2005a). To clone the *ITB3* gene, we further mapped the *itb3* mutation relative to simple sequence length

polymorphism (SSLP) markers (Bell and Ecker, 1994) to BAC clone F25P12 (Figure 2-1). Because the *itb3-27* allele was isolated from a fast neutron mutagenized population, we screened BAC clone F25P12 for deletions by amplifying short regions spaced approximately every 1000 bp along F25P12. An approximately 42-kb deletion was found between the 92.4 and 134.4 kb positions in F25P12, but the deletion did not occur in wild type. In the deleted region, there were 16 putative genes (Figure 2-1).

The SALK T-DNA insertion database was searched for insertions in these genes, and the resultant insertion lines (Alonso and Stepanova, 2003) were screened for plants showing the *itb3* trichome phenotype. Salk_073071 segregated plants that had strong *itb3* phenotypes; Salk_15997 line also segregated plants with a weak *itb3* trichome phenotype. These three lines all had a T-DNA insertion in At1g56580. The *itb3-27* mutant was crossed to these three lines for complementation tests. The results indicated that the insertion mutations in the three lines were allelic to *itb3* (data not shown), which demonstrated that *ITB3* is At1g56580.

The trichomes on the leaves of all three *itb3* mutant alleles fit the criterion set for irregular trichome branching, where at least one branch that is shorter than the others in length, or at least two branch points positioned separately on the stalk. Additionally, the trichome size and branch number of *itb3* mutants decreased when compared with wild type (Zhang et al., 2005a). To determine why these defects occur in *itb3* mutants, we examined the cytoskeletons in *itb3* and wild type trichomes by immunostaining with antibodies against actin and tubulin. Compared to wild type, the microtubules in *itb3* trichomes showed no apparent difference (data not shown), but the actin filaments in *itb3* trichomes were disorganized (Figure 2-2). In trichomes of developmental stage 2-3, the actin cables in *itb3* mutants accumulated near the bottom of the stalk (Figure 2-2C), whereas in wild type more actin cables were distributed close to the top of

the trichome (Figure 2-2B). At stage 3, the disorganization of actin cables in *itb3* mutants was more pronounced. Most of the actin cables were parallel to the long axis of the stalk in the *itb3* trichomes (Figure 2-2F), whereas in wild type actin cables were more abundant in the region between branches (Figure 2-2E). At stage 4, more disorganized actin cables were arranged under the trichome branch points in the *itb3* mutant (Figures 2-2I, 2-3A) compared with wild type (Figures 2-2H, 2-3B). The greatest difference was the formation of actin rings in *itb3* mutants after stage 3, but these actin rings were rarely found in wild type (Figures 2-3I, 2-4).

ITB3 is a Plant-specific Gene

ITB3 encodes an unknown protein with a mass of about 18 KD and a pI of 6.64. No signal peptide or other known motif was found in the ITB3 protein sequence. Using ITB3 to search the complete *Arabidopsis* genome, we found a family consisting of 22 members. This family can be grouped into two distinct clades: the *ITB3-Like* (*AtITB3L-02-05*) clade in the green square and *ITB3 Related* (*AtITB3R-01-13*) clade in the yellow square, with 100% bootstrap support for their occurrence (Figure 2-5). The search of all available genomes of other organisms indicated that *ITB3* is a plant-specific gene that is present in all land plants, including moss (Figure 2-6).

ITB3 Over-Expression Did Not Generate Novel Phenotypes

Over-expression of *ITB3* using the 35S promoter completely complemented the defective trichome phenotype and no additional phenotypes were found. Over-expression of *ITB3* with the same construct in wild type did not display any visible changes in the trichome shape or other phenotypes (data not shown).

ITB3 Has No Specific Subcellular Location

When the *ITB3-GFP* fusion construct was transferred into onion epidermal cells through particle bombardment, the GFP signal was located in the cytoplasm and nucleus of transformed cells and was both indistinguishable from that of the control of GFP alone and remarkably

different from the control of the nucleus-localized GFP (Figure 2-7). The same gene fusion was used to stably transform *itb3* mutants. The signal distribution in the trichomes was the same as that in the transgenic onion epidermal cells. Additionally, the *itb3* mutant trichomes were rescued into wild type trichomes (data not shown), which indicated that the ITB3-GFP carried out normal functions in living cells.

ITB3 Interacts With ADF3 in Yeast

To search for ITB3 interactors, a yeast two-hybrid screen was performed using a rice cDNA library as the prey and ITB3 as the bait. On the plate without Trp, the yeast containing the bait plasmid, pDBLeu-ITB3, grew, but those containing the prey plasmids, pPC86-ADF3 and DCD, did not. On the plate without Leu, the yeast containing the prey plasmids pPC86-ADF3 and DCD grew, but those containing the bait plasmid, pDBLeu-ITB3, did not. On the plate lacking both Trp and Leu, the yeast with both bait and prey plasmids grew. Additionally, this yeast also grew on the plate without Trp, Leu, and His (Figure 2-8). This result indicated that His was produced by transcription activation through ADF3 or DCD bound to ITB3. Therefore, rice ADF3 and DCD proteins are able to interact with *Arabidopsis* ITB3 in yeast cells.

ITB3 Directly Binds with ADF3 in Vitro

To further confirm the interaction between ITB3 and ADF3, we carried out a pull down experiment. The purified His-tagged ITB3 pulled down GST-tagged AtADF1 in vitro, but did not pull down GST-tagged profilin (Figure 2-9). This data further supported the results from the yeast two-hybrid assay.

The Trichomes are Defective in the Mutants of *adf*, *itb3l-4* and Their Double Mutants

To search for additional genetic evidence that ADF is involved with ITB3 in controlling trichome development, the knockout lines of *ADF* and other *ITB3* family members were examined for trichome phenotypes. A T-DNA insertion in *ITB3L-4* gave rise to trichomes with

fewer numbers of branches compared to wildtype. Plants homozygous for a T-DNA insertion in *ADF3* showed caused an increase in trichome branch number (Figure 2-10).

Double mutants of *adf3* and *itb3* displayed trichomes with more branches than *itb3* mutants and fewer branches than *adf3* mutants. The mutation of *ITB3* is additive to the mutation of *ADF*. However, double mutants of *adf3* and *itb3l-4* displayed trichomes with fewer branches than their parents. Double mutants of *itb3* and *itb3l-4* had much more severe decreases in branch number compared to either parent. Therefore, these two mutations appear to be synergistic in controlling trichome branching.

The transgenic plants of the *itb3-27* mutants with *35S*:*ITB3GFP* or *35S*:*ITB3CFP* displayed the wild-type trichome phenotype. However, the transgenic plants of either the *itb3l-4* mutants with *35S*:*ITB3L4CFP* or the *adf3* mutants with *35S*:*ADF3YFP* exhibited mutant trichome phenotypes. These results led us to devise the constructs that contain their own endogenous promoters for driving the fusion gene expression in the future (data not shown).

Discussion

Disruption of Actin Cytoskeleton Organization Leads to Misshapen Trichomes

Pharmacological disruption of actin filaments with actin-specific drugs severely affects trichome morphogenesis and changes trichome shapes (Mathur et al., 1999; Szymanski et al., 1999). When the *Arabidopsis* trichomes were treated with the actin polymerization inhibitor Latrunculin B, no effect was found at the initial developmental stages, but after the branching events, the trichome cells rapidly expand. The inappropriately extended trichomes generate distortion, shortened branches, and separate branch points. Genetic disruption of the actin filament dynamics through loss-of-function mutations of the distorted class of *Arabidopsis* genes gives rise to the aberrant trichome phenotypes, similar to those in the pharmacological experiments. The distorted class genes encode subunits of the Arp2/3 complex and its activation

complex. Mutations in the distorted class genes disrupt actin filament dynamics, which causes an altered distribution of cortical actin cables (Mathur et al., 2003). The *dis* mutants display changes of overall trichome shape, a reduction of branch length, and an increase in the distance between two branch points (Basu et al., 2005; Zhang et al., 2005b). These changes are similar to the trichome defects seen in *itb3* mutants. Although the distortion defect was considered as the criterion for mutations in the DIS class genes (Hulskamp et al., 1994), it disappears in some genetic backgrounds. For example, the *itb1-1* allele, (*dis3*) does not display the distorted trichomes in the Wassilewskija (WS) genetic background. However, this mutant still exhibits the *itb* trichomes (Zhang et al., 2005b). In *itb3* mutant trichomes, the actin cytoskeleton is severely disorganized. Therefore, our results strongly support the idea that the actin cytoskeleton has a crucial role in the regulation of trichome morphogenesis.

The Precise Role of the Actin Cytoskeleton in Trichome Morphogenesis

A wealth of cellular observations indicates that a fine actin filament meshwork or diffuse actin patches promote cell expansion, whereas dense actin bundles or actin cables serve as structural scaffolds or tracks for myosin-based motors to transport organelles and vesicles. The precise role of actin filaments in cell expansion is dependent on actin types and subcellular locations. Our results show that the fine actin filament meshwork is abundant close to the rapidly growing sites of normal trichomes. However, at rapid growth stages, the *itb3* mutant trichomes did not show this meshwork. We hypothesize that these fine actin meshworks promote cell expansion. Similar actin patches have been observed in other cell types, such as root hairs (Baluska et al., 2000) and elongating lobes of epidermal pavement cells (Fu et al., 2005). Although dense actin cables were observed in both wild type and *itb3* mutants, many of the actin cables formed rings in *itb3* mutants. These rings are unlikely to be normal tracks for vesicles. It is conceivable that the rings caused reduced and misdirected delivery of vesicles to the cell

cortex, ultimately resulting reduced growth. This might be a reason why the trichome size of *itb3* mutants is reduced when compared to normal trichomes.

Actin Filament Reorganization Is Required for Cell Expansion

In response to internal and external signals for cell expansion Actin filaments are rapidly remodeled by multiple regulators. Some of the regulators modulate the size and activity of the monomeric actin pool through interaction with actin monomers. Others change the disassembly property of filamentous actin through binding to the filament sides (Staiger and Blanchoin, 2006). Actin and its regulators establish a complex and adjustable system for plant cells in various environments. When the delicate balance is impaired by loss of function of some regulators, unusual consequences occur in actin assembly and cellular architecture. Additionally, recent findings suggest that a class-specific interaction of actin with its regulators exist for proper remolding of the actin filaments (Kandasamy et al., 2007). ADF is a key regulator of actin. It binds with both actin monomers and filaments. ADF severs filaments, thereby generating new barbed ends for subunit addition (Staiger and Blanchoin, 2006). ADF severing activity is regulated by profilin (Didry et al., 1998), ACP1 (Bertling et al., 2004; Chaudhry et al., 2007), AIP1 (Okada et al., 2002; Mohri et al., 2006), phosphorylation (Huang et al., 2006), and pH (Gungabissoon et al., 2001; Chen et al., 2002). Our results show that plant ADF binds with ITB3. Additionally, ADF activity is inhibited by ITB3 binding (Oppenheimer and Grey, unpublished data). Our results provide new insight into differences in actin filament dynamics between plant cells and animal cells, which in plant cells is the high ratio of monomeric to filamentous actin (Snowman et al., 2002; Wang et al., 2005a).

ITB3 is a Plant-Specific Regulator of Actin Organization

A search of all known organisms shows ITB3 is present only in the plant kingdom. Although actin and ADF both are conserved in all eukaryotic cells, only 31 of the 67 animal

actin-binding proteins appear to be conserved in plants (Hussey et al., 2002). In addition, plants have a higher percentage of monomeric actin in the total actin pool (Gibbon et al., 1999; Snowman et al., 2002; Wang et al., 2005a). Therefore, plant-specific actin regulators like ITB3 may provide the functions of the animal proteins that are missing from plants.

Future Perspectives

Plant cell shapes are controlled by the cytoskeleton. Our data show that Irregular Trichome Branch 3 (ITB3) is a novel regulator of actin cytoskeleton organization. Mutations in *ITB3* caused disorganization of the actin cytoskeleton in trichomes resulting in an altered trichome shape. We showed that ITB3 interacts with and negatively regulates the function of actin depolymerizing factor (ADF) *in vitro*. However, two important questions remain: First, how do ITB3 and ADF work together to regulate actin organization, and second, how does this interaction lead to site-specific cell expansion to generate normal trichome shape.

To answer the first question, we need additional information on the molecular mechanism of ITB3 interaction with ADF. For example, does ITB3 regulate ADF binding to actin filaments? Does ITB3 regulate ADF phosphorylation or dephosphorylation? To address these questions, we can use actin depolymerization assays and actin filament-severing assays with purified ADF, in the presence or absence of ITB3. In vitro polymerized actin filaments can be labeled by including pyrene-labeled actin monomers in the assay, and fluorescence microscopy can be used to visualize the actin filaments. The kinetics of F-actin depolymerization can be monitored by continuous pyrene fluorescence measurements by using a Cary Eclipse fluorescence spectrophotometer (Yokata et al., 2005). Although we have shown convincingly that ITB3 interacts with ADF *in vitro*, it is important to confirm this interaction *in planta*. To this end, Förster resonance energy transfer" (FRET) can be used. An *ITB3-CYP* fusion can be used as the donor; an *ADF-YPF* fusion can be used as the acceptor. The gene fusions are transferred into

Arabidopsis leaf epidermal cells through biolistic bombardment, and the FRET efficiency can be determined. The higher the FRET efficiency, the higher the number of ITB3 and ADF interactions.

Also, we know that both ADF and ITB3 are members of moderately sized families in Arabidopsis. It is possible that there are family member specific interactions between ITB3 and ADF proteins. Plant ADF family members are grouped into the vegetative and reproductive ADFs based on expression pattern. There are sequence and activity differences between the two groups of ADFs. The ITB3 family has been divided into two groups based on protein sequence differences. Can ITB3 family members also be organized into vegetative and reproductive groups? This can be done by examining the expression of the ITB3 family members in microarray data sets. To address the binding of specific ITB3 members with specific ADF members, two approaches can be applied. The first approach is to determine expression patterns of *ITB3* and *ADF* family members in trichomes using *in situ* hybridization. If two members are co-expressed in specific tissues or organs, they may be binding partners. The second approach is to use the yeast two-hybrid assay. Putative positives from this assay can be confirmed with pull down assays *in vitro*, and *in planta* using FRET analysis.

Table 2-1. Primers used in this study

Primer name	Sequence (5' – 3')	Used for*
F6D8-25F	CTACATTTGTTCATATACAGGGAGTTC	RLD 134/Ler 109
F6D8-25R	GCCGAGATATACTTGGATCATACTG	
F12P19-26F	CTGGAAATATCTGCGAAGTGGAA	RLD 119/Ler 93
F12P19-26R	CATGAACTGTTTGTGCATCTCTG	
F5I14-55F	CGGATGCGGTTATATAAATAGAGA	RLD 231/Ler 176
F5I14-55R	CCCTCCCTTTTCTTGCTACAAA	
T30E16-57F	ACACTCTTTACTGGAAGATGCAA	RLD 138/Ler 81
T30E16-57R	AACACACCCATGCAAGTGAA	
F7F22-17F	GCTCACACTTTCCAATGGTGT	RLD 82/Ler 95
F7F22-17R	CCTTGGAAGCGTAGACCCA	
F25P12-14F	GCACGATCCTATGAGTTAGCA	RLD 101/Ler 87
F25P12-14R	TTACACGCGAGGAATGAAGA	
F23H11-39F	TTTGATGGAGATTTTGCTGATT	RLD 119/Ler 80
F23H22-39R	ACCATTGACAGTGGAGCTACATT	
T14G11-12F	TTTGGATGGATTTGTGCGTG	RLD 81/Ler 69
T14G11-12R	CGATGAGGTCAATCCTAAAGATCAG	
T5A14-14F	GACCAATACAGAGATACAAAGCAA	RLD 89/Ler 103
T5A14-14R	TCCGCTAACTTATCCGACAA	
T6H22-11F	GACAATTTTCTTCTATATAAGGATGTGG	RLD 127/Ler 116
T6H22-11R	GGTCATCCTTGCAAGATATCAA	
ITB3enF	GGGTGATTTCATACCACACCACC	ITB3 over expression
ITB3enR	TGGCTATGAAGTAACCGCTGAGAT	
ITB3GSTpF	ATGGGTTTGG TTACAGATGAAGTG	GST-ITB3 protein
ITB3GSTpR	AGCATCTGTGACTGCAACAGCTTC	
ITB3HISpF	ATGGGTTTGGTTACAGATGAAGTGAGAGC	His-tagged ITB3
ITB3HISpR	CTAAGCATCTGTGACTGCAACAGC	

*Note: A majority of primers are used for *ITB3* positional cloning, for example, RLD 134/Ler 109 is a SSLP marker that has PCR products of 134 bp in RLD wild type and 109 bp in Ler wild type.

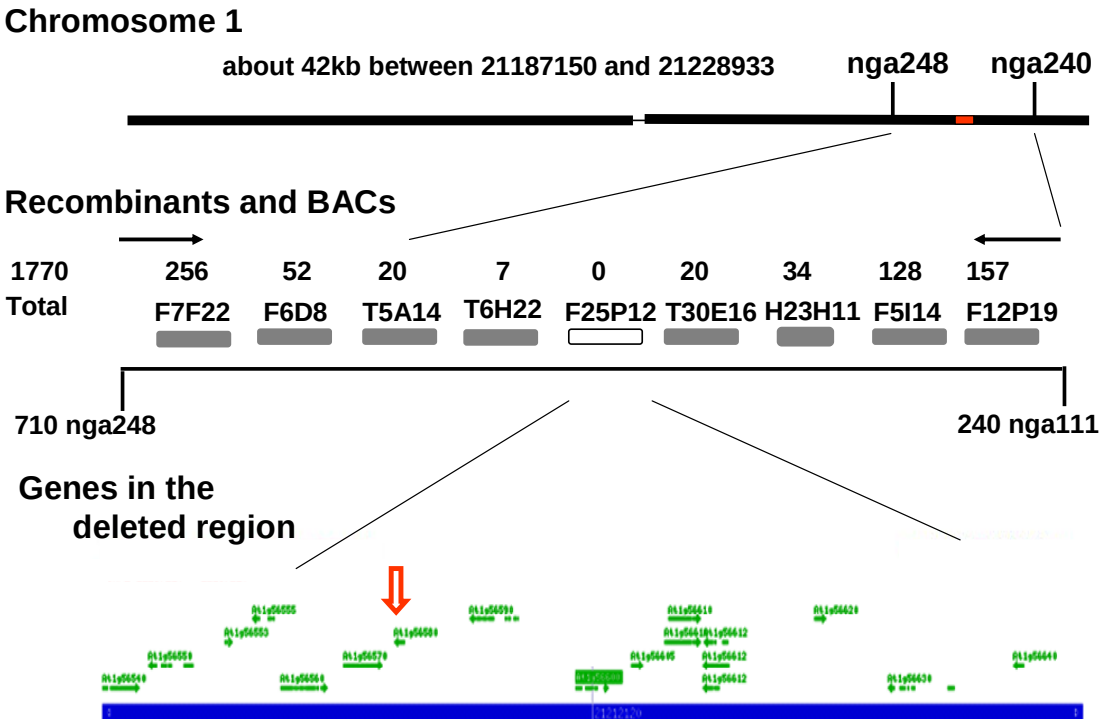

Figure 2-1. Positional cloning of *ITB3*. The *itb3* mutation was mapped near SSLP marker ATPase on chromosome 1. Additional molecular markers were used to map the *itb3* mutation to BAC clone F25P12. The numbers of recombinants (out of 1770 chromatids screened) are given above BAC clones. The locations of all putative genes on BAC clone F25P12 are listed. The numbers inside the flags above specific genes are numbers of recombinants for that marker. *ITB3* is indicated by the vertical arrow.

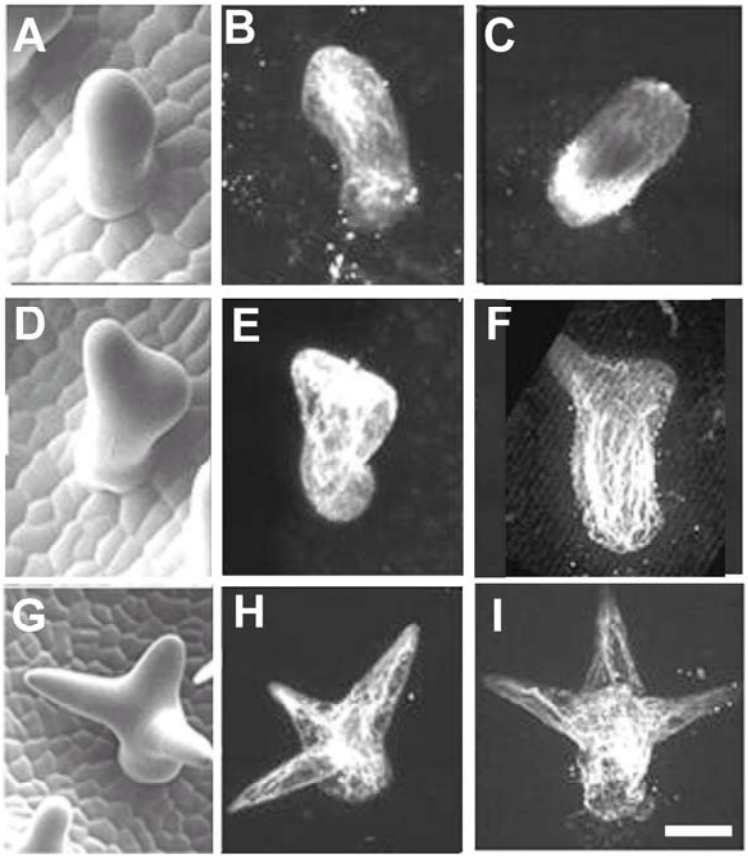

Figure 2-2. Actin cytoskeleton is disorganized in the *itb3* mutant. (A), (D), and (G) are wild-type trichomes showing different developmental stages through scanning electronic microscope (SEM). (B), (E), and (H) are wild-type trichomes showing the normal organization of actin cytoskeleton with the identical developmental stages with (A), (D) and (G). (C), (F), and (I) are the *itb3* mutant trichomes at the same developmental stages as wild type showing disorganization of the actin cytoskeleton through immunostaining and fluorescent microscopy. Bar = 100 μm in all images.

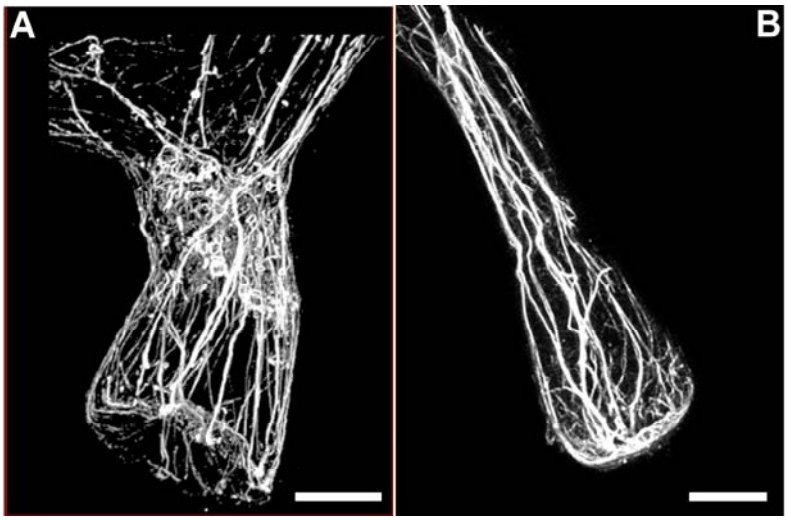

Figure 2-3. Actin cable organization in the stalk of trichomes. (A) The *itb3* mutant trichome stalks showing clear differences in actin organization compared to the wild type in (B). Bar = 10 μm.

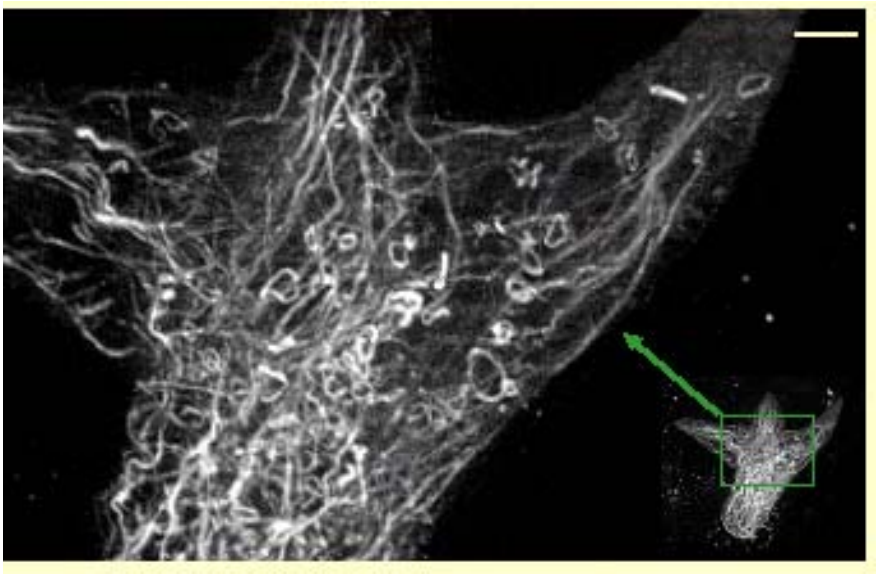

Figure 2-4. Actin rings in the *itb3* mutant. Bar = 5 μm

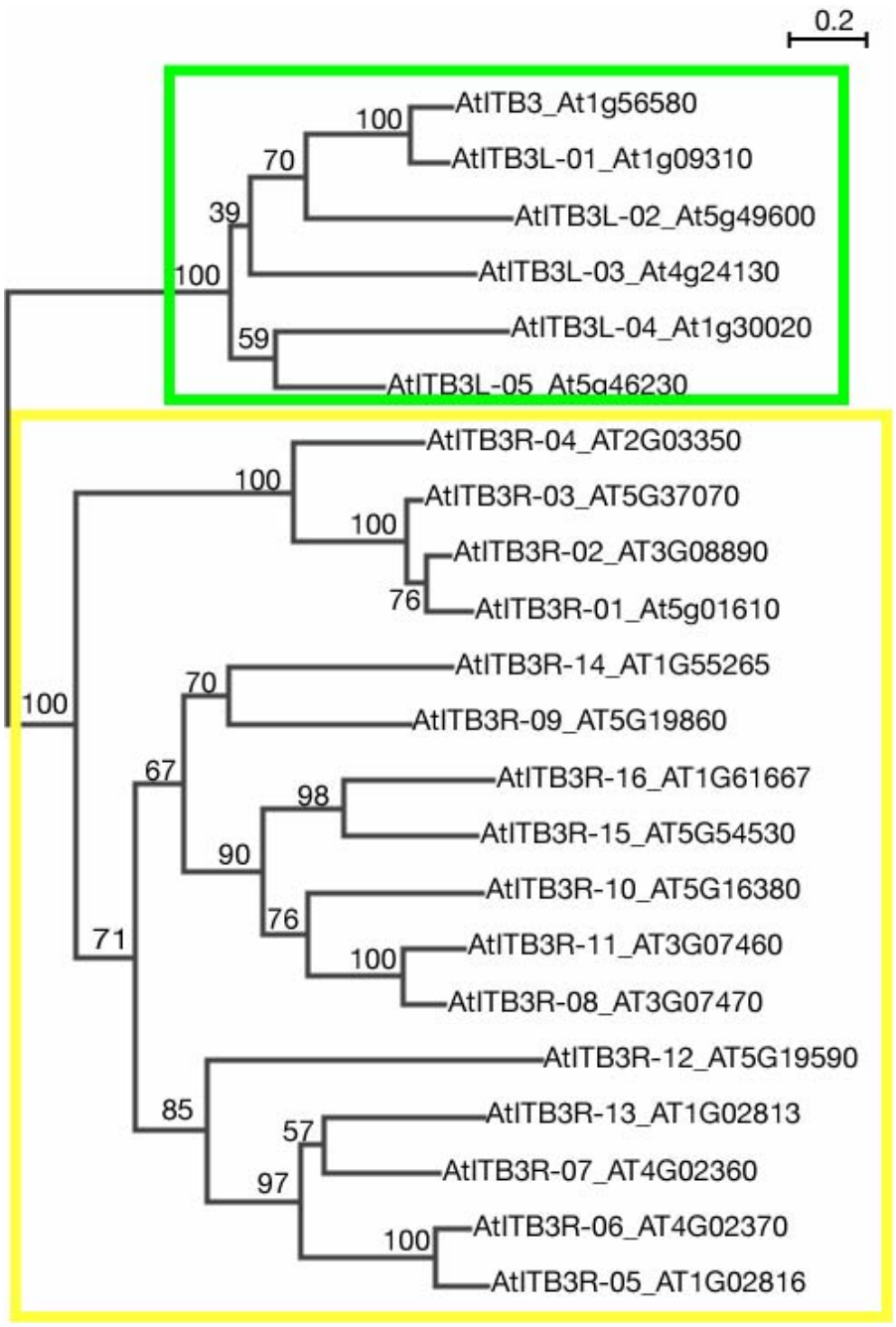

Figure 2-5. Phylogenic tree of the Arabidopsis ITB3 family members

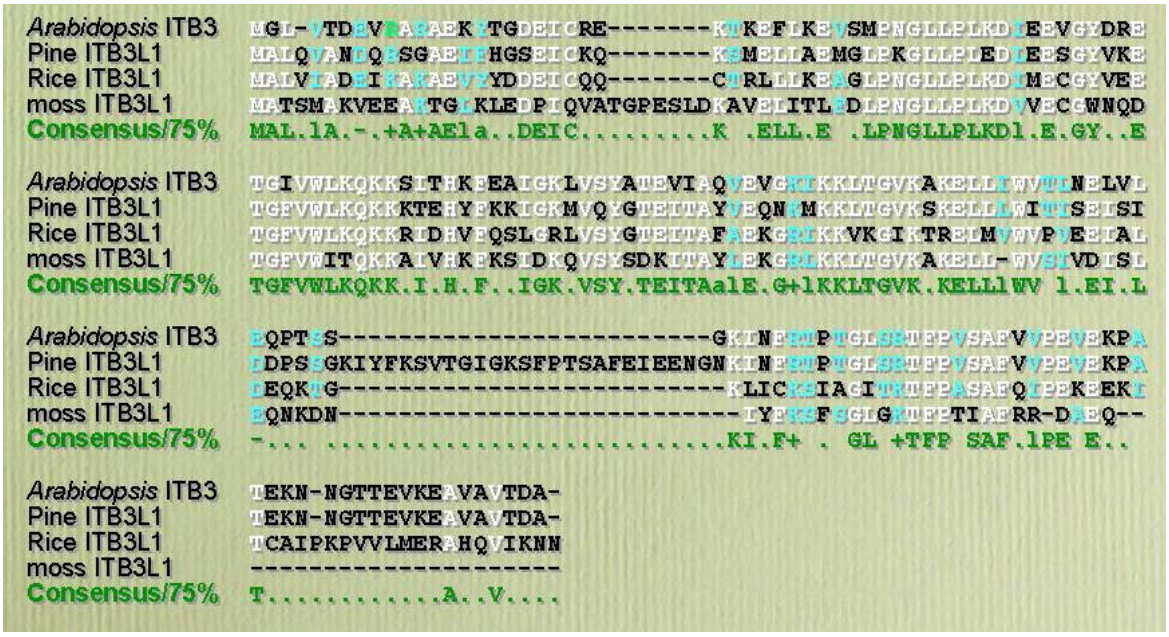

Figure 2-6. Alignment of ITB3 protein sequence with its homologs in other plants

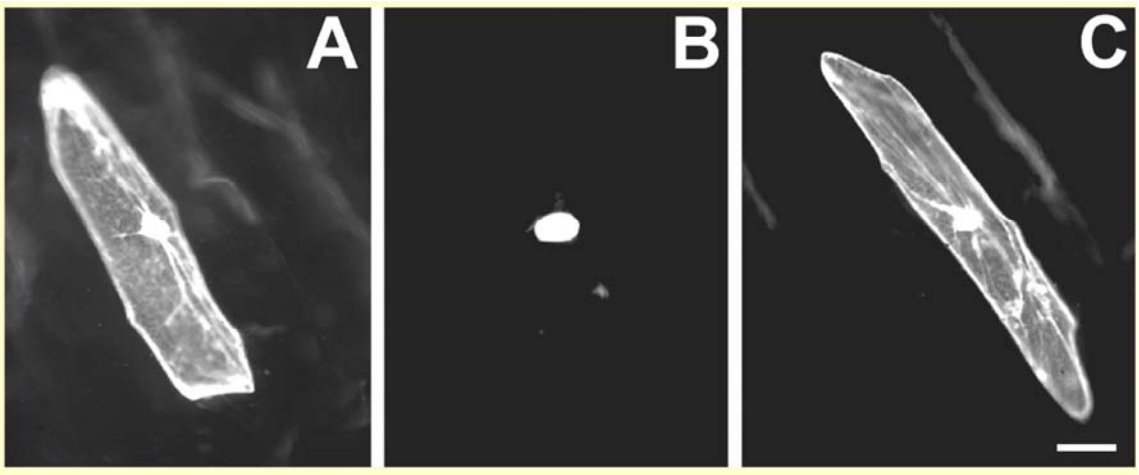

Figure 2-7. ITB3-GFP is not specifically localized to any subcellular structure in transformed onion epidermal cells. (A): GFP alone; (B): GFP-NIa in nucleus; (C): ITB3-GFP. Bar = 5 μm

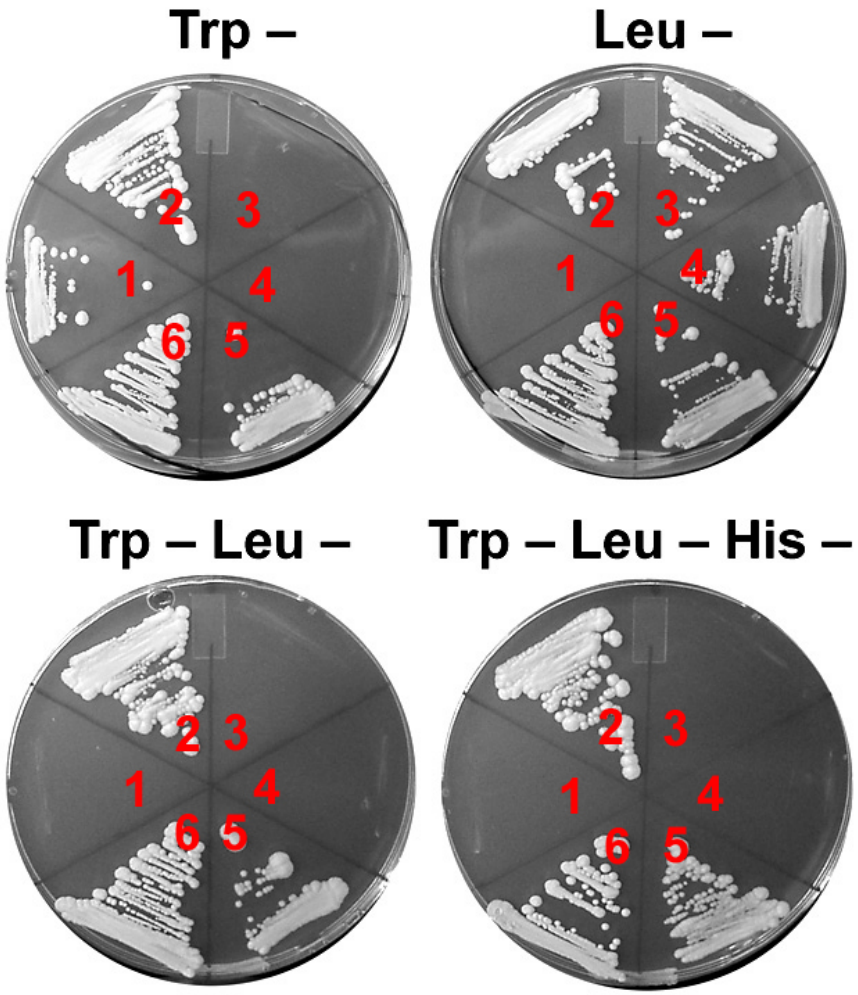

Figure 2-8. Yeast two-hybrid screen for ITB3 interactors. (1): Bait ITB3; (2): bait ITB3 and prey ADF; (3): prey ADF; (4): pre DCD; (5): bait ITB3 and prey DCD; (6): positive control.

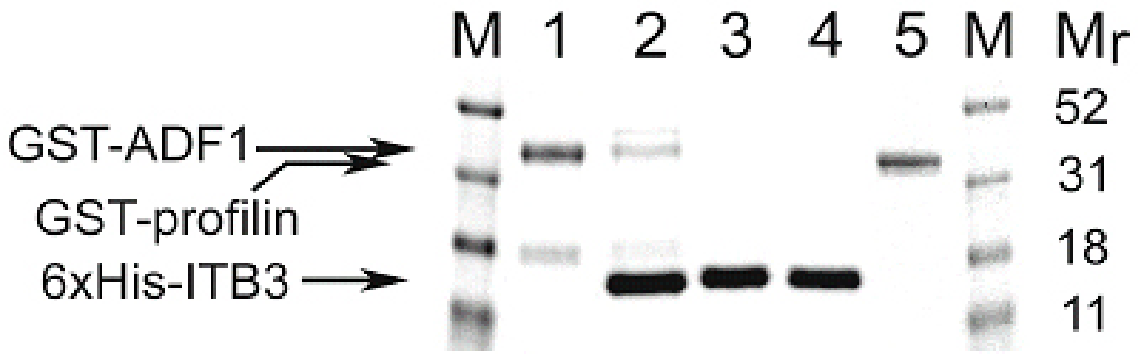

Figure 2-9. ITB3 directly interacts with ADF in vitro. (1): GST-ADF; (2): the GST-ADF is pulled down by His-ITB3; (3): the GST-profilin fails to be pulled down by His-ITB3; (4) His-ITB3 alone; (5): GST-profilin alone.

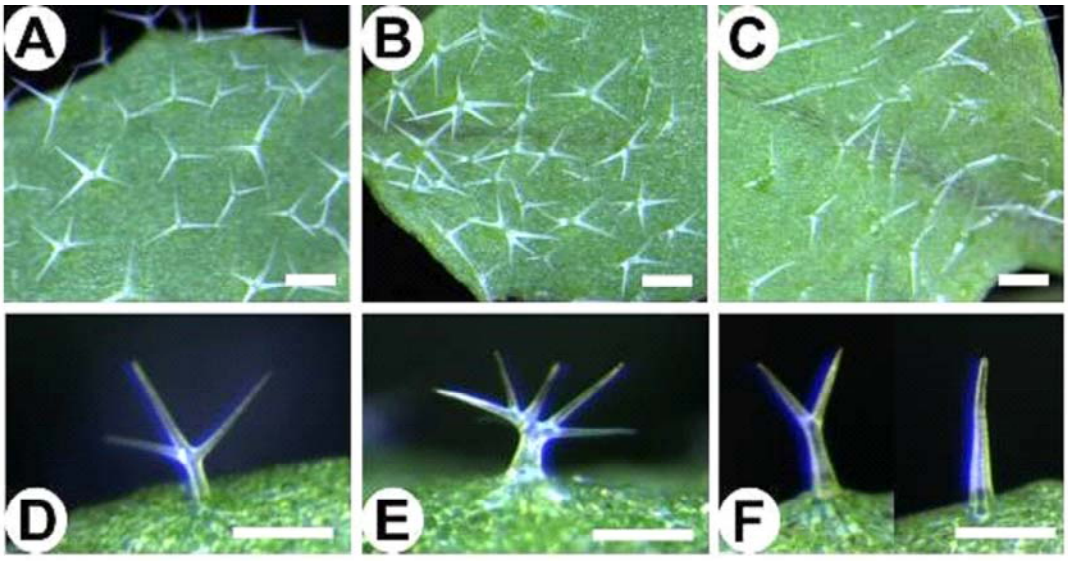

Figure 2-10. Trichome shapes are defective in *adf3* and *itb3l-4* mutants. (A) and (D): Col wild type; (B) and (E): *adf3*; (C) and (F): *itb3l-4*. Bar = 100 μm

CHAPTER 3
IRREGULAR TRICHOME BRANCH 2 (ITB2) IS A PUTATIVE AMINOPHOSPHOLIPID TRANSLOCASE THAT REGULATES TRICHOME BRANCH ELONGATION IN ARABIDOPSIS

Introduction

Lipids are the major components of all eukaryotic membranes. They mainly include phospholipids, sphingolipids, and sterols, which are distributed asymmetrically within bilayer membranes. Phospholipids form the main homogenous planar architecture, but sphingolipids and sterols are rich in microdomains called lipid shells/rafts, which theoretically float freely in the more fluid surrounding membranes analogous to the so-called ‘‘liquid disordered’’ phase. Distinct lipids also specifically localize the two leaflets of membranes. In general, the aminophospholipid, phosphatidylserine (PS), and phosphatidylethanolamine (PE) are concentrated in the cytosolic leaflet, whereas phosphatidylcholine (PC) and sphingolipids are enriched in the exoplasmic leaflet (Holthuis and Levine, 2005; Pomorski and Menon, 2006).

The asymmetric distribution of lipids is generated by energy-dependent flippases that hydrolyze ATPs for energy to translocate specific lipids across the lipid bilayer (Pomorski and Menon, 2006). The P-type ATPase is such a flippase and its translocase activity was found not only in the plasma membrane (PM) (Pomorski et al., 2004), but also in the membranes of distinct vesicles (Zachowski and Gaudry-Talarmain, 1990; Alder-Baerens et al., 2006) and the *trans* Golgi network (Natarajan et al., 2004). In yeast, the *DRS2* gene codes for Drsp, a member of the P4-ATPase family in the P-type ATPase superfamily (Ripmaster et al., 1993). Mutations in *DRS2* caused an absence of low temperature uptake of a labeled PS analog at the PM (Tang et al., 1996; Gomes et al., 2000). Additionally, loss of the Golgi-associated P4-ATPases Drs2p and Dnf3p abolished the asymmetric

arrangement of endogenous PE in post-Golgi secretory vesicles (Alder-Baerens et al., 2006). These findings indicated an essential role for P4-ATPases in generating and maintaining lipid asymmetry during membrane flow through the Golgi. Additional P4-ATPase family members also have been identified, and they are all associated with lipid translocation in other species (Ujhazy et al., 2001; Perez-Victoria et al., 2003; Wang et al., 2004), including plants (Gomes et al., 2000).

P4-ATPase is involved in vesicle formation. During the biogenesis of intracellular transport vesicles, lipids need to translocate from the inner leaflet to the outer one by flippases in membranes (Pomorski and Menon, 2006). In yeast, the absence of the two PM associated P4-ATPases, Dnf1p and Dnf2p, resulted in a cold-sensitive defect in the biogenesis of endocytic vesicles (Pomorski et al., 2003) and inactivation of Drs2p caused a decrease in clathrin-coated vesicle budding from the trans-Golgi (Gall et al., 2002; Natarajan et al., 2004). Stimulation of PS and PE inward translocation induced the formation of endocytic vesicles in red blood cells (Birchmeier et al., 1979; Muller et al., 1994). Conversely, enhancement of outward directed lipid translocation led to a defect in endocytosis (Kean et al., 1997; Decottignies et al., 1998). The role of flippases in vesicle biogenesis was considered a direct and mechanical action on vesicle budding. P4-ATPases interacted with such cytosolic proteins as guanine nucleotide exchange factors (GEFs) and small GTPases, which are crucial for the recruitment of such coat proteins as clathrin at sites of the lipid translocation (Pomorski and Menon, 2006; Liu et al., 2007). The membrane curvature, which is generated by lipid translocation that creates an area difference between the two leaflets, promotes vesicle budding (Pomorski and Menon, 2006).

Vesicle-mediated membrane trafficking plays a crucial role in cell expansion. Polar expansion such as elongation of pollen tubes and root hairs requires vesicles for transporting materials to build cell walls (Samaj et al., 2006). Abundant vesicles are transported and deposited cell wall molecules at growing sites. Normal vesicle trafficking is also necessary for other cells to initiate or execute anisotropic expansion. Aberrant vesicle trafficking caused lobe reduction of *Arabidopsis* epidermal pavement cells and shape changes of trichomes (Zheng et al., 2005). In this study, we cloned the Arabidopsis *ITB2* gene through a map-based strategy. ITB2 is identical to ALA3, a member of the putative aminophospholipid translocase (ALA) subfamily in the P4 ATPase family in the P-type ATPase superfamily. Mutations in *itb2* mutants reduced the trichome branch length. We provide the evidence that plant P4 ATPases regulate cell expansion, likely through contribution to the vesicle formation.

Materials and Methods

Plant Materials and Growth Conditions

The *itb2-28*, *itb2-29*, and *itb2-12* (*9412-12*) mutants were isolated in the Rschew (RLD) genetic background (Zhang et al., 2005). The *itb2-4* (Salk_015929) mutant is a T-DNA insertion line in the Columbia (Col) ecotype, based on the SALK T-DNA Expression Database (http://signal.salk.edu/cgibin/tdnaexpress). The wild type used for construction of the mapping population is the Landsberg *erecta* (Ler) ecotype. Seeds of the SALK lines, SALK_015929, 006470, 067322, 139762, 129494, 133319, 082561, 066531, and 109350, were ordered from the *Arabidopsis* Biological Resource Center (The Ohio State University, Columbus, OH).

Seeds were sown on a soil-less potting medium, Fafard 2 Mix (Conrad Fafard, Inc., Agawam, MA). Seedlings were grown at 24°C under constant light, provided by 40W cool

white fluorescent tubes. Plants were watered with PGP nutrient solution (Pollock and Oppenheimer, 1999) every two weeks.

Positional Cloning of *ITB2*

The mapping population for cloning the *ITB2* gene was generated as described by Zhang et al., (2005). The phenotypically *itb2* mutant plants were selected from the F2 generation of plants. From each selected plant, one of the cotyledons was removed for DNA extraction using the RED Extract-N-Amp Plant PCR Kit (Sigma-Aldrich, St. Louis, MO). The isolated DNA was used to map the *itb2* mutation relative to simple sequence length polymorphisms (SSLPs) (Bell and Ecker, 1994; Lukowitz et al., 2000). Because the itb2 mutant was isolated from a fast neutron mutatgenized population, after the *itb2* mutation was mapped to a relatively small region, the presence of a deletion was tested by using *itb2-28* DNA as the template to amplify about 500 bp target fragments. After the deletion was found, all the genes in the deleted region were sequenced to check for mutations using PCR products amplified from *itb2-19* DNA.

Plasmid Construction

To complement the *itb2* mutant, the 2146 bp element at the 5' end of *ITB2* replaced the 35S promoter on pAM-PAT-GW through *Xho*I and *Asc*I, and the 1380 bp-element at the 3' end of *ITB2* was directionally cloned into the pAM-PAT-GW backbone using the *Pst*I restriction site. Because of the large size of the *ITB2* genomic sequence, its cDNA was used for construction. The full length coding sequence of *ITB2* cDNA was amplified by RT-PCR from total RNA of from Col wild type. The PCR fragment was cloned into the pBluescript SK II (+) vector. The amplified PCR products were sequenced to identify any mutations that were introduced during PCR. The mutations in the cloned cDNA of *ITB2* were corrected in the Col wild-type version by multiple substitutions with the correct PCR

fragments. The resultant wild type *ITB2* cDNA was cloned into pENR1A (Invitrogen, Carlsbad, CA) using the *Bam*HI and *Eco*RI sites. Finally the *ITB2* cDNA was transferred into the modified pAM-PAT-GW vector through an LR reaction.

For overexpression of *ITB2*, the *35S:ITB2* and *GL2:ITB2* constructs were made. The *ITB2* cDNA of the Col wild-type version was transferred into pAM-PAT-GW (Bekir Ulker, Max Planck Institute for Plant Breeding, Cologne, Germany) for expression from the 35S promoter, or pCK86 (Arp Schnittger, Max Planck Institute for Plant Breeding) for expression from the GL2 promoter through an LR recombination.

To localize ITB2, a *35S:ITB2-CFP* gene fusion was made. Cyan fluorescence protein (CFP) was amplified by PCR using the pAVA574 (von Arnim et al., 1998) plasmid as a DNA template. The stop codon was removed from pENR1A-ITB2 through sequence substitution at the 3' end containing *Nde*I with the PCR product. The two PCR products were ligated together through blunt ends. The fused fragment was cloned into pENR1A-ITB2 using the *Nde*I and *Eco*RI sites. Finally the *ITB2-CFP* gene fusion was transferred into pAM-PAT-GW for expression from the 35S promoter through an LR reaction.

RNA Extraction and RT-PCR

Total RNA was extracted from six-week-old Col wild-type plants using the RNeasy Plant Mini Kit (Qiagen, Valencia, CA) according to the manufacturer's instructions. The full length *ITB2* cDNA was amplified, following the instructions for the cMaster RT plus PCR System (Eppendorf AG, Hamburg, Germany). The first strand DNA synthesis was primed using oligo $(dT)_{20}$. The cDNA was amplified using specific primers of *ITB2*. The PCR products were sequenced by the Interdisciplinary Center for Biotechnology Research (ICBR) at the University of Florida.

Plant Transformation

The constructs, *5' untranslated region* (*UTR*):*ITB2*:*3'UTR*, *35S*:*ITB2*, *GL2*:*ITB2*, and *35S*:*ITB2-CFP,* were transferred into *itb2-28* mutants by the floral dip method (Clough and Bent, 1998). The transgenic plants were selected using a 1000X dilution of Finale (Farnam Companies, Phoenix, AZ) with 5.78% glufosinate-ammonium 5.78%.

Results

Characterization of the *itb2* Mutants

ITB2 controls the trichome shape mainly through regulation of branch expansion. All the *itb2* mutant alleles displayed defective trichomes in which one branch is longer than others (Zhang et al., 2005a). The *itb2-12*, *itb2-19,* and *itb2-28* mutant alleles are in the RLD genetic background; and *itb2-4* is in the Col genetic background. All mutants display identical trichome shape that is a weak distortion and at leas one branch longer than others (Figure 3-1G-L). In the RLD genetics background, cotyledon shape also was altered in *itb2* mutants. A kidney- shape d cotyledons are shown in Figure 3-1A-F. In addition to this effect, the genetic background also influences the frequency of the phenotypically *itb2* mutant plants in F2. The segregation of the *itb2* allele does not fit the monogenic model for Mendelian segregation (Table 3-1). In the RLD and Col ecotypes, the ratio of wild-type and mutant plants in F2 was approximately 15:1, which is closer to the segregation ratio expected for two loci segregating independently. However, in the Ler genetic background, the ratio was much lower, which also seems to indicate that the *itb2* phenotype results from multiple independent lesions (Table 3-1).

Cloning of the *ITB2* Gene

ITB2 was mapped between *ITB3* and *ITB4* on chromosome I (Zhang et al., 2005a). To clone the *ITB2* gene, we executed its fine mapping relative to SSLP markers. Because

the *itb2-28* mutant is in the RLD genetic background, additional SSLPs markers were developed between the RLD and Ler ecotypes. In addition, we screened for DNA deletions in the *itb2-28* mutant. One set of PCR primers did not produce a product when *itb2-28* DNA was used as the template, but produced products when wild-type DNA from RLD or Ler was used. Additionally, the primers in this reaction are complementary to the sequences that are located to the middle of the mapped region, the BAC clone F23H11 (Figure 3-2A). To determine the exact position of the detected deletion, we screened F23H11 through amplification of short regions spaced approximately every 500 bp along this BAC clone. Finally, an approximately 19-kb deletion was found between positions 62757 bp and 81830 bp on F23H11. The sequencing data showed that the breakpoint was TTTAAGCCATGACGCTGAGCGAT//AAAAAGCTTTGATCGTCTTTGAT. The right deletion breakpoint includes 779-bp cDNA of the At1g59780 gene. The letf side of the deletion covered a 1336 bp deletion of the At1g59820 gene. Additionally, the deleted region covered only five genes (Figure 3-2B), all of which were sequenced using the genomic DNA from the *itb2-19* allele as the template for PCR amplification. We identified an approximately 800 bp deletion in the gene At1g59820 in this mutant and further sequenced the *itb2-12* allele. The same deletion as the *itb2-19* allele was found. These results indicated that *ITB2* was identical with At1g59820, and that the *itb2-19* and *itb2-12* alleles were likely to derive from the same allele.

For an allelism tests, the *itb2-28* mutant was crossed with *itb2-19* and *itb2-12* mutants. Their F1 generation all displayed the *itb2* mutant trichome phenotype. To search for more alleles of the *itb2* mutant, the Salk T-DNA insertion lines were examined. The Salk_015929 line segregated into two kinds of phenotypic plants, one of which displayed

the *itb2* mutant trichomes. The PCR analysis indicated the two plants with the *itb2* mutant trichomes were homozygous for the T-DNA insertion in At1g59820. The *itb2-28* mutant was crossed with the homozygous T-DNA lines of Salk_015929 as a complementation test. The F1 plants all displayed the *itb2* mutant trichome phenotype indicating that the plants from SALK_015929 with the *itb2* phenotype were *itb2* alleles.

The *ITB2* gene is relatively large, with an 8425-bp genomic coding sequence and a 3642-bp cDNA sequence. The coding sequence consists of 27 exons (Figure 3-2C). Compared to the gene in the Col ecotype, the RLD ecotype has six single nucleotide-alterations were identified. Among the SNPs detected, five alterations were located in introns and one alteration was located in the last exon, but this transition causes no change in the protein sequence. Through RT-PCR, the same size the *ITB2* cDNA was amplified using the total RNA from Col wild type. The results from sequencing the *ITB2* cDNA indicated that the *ITB2* structure is identical with the annotation of The Arabidopsis Information Resource (TAIR) in Figure 3-2C.

Complementation of the *itb2* Mutant and Over-expression of the *ITB2* Gene

To complement *itb2* mutants and over-express *ITB2*, we made constructs using the *ITB2* cDNA. One reason for using the *ITB2* cDNA is that it is much smaller size than the genomic DNA. The *ITB2* cDNA that was cloned into the pBluescript SK II (+) vector (SK-ITB2) had 9 base changes (Figure 3-3) compared to the Col wild type. Among these mutations, five cause amino acid changes: at 878 (the position in the cDNA beginning with 1 at A of ATG), A to G (the amino acid transition, K to R); at 2554, A to G (M to V); at 2690, T to C (L to P); at 3265, A to G (M to V); and at 3289, A to G (T to A). The transition of L to P and T to A is likely to affect protein function and others are not, because similarity of mutated amino acids with the wild type in structure and property.

The re-cloning of the full length *ITB2* cDNA was unsuccessful and no full length *ITB2* cDNA clones were available from the stock center. To correct the mutations in the resultant clone of the *ITB2* cDNA, two EST clones from the *ITB2* gene, G7B4 and M65O03, were ordered from the ABRC (The Ohio State University, Columbus, OH). These two clones both contain about a 1 kb sequence at the 3' end region of the *ITB2* cDNA, which can be used for substitution of the mutated part of SK-ITB2. The host cells that contain G7B4 grew well and the plasmids could be isolated through mini-preparation. However, the host cells that contain M65O023 grew slowly and the plasmids could not be isolated through standard metheds. The isolated plasmids were sequenced and a TC-deletion was found in the G7B4 clone at the 2946-bp position of the *ITB2* cDNA. The target fragments were amplified through PCR using the M65O03 DNA as the template and cloned into pBluescript SK. The cells that hosted the resultant construct also grew slowly and compared to the G7B4 clone, much less plasmid DNAs could be isolated using standard plasmid isolation procedures. Therefore, in the later experiments, we added 0.5% glucose to the medium to prevent expression of the genes of interest in the host cells. Through multiple substitutions, all the changed bases in SK-ITB2 were corrected into the Col wild-type version (Figure 3-3).

To complement the *itb2* mutant, both the 2146-bp element of the *ITB2* gene at the 5' end of *ITB2* and the 1380-bp element at the 3' end drove the *ITB2* cDNA coding sequence of the Col wild type version. The transgenic plants in the *itb2-28* background displayed the wild type trichome phenotype (Table 3-2 and Figure 3-4). This result provided further evidence that the *ITB2* gene is At1g59820.

To over-express *ITB2*, the *ITB2* cDNAs were cloned into either pAM-PAT-GW for expression by the *35S* promoter or pCK86 for expression by the *GL2* promoter through a homologous recombination. The transgenic plants containing the mutated *ITB2* cDNA in the *itb2-28* mutant background displayed the *itb2* mutant trichome phenotype (data not shown). However, the transgenic plants of the same genetic background as the Col wild-type *ITB2* cDNA version exhibited wild-type trichomes (Table 3-2 and Figure 3-4). This result indicated that the C-terminus is crucial for functionality. Additionally, no novel visible phenotypes were observed for these transgenic plants.

To localize ITB2, we constructed the *ITB2* gene fusion with CFP, using the Col wild type *ITB2* cDNA. The transgenic plants in the *itb2* mutant background with the *35S: ITB2-CFP* construct displayed the *itb2* trichome phenotype. This result further supports the hypothesis that the C-terminus of ITB2 is crucial for functionality.

Discussion

Membrane trafficking is essential for establishment and maintenance of plant cell polarity, especially for such tip growth as the elongation of pollen tubes and root hairs. At the cellular level, tip growth is achieved through polar-specific and cell domain-specific trafficking of vesicles (Hepler et al., 2001); at the molecular level, the tip growth machinery is assembled mainly by small GTPases in the Rab, Arf, and Rop/Rac families and their regulatory proteins such as Rho guanine nucleotide exchange factors (GEFs) and GTPase activating proteins (GAPs) (Samaj et al., 2005; Yang and Fu, 2007). A trans-Golgi network (TGN) was further proposed as a tip-localized vesicular compartment integrating targeted secretion and endocytosis within the growing tip (Samaj et al., 2006).

When pollen tubes are growing, endomembrane trafficking activity transports secretory vesicles along the flank of the tube to the tip; meanwhile, endocytic recycling

vesicles move back distally along the center of the tube, which forms a reverse-fountain cytoplasmic streaming pattern (Hepler et al., 2001). The secretory vesicles accumulate within the tip clear zone where they form clusters and fuse with the apical membrane, depositing new membrane, proteins, and cell wall materials to support growth (Samaj et al., 2006). The behavior of vesicles in the growing root hairs is reminiscent of that in growing pollen tubes (Hepler et al., 2001; Voigt et al., 2005).

Although trichome branching is not considered to belong to the tip growth, its process is a typical anisotropic cell expansion. Endomembrane trafficking also plays an important role in plant epidermal cell expansion, such as *Arabidopsis* leaf pavement cells and trichomes (Smith and Oppenheimer, 2005). The defective endocytic membrane traffic can cause changes in the shapes of these cells. Using FM4-64 to track endocytic membrane traffic, the larger vesicle clusters aggregated and were surrounded with an ring of Golgi stacks in the leaf pavement cells of the *cer10* mutant (Zheng et al., 2005). These defects resemble the compartments found in the brefeldin A (BFA)-treated cells. BFA is an inhibitor that disrupts exocytosis (Baluska et al., 2002; Samaj et al., 2004). The *cer10* mutant leaf pavement cells were considerably smaller with less pronounced lobes, and the *cer10* trichomes were smaller with short, crooked, and aberrant swollen stalks and branches (Zheng et al., 2005). The alterations of these cell shapes indicated that their anisotropic expansion was compromised, because of defects in endocytic membrane trafficking. A further molecular model was proposed after analysis of Kinesin-13A, ZWI, and AN functions (Lu et al., 2005; Smith and Oppenheimer, 2005). The plant Golgi apparatus and secretory vesicles are transported by myosin(s) from the perinuclear region to the cell cortex, dispersed to cell expanding sites by Kinesin-13A along the cortical microtubules.

Mutations of *AtKinesin-13A* increased the trichome branch number and a compromised anisotropic trichome cell expansion. In the trichomes of the *kinesin-13a-1* mutant, the Golgi stacks aggregated (Lu et al., 2005). Further support for this modelcomes from the aberrant trichome shapes found in myosin mutants (Ojangu et al., 2007).

ITB2 is putative aminophospholipid translocase 3 (ALA3) in the P4 ATPase family. Although 12 members (ALA1-12) in this family were identified in *Arabidopsis*, their biological functions are less known (Axelsen and Palmgren, 2001). Evidence suggests that ALA1 is involved in generating membrane lipid asymmetry. Down-regulation of ALA1 results in a significant reduction in plant size and an alteration of plant morphology at low temperatures (Gomes et al., 2000). It is likely that the aberrant plants resulted from defective cell expansion. ITB2 regulates anisotropic expansion in trichome morphogenesis most likely through its role in generating membrane lipid asymmetry for vesicle formation during endomembrane trafficking. To confirm our explanation, we will track membrane trafficking in the *itb2* mutants.

Future Perspectives

ITB2 is a putative flippase that translocates aminophospholipids from one leaflet to another. It belongs to the P4 ATPase family. Our results show that mutations in *ITB2* cause a defective trichome shape phenotype and a slight change in cotyledon shape. These mutants provide good experimental materials for further studies on function of ITB2 in controlling plant cell shape. Recently published data showed that aminophospholipid translocase 3 (ALA3) is identical to ITB2 (Poulsen et al., 2008). It was shown that ALA3 localizes to the Golgi. We predict that defective Golgi localization can also be observed in *itb2* mutant trichomes.

To observe Golgi localization in developing trichomes, we can cross the *ST-YFP* construct to *itb2* mutants. The *ST-YFP* construct is a fusion of the Golgi-localized sialyltransferase enzyme to yellow fluorescent protein. This construct labels Golgi stacks in transformed plant cells. Once this construct is introgressed into the *itb2* mutant background, localization of Golgi can be observed in living, developing trichomes using confocal microscopy. By comparing the localization pattern and dynamics of Golgi stacks in *itb2* mutants with that of wild type trichomes, we can determine if Golgi dynamics and localization is affected in *itb2* mutants. If this is found, then it suggests that proper Golgi localization is a key to directional cell expansion. Also this result would suggest that flippase activity is important for Golgi function.

The key question that remains to be answered is whether or not ALA3/ITB2 is actually a flippase. For this to be shown, flippase activity has to be reconstituted in vitro. Many groups have attempted this, but have not been successful.

Table 3-1. Segregation of the mutant plants in F2 with different genetic background

Cross name	Number of wt plants	Number of mutant plants	X^2 value*	P value*
itb2-28/RLD wt	424	28	0.0022	>0.900
itb2-28/Col wt	867	52	0.5495	>0.500
itb2-28/Ler wt	1441	46	25.2859	<0.001

* is for 15:1 ratio.

Table 3-2. Trichome shapes of the transgenic plants

Construct name	Promoter	% irregular	% normal	Total
XG61	ITB2	10.7	89.3	799
XG62	35S	8.2	91.8	972
XG63	GL2	5.4	94.6	815
RLD	-	3.5	96.5	713
itb2-28	-	89.3	10.7	651

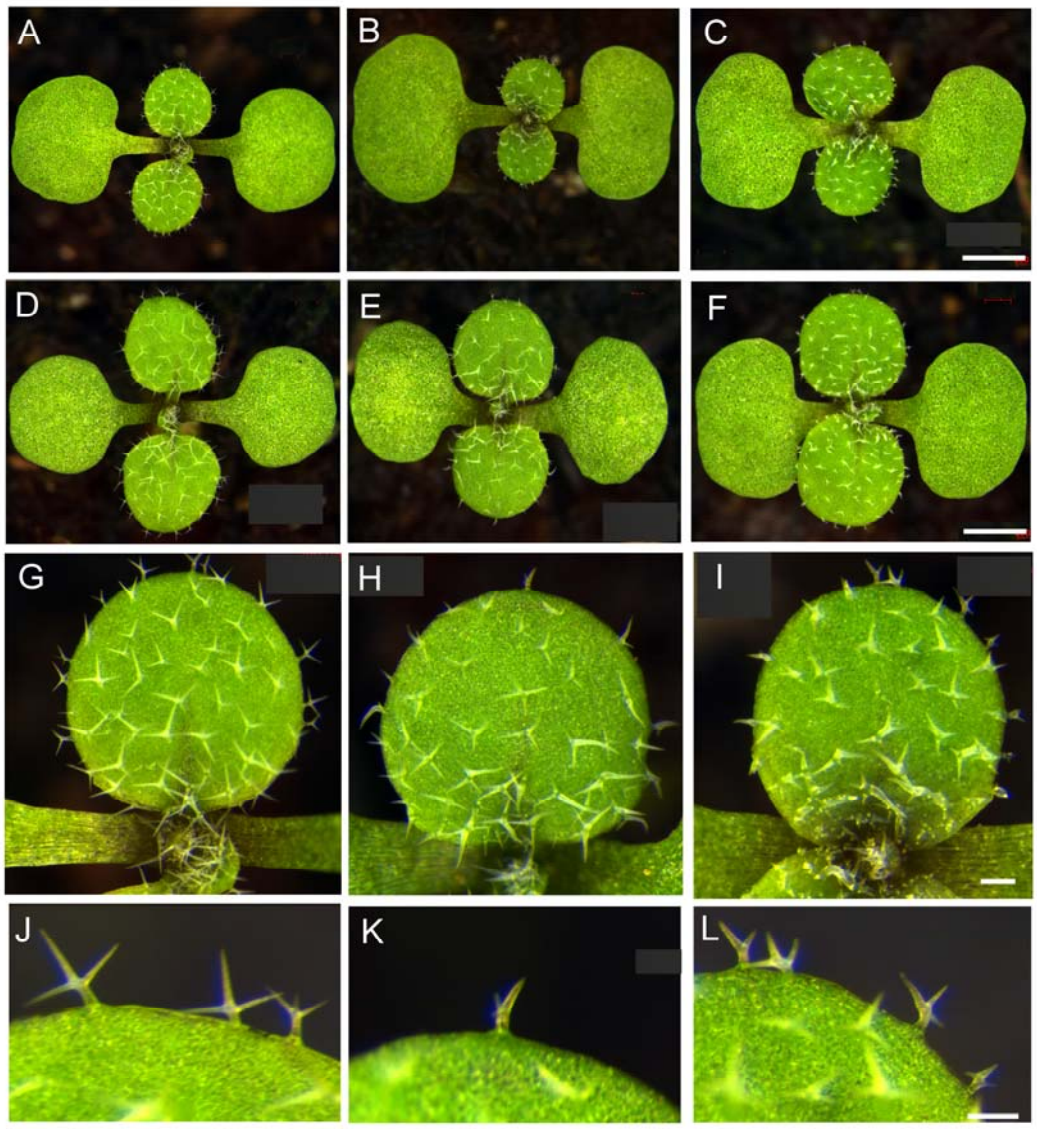

Figure 3-1. Defects in leaf trichome and cotyledon shape of *itb2* mutants. (A), (G), and (J): RLD wild type; (D), Col wild type; (B), (H), and (K), *itb2-28*; (C), *itb2-19*; (E), (I), and (L), *itb2-4*; (F), *itb2-12*. Bars = 1000 µm in (A)-(F); 200 µm in (G)-(I); 100 µm in (J)-(L)

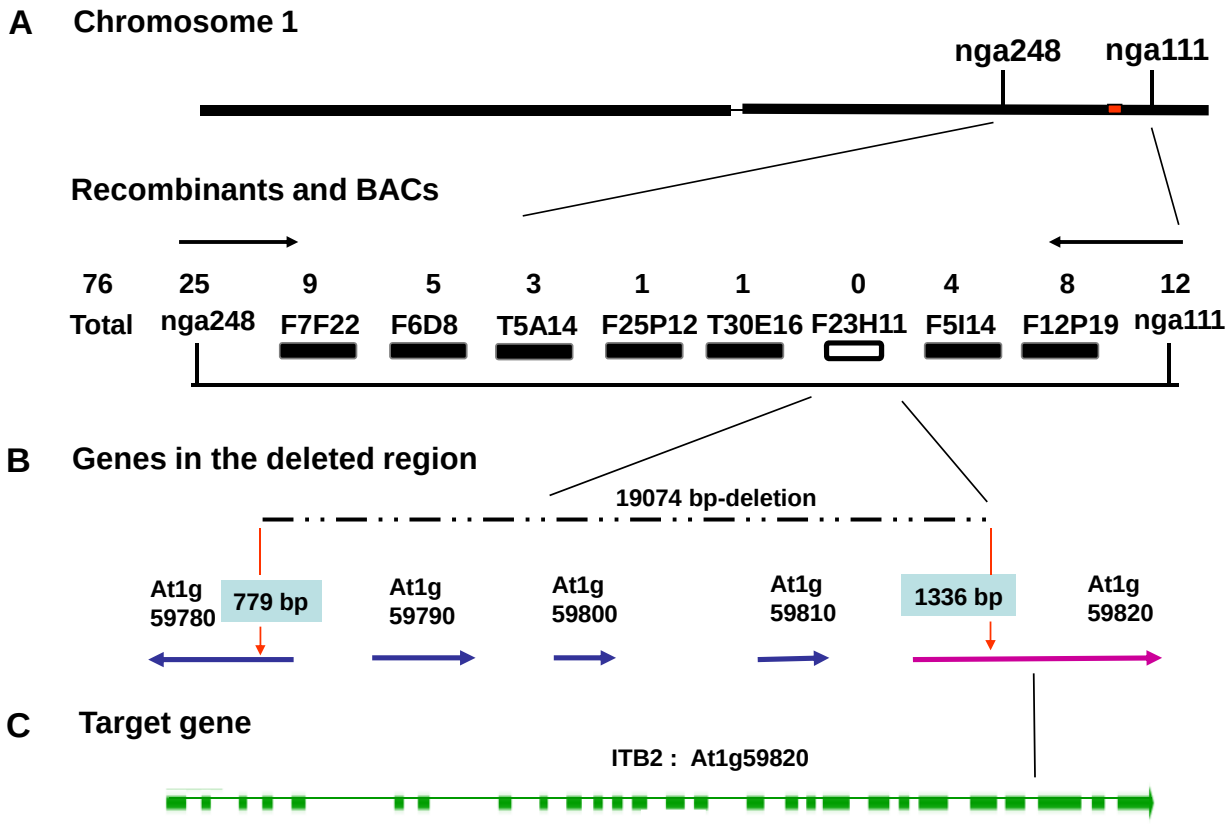

Figure 3-2. Positional cloning and gene structure of *ITB2*. The *itb2* mutation was mapped near SSLP markers between nga248 and nga111 on chromosome 1. Additional molecular markers were used to map the *itb2* mutation to BAC clone F23H11. The numbers of recombinants (out of 76 chromatids screened) are given above BAC clones. All putative genes inside the identified deletion on BAC clone F23H11 are listed. *ITB2* structure is shown in (C). The thick bars in (C) represent exons.

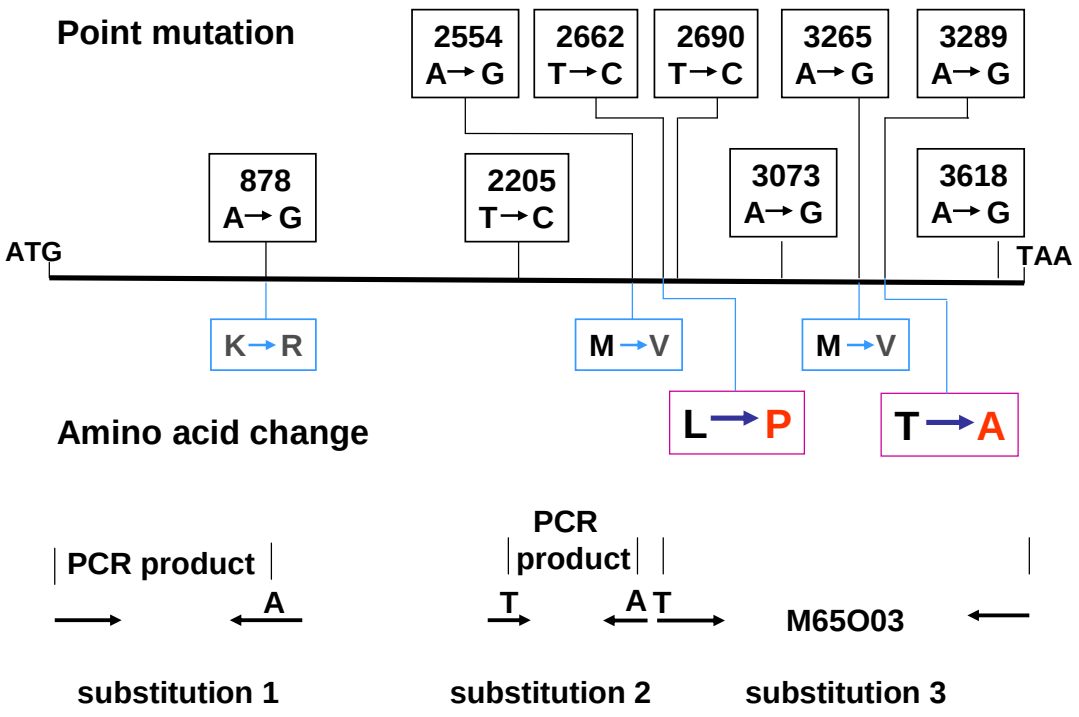

Figure 3-3. Mutations and corrections of *ITB2* cDNA. All mutations of the cloned *ITB2* cDNA are listed in the vectanglar boxes. The numbers on the above bases are the positions of mutated bases. The respective amino acids encoded by the change genetic codes are also listed below the thick line representing *ITB2* cDNA. Approximate positions of the PCR primers used for substitution are shown by the black arrows with the corrected base above them.

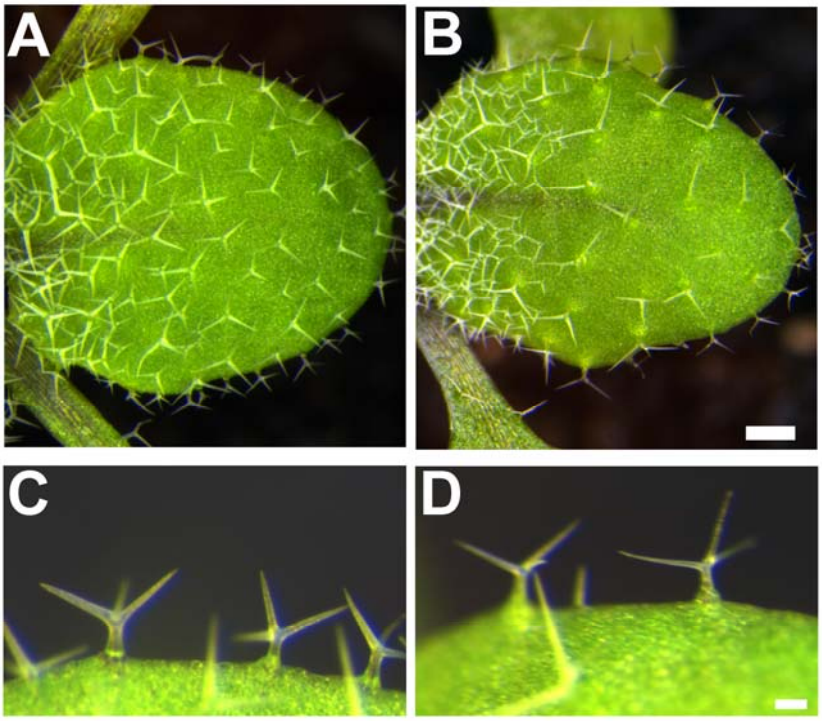

Figure 3-4. Transgenic plants with *ITB2* cDNA. (A) and (C), RLD wild type; (B) and (D) the transgenic plant. Bars = 500 µm in (A) and (B); 100 µm in (C) and (D)

CHAPTER 4
DISPROPORTIONATE (DPP) ENCODES A KETOACYL REDUCTASE INVOLVED IN TRICHOME CELL EXPANSION

Introduction

The control of plant cell shape has been suggested to occur in three sequential steps: First, cell polarity is established by intracellular mechanisms and/or extracellular cues. Second, using the established polarity, cytoskeletal rearrangements take place. Third, the cytoskeletal changes enable polarized cell expansion, which includes the incorporation of membrane and cell wall material at defined areas of the cell periphery (Hulskamp et al., 1998; Smith and Oppenheimer, 2005).

Arabidopsis trichomes are and excellent model for studies on the control of plant cell shape. Through a forward genetic approach, more than 20 genes that regulate trichome development have been cloned (Marks, 1997; Schellmann and Hulskamp, 2005). The products of these trichome genes are diverse; their functions include transcription initiation, cytoskeletal organization and vesicle trafficking. For example, *GL1*, *GL2*, *GL3*, *EGL3*, *TTG1*, *TRY*, *ETC*, *MYB23* and *CPC* all function as transcriptional regulators (Schellmann and Hulskamp, 2005). *DIS1*, *DIS2*, *DIS3*/*ITB1*, *WURM*, *CRK*, *GRL*, *ATRK1* and *PIR*/*KLK* belong to the "distorted" group of trichome genes that encode regulators of the actin cytoskeleton (Schellmann and Hulskamp, 2005; Szymanski, 2005). *AN*, *ZWI*, *MYA2* and *KINESIN-13A* are known or predicted to be involved in vesicle trafficking (Smith and Oppenheimer, 2005). Recently, a group of genes identified by wax and cuticle phenotypes whose products are involved in wax synthesis and transport (Kunst and Samuels, 2003) have been shown to be involved in trichome morphogenesis (see below).

Wax is derived mainly from very long chain fatty acids (VLCFAs), which are required for sphingolipid synthesis. VLCFA moieties in sphingolipids are essential for

determining the physical properties and characteristics of membranes. Sphingolipids are an important class of lipids in the plasma membrane and the endomembrane system (Simons and Toomre, 2000). In yeast and mammalian cells, sphingolipids are concentrated in lipid rafts, which are involved not only in cellular trafficking of certain plasma membrane proteins, but also play important roles in signal transduction and generation or maintenance of cell polarity (Rajendran and Simons, 2005). Plant lipid rafts are also enriched in sphingolipids, but their role in generation or maintenance of cell polarity has rarely been reported (Bhat and Panstruga, 2005; Grennan, 2007).

VLCFA synthesis is a complex process including two stages in different cellular compartments (Kunst and Samuels, 2003). The de novo fatty acid synthesis of C16 and C18 acyl chains occurs in the stroma of plastids by the soluble enzyme complex called the fatty acid synthase (FAS). The synthesized fatty acyl precursors are further extended to C34 VLCFA chains through the same reactions as the de novo fatty acid synthesis, but these reactions are catalyzed by membrane-bound enzyme complexes called fatty acid elongases (FAE) located in the endoplasm reticulum. FAE is composed of four enzymes that catalyze four sequential reactions: These are 1) condensation of malonyl-CoA to acetyl-CoA by 3-ketoacyl-CoA synthase (KCS), 2) reduction of 3-ketoacyl-CoA by 3-ketoacyl-CoA reductase (KCR), 3) dehydration of 3-hydroxyacyl-CoA by 3-hydroxyacyl-CoA dehydrase (DCH), and 4) reduction of trans-2-enoyl-CoA by enoyl-CoA reductase (ECR). The resultant VLCFAs are finally modified into different kinds of waxes (Kunst and Samuels, 2003). Wax monomers are exported to the cell surface by the ABC transporters such as ABCG12/CER5 (Pighin et al., 2004) and ABCG11/WBC11 (Bird et al., 2007).

LACERATA (LCR) encodes a monooxygenase, which catalyzes ω-hydroxylation of fatty acids ranging from C12 to C18. The trichomes on *lcr* mutant leaves exhibited under-development with a variety of aberrant shapes (Wellesen et al., 2001). The *FIDDLEHEAD (FDH)* gene codes for a KCS. Mutations in *FDH* have a deleterious effect on trichome differentiation because leaf trichome number was reduced 2-fold in *fdh* mutants (Yephremov et al., 1999). *ECERIFERUM10* (*CER10*) encodes an ECR; mutations in this gene caused defective leaf trichomes, which had short, crooked, and abnormally swollen stalks and branches (Zheng et al., 2005). The *BODYGUARD* (*BDG*) gene encodes a putative extracellular synthase responsible for the formation of the cuticle. The *bdg* mutants displayed many misshapen leaf trichomes including ones with flat, bent, and collapsed shapes (Kurdyukov et al., 2006). The maize (*Zea mays*) *GLOSSY1 (GL1)* gene codes for a component in the pathway leading to cuticular wax biosynthesis in seedling leaves. The *gl1* mutation results in leaf trichomes that are smaller than normal (Sturaro et al., 2005). Mutations in *YORE-YORE* (*YRE*), a putative *GL1* homolog in Arabidopsis, also led to small trichomes. In addition, the trichome shape of *yre cer1* double mutants was greatly deformed (Kurata et al., 2003). Genetic lesions in (*DESPERADO*) *DSO*/*AtWBC11*, an ATP binding cassette (ABC) transporter for wax export, led to a dramatic alteration in wax load and trichome development. The *dso/atwbc11* mutants had waxless stems and collapsed and underdeveloped trichomes (Bird et al., 2007; Luo et al., 2007; Panikashvili et al., 2007). Here, we report the cloning of the *DPP* gene through a novel strategy amenable to the map-based cloning of other dominant, homozygous lethal mutations. We show that *DPP* codes for a KCR, and *dpp* mutations lead to a waxless phenotype in addition to dramatically altered trichome shape.

Materials and Methods

Plant Materials and Growth Conditions

The *dpp* mutant was isolated in a genetic screen of fast-neutron mutagenized seeds, in the Rschew (RLD) genetic background, which were purchased from Lehle Seeds (Round Rock, TX). The Landsberg *erecta* (Ler) ecotype was used as wild type for construction of the mapping population. Wild-type plants of the Columbia (Col) ecotype were used for transformation. Seeds were sown on a soil-less potting medium, Fafard 2 Mix (Conrad Fafard, Inc., Agawam, MA). Seedlings were grown at different temperatures (18° C, 20° C, 22° C and 24° C) in growth chambers under 16 hr light and 8 hr darkness. Light was provided by 40W, cool white fluorescent tubes. Plants were watered with PGP nutrient solution (Pollock and Oppenheimer, 1999) every two weeks.

Positional Cloning

For cloning *DPP,* a mapping population was generated from a cross between the *dpp* mutant and Ler. Because the *dpp* mutant was dominant and homozygous lethal, 646 phenotypically wild type plants were selected from the F2 population for mapping. The first leaf pair from each individual was used for DNA extraction, following a standard protocol (Edwards et al., 1991). The isolated DNA was used as a template for PCR to map the *dpp* mutation relative to simple sequence length polymorphisms (SSLPs) (Bell and Ecker 1994, Lukowitz et al. 2000) and cleaved amplified polymorphic sequences (CAPS) (Konieczny and Ausubel, 1993). After the *dpp* mutation was mapped into a narrow region, all the candidate genes in the mapped region were amplified by PCR of genomic DNA from the *dpp* mutant to check for deletions, as expected in a mutant isolated from fast neutron mutagenesis. Primers sequences are listed in Table 4-1.

To determine the lesion in the dpp mutant, we crossed dpp plants to SALK lines that were homozygous for T-DNA insertions in the candidate genes located within the mapped region. The SALK lines were obtained from the Arabidopsis Biological Resource Center (The Ohio State University, Columbus, OH). Plants homozygous for the T-DNA insertions were identified through PCR with T-DNA and gene-specific primers designed using the SALK T-DNA insertion primer design website (http://signal.salk.edu/tdnaprimers.2.html). The homozygous T-DNA insertion lines were used as the female and the *dpp* mutant was used as the male for the crosses. The F1 progeny were grown at temperatures below 20°C to ensure that the dpp trichome phenotype was visible. The segregation of the trichome phenotype in the F1 plants was recorded. DNA was extracted from the F1 plants using the DNeasy Plant Mini Kit (Qiagen, Valencia, CA), following the manufacturer's instructions. The candidate genes were amplified by PCR, and the products were sequenced to check for mutations. The sequences were compared to that of RLD wild type.

Plasmid Construction

Genomic DNA from *dpp* mutants was used as the template for amplification of At1g67730 using primers DEd7 and DEd8. PCR reaction conditions were as follows: 94º C, 3 minutes; 25 cycles of 94º C, 30 seconds; 64º C, 30 s; 68º C, 3 minutes. KOD XL DNA polymerase (Novagen, Madison, WI) was used to amplify the entire At1g67730 coding sequence, which comprised 4967 bp. The PCR products were cloned into pBluescript SK using the *Pst*I and *Eco*RV sites. Positive clones were sequenced to check for mutations in the cloned gene. The GC-deleted *dpp* allele was also cloned into pAM-PAT-GW (Bekir Ulker, Max Planck Institute for Plant Breeding, Cologne, Germany) using the *Asc*I and *Pst*I sites. This clone was used to transform Col and RLD wild type plants to regenerate the dominant *dpp* trichome phenotype.

Plant Transformation

Plants were transformed by the floral dip method (Clough and Bent, 1998). Transgenic plants were grown at 16º C, and sprayed with a 1000X dilution of Finale (5.78% glufosinate-ammonium) (Farnam Companies, Inc., Phoenix, AZ).

Results

Characterization of *dpp* Mutants

To gain additional insight into trichome morphogenesis, we screened fast neutron-mutagenized *Arabidopsis* populations for plants that displayed defects in trichome shape. One of the mutants isolated in this screen showed shorter branches and longer stalks (Figures 4-1B, 4-1C) than wild type (Figures 4-1E, 4-1F). This mutant was named *disproportionate* (*dpp*). During routine plant growth, we noticed that the *dpp* phenotype was temperature sensitive; at temperatures below 22°C, plants displayed the *dpp* phenotype, while at temperatures above 24°C, the trichomes developed normally. At temperatures between 22°C and 24°C, most of the trichomes on the first leaf pair had a *dpp* phenotype, but later leaves had a higher proportion of normal trichomes. In addition, *dpp* leaf blades adhered to each other at an early developmental stage (Figure 4-1A), whereas the wild type leaves are open at the same stage (Figure 4-1D).

When *dpp* plants were crossed to other wild type plants, the resulting F1 plants segregated for the *dpp* phenotype. This result showed that the *dpp* mutation was dominant. The resulting F2 progeny also displayed segregation of both *dpp* and wild type plants in a ratio of 2:1, which fits a monogenic model for *dpp* (Table 4-2), assuming that the *dpp* homozygotes are lethal. We also noticed that all *dpp* plants segregated both *dpp* and wild type plants in the next generation. This phenomenon was examined in more detail by scoring the phenotypes of at least 50 progeny from 108 individual *dpp* plants. The plants in

all the observed populations segregated for *dpp* and normal trichomes. This result indicated that the populations were derived from the homozygous plants. Therefore, *dpp* plants are homozygous embryo lethal because no homozygous plants were found.

To test transmission of the *dpp* allele, the *dpp* mutant was reciprocally crossed with RLD wild type or Salk_143503. When the *dpp* mutant was used as the female parent, a higher frequency of F1 plants with the *dpp* phenotype occurred than when the *dpp* mutant was used as the male parent (Table 4-3). Because *dpp* mutants are heterozygous, when *dpp* is used as the male parent, both *dpp* and wild type pollen are transferred to the stigma. This result indicated that the *dpp* pollen was less competitive than wild type pollen during pollination and/or fertilization.

Positional Cloning of *DPP*

To clone the *DPP* gene, we generated an F2 mapping population consisting of 646 wild type plants. Wild type plants were used because the *dpp* homozygotes do not survive, and known homozygous plants need to be genotyped to identify recombinants. The *DPP* locus was mapped relative to SSLP markers to two BAC clones, T1F15 and F12A21. It was further mapped relative to CAPS markers to an 82 Kb region on F12A21. According to the TAIR database, this region covers 34 putative genes (Figure 4-2).

Because the *dpp* mutant was isolated from fast neutron-mutagenized seeds, we expected this mutation was caused by a deletion. We designed primers to amplify 0.5 Kb to 3 Kb fragments that cover the region of F12A21 that contained *dpp*. PCR products were amplified from both wild type and *dpp* mutants, and the sizes of the PCR products were compared with each other to determine the deletion position. Results showed that PCR products that differed in size from those predicted for wild type were generated by non-specific binding of the primers, and not due to a deletion in the *dpp* mutant. The PCR

products were further sequenced through amplification of the coding sequences of the putative genes in this region using the genomic DNA from the *dpp* mutant plants. This strategy identified single nucleotide polymorphisms (SNPs) between the of RLD and Ler ecotypes (Table 4-4 and Figure 4-3), and these SNPs were used as the markers for further mapping the *dpp* mutation. Many sequencing results were equivocal because the genomic DNA used for sequencing was extracted from the heterozygous *dpp* plants. For example, see sequencing results of At1g67760 (Figure 4-4) and At1g67730 (Figure 4-5, 4-6). At1g67760 encodes a chaperonin and At1g67730 encodes a ketoacyl reductase. There were no clear connections between these two gene products and the regulation of trichome shapes. Therefore, they were not immediately pursued further.

Identification of *DPP*

The homozygous lethality of the *dpp* mutation presented a challenge to identify the molecular lesion in the *dpp* allele because all *dpp* plants were heterozygous. Therefore, to identify the lesion in the *dpp* allele, we developed a strategy whereby we could specifically amplify the *dpp* allele from the heterozygous *dpp* plants, which was accomplished by crossing the *dpp* mutant to a homozygous SALK lines (Figure 4-7).

The *dpp* mutation is dominan, the heterozygous plants grow normally except for the *dpp* trichome phenotype, and the homozygous *dpp* plants are lethal. If the T-DNA insertion in the Salk lines causes a decrease in *DPP* gene expression, the F1 plants may display a novel phenotype. The result of phenotypic segregation in the F1 plants from crosses of *dpp* to homozygous SALK lines confirmed this prediction. Among the 10 homozygous SALK lines (with T-DNA insertions in 7 distinct genes) two F1 families showed lower transmission of the *dpp* mutation (Table 4-5). These two SALK lines had a T-DNA inserted in the 5' UTR of At1g67730. The F1 plants from one of these combinations segregated for

a novel phenotype: crinkled leaves, collapsed trichomes, waxless stems, and fused floral organs (Figure 4-9). Some of these phenotypes are similar to those displayed by *deadhead* (*ded*) mutants (Lolle et al., 1998).

The crinkled leaves and severe defective trichomes led us to focus our attention on At1g67730. We re-sequenced the PCR products using the DNA from the *dpp* plants as the template. The result remained equivocal (Figure 4-10). However, the forward reaction worked well with the same DNA sample (Figure 4-11), suggesting that a deletion or insertion likely occured in this gene. When the F1 plants that had the novel phenotypes grew larger, DNA was isolated from their leaves for further analysis. By designing primers that flank the T-DNA insertion, such as primers 720S1 and 720S2 or 730S1 and 730S2 (see Table 4-1 and Figure 4-12), we could specifically amplify the *dpp* allele, using the isolated DNA from the F1 plants. Sequencing of the PCR product revealed a 2 bp deletion (GC) at position 1595 and 1596 of the coding sequence of gene At1g67730 (Figure 4-13). This deletion was not observed in the sequence of PCR products from DNA extracted from F1 plants that had a wild type trichome phenotype (Figure 4-14). To confirm that the GC-deletion also exsits in the *dpp* mutant and that *DPP* is At1g67730, the entire coding sequence of At1g67730 including upstream and downstream intergenic regions was amplified from DNA isolated from *dpp* plants using primers DEd7 and DEd8 (Figure 4-12). The PCR products were cloned into the pBluescriptSK vector. The plasmid DNAs from two individual colonies were sequenced. One of them showed the GC-deletion (Figure 4-15) (and other was wild type (Figure 4-16). The GC-deleted *DPP* was used to transform wild type plants. Plants transformed with this GC-deleted transgene showed the same trichome defect as the original *dpp* mutant (Figure 4-17). These results further

confirm that *DPP* is At1g67730, which encodes a ketoacyl reductase, basing on the gene annotation (Arabidopsis Information Resource).

Discussion

DPP Encodes a β-ketoacyl Reductase

We isolated the *dpp* mutant during a screen for mutants with altered trichome shape. We found that the *dpp* mutation was dominant and homozygous lethal. In addition, the *dpp* mutants had a temperature sensitive phenotype; at 24°C and above, the trichomes appeared perfectly normal, whereas at 22°C and below, the trichomes displayed an elongated stalk and short branches. To clone *DPP*, we combined microarray information from laser-capture microdissected trichome cells with traditional positional cloning methods to identify the most likely candidate gene, At1g67730, for further analysis. At1g67730 encodes a β-ketoacyl reductase (KCR) that is involved in cuticular wax biosynthesis. To overcome the problems associated with identifying the *dpp* mutation from DNA isolated from heterozygous plants, we devised a novel strategy using primers flanking a T-DNA insertion in At1g67730. Using these primers and DNA from F1 plants from a cross of *dpp* with At1g67730 T-DNA insertion, only the *dpp* allele was amplified by PCR and the *dpp* mutation unequivocally identified. Recapitulation of the *dpp* phenotype in wild type plants containing the mutant *dpp* transgene confirmed that At1g67730 is *DPP*. The straightforward cloning of *dpp* demonstrates the efficacy of our approach for the positional cloning of other dominant, homozygous lethal alleles.

DPP Has Pleiotropic Functions in Cell Expansion and Wax Synthesis

The mutation in the *dpp* mutant caused a 31amino acid-deletion at the C-terminus of KCR. The mutated KCR resulted in plant lethality, but heterozygous plants in the RLD ecotype background, at the restrictive temperature, exhibited a trichome phenotype.

Otherwise the plants grew normally. Expression of the truncated KCR with the endogenous promoter in Col wild type plants exhibited novel phenotypes such as waxless stems, crinkled leaves, fused organs and severe aberrant trichome shapes. These phenotypes are similar to those seen in the F1 plants from the cross of the *dpp* mutant with the T-DNA insertion line, except that the phenotype of the transgenic plants is less severe. This may be due to the fact that only one mutant copy of *dpp* is present along with two- copies of wild type *DPP* in the transgenic plants. This suggests that the severity of the phenotype is dependent on the dosage of the DPP gene relative to the mutant allele.

The truncated DPP protein encoded by the *dpp* allele is likely to have less function compared to wild type. The more dpp protein that gets assembled into FAE, the less VLCFAs are synthesized. The *dpp*-homozygous plants are lethal because of the VLCFA deleption. Therefore, these long-chain fatty acids are essential for plant viability. The possibility that the dpp protein is a gain-of-function allele cannot be excluded. For example, the dpp protein might interfere with wax synthesis or transport.

Plants with the *dpp* allele in the Col genetic background lacked cuticular wax and had fused leaves and floral organs. These phenotypes are typical of the defects resulting from mutations in genes that are involved in wax synthesis.

The *GL8* gene in maize (Zea mays L.) codes for a KCR. *gl8* mutants reduced the amount and altered the composition of seedling cuticular waxes (Xu et al., 1997). The disruption of *CER6/CUT1* coding for a KCS reduced wax accumulation on stems (Millar et al., 1999; Fiebig et al., 2000). The *FIDDLEHEAD (FDH)* gene encodes another KCS (Fiebig et al., 2000; Pruitt et al., 2000). This mutant displayed defects in organ fusion (Lolle et al., 1992). Mutation of the *CER10* gene, which encodes an ECR, caused a

reduction of wax abundance (Zheng et al., 2005). However, the *dpp* mutation in the RLD background did not cause a reduction in wax accumulation or organ fusion. The reason for this difference is not known, but this difference was also observed in other studies. For example, the appearance of crinkled and fused leaves in the *abnormal leaf shape1* (*ale1*) mutant depended on the genetic background, and the mutant phenotypes could be observed in the Landsberg *erecta* background but not in the Columbia and Wassilewskija genetic backgrounds (Watanabe et al., 2004).

Mutations in CER10/ECR caused a change in the VLCFA content of sphingolipids (Zheng et al., 2005). Sphingolipids play a role in generation and maintenance of cell polarity. Genetic or pharmacological inactivation of sphingolipid synthases not only prevents polarized hyphal growth, but it also abolishes cell polarity establishment (Cheng et al., 2001). This result was further confirmed by distinct sphingolipid synthases with a chemical genetic approach (Li et al., 2006). The epidermal leaf pavement cells in the *cer10* mutants displayed a three-fold reduction in size and less pronounced lobing, when compared to these cells in wild-type leaves. Aberrant cell shapes were caused by a disruption of trafficking since the Golgi stacks aggregated, forming ring-like structures in the *cer10* mutants (Zheng et al., 2005). The *dpp* mutant in the RLD background also exhibited a change in the trichome shape at the restrictive temperature, but the wax and other phenotypes were normal.

DPP is Vital for Plant Viability

DPP codes for a KCR, a subunit of FAE for VLCFA synthesis. In distinct FAEs, specificity of each elongation reaction on different chain length substrates is determined by the selectivity of a KCS (Millar and Kunst, 1997). A large family of 21 KCS-like sequences in the Arabidopsis genome contributes to wax biosynthesis, which takes place

in several different tissues at different stages of plant development (Kunst and Samuels, 2003; Costaglioli et al., 2005; Suh et al., 2005). In contrast, two KCRs apparently have no particular acyl chain length specificity and are shared by distinct FAEs (Kunst and Samuels, 2003). In the yeast genome, because only one gene was found to code for each KCR, *TSC13* coding for ECR is essential for yeast viability (Kohlwein et al., 2001), but *YBR159w* coding for a KCR is not essential (Beaudoin et al., 2002). In the Arabidopsis genome, five genes code for ECRs (Costaglioli et al., 2005). Mutations in CER10/ECR disrupted normal shoot development and cell expansion, but plants were viable (Zheng et al., 2005). The genes coding for KCR are At1g67730/DPP and At1g24470. These two proteins are 44% identical and 68% similar to each other (Kunst and Samuels, 2003). Based on microarray analysis, At1g67730 was expressed to significant levels, but At1g24470 expression is low (Costaglioli et al., 2005). Therefore, it is likely that DPP is the major component of FAE. The Salk-096487 line having a T-DNA inserted in an exon of At1g24470 displayed no visible phenotype (Xiaoguo Zhang, Unpublished data).

DPP is Likely to be _DEADHEAD_

The *deadhead* mutation was mapped to chromosome I. It maps to the same location as the *dpp* mutation. More importantly, among *deadhead*, *bulkhead* and *hothead*, only the *deadhead* mutant displayed no wax on stems (Lolle et al., 1998). The F1 from the combination of the *dpp* mutant and Salk line143505 also displayed this waxless phenotype on stems. Therefore, it is possible that the *DPP* gene is the *DEADHEAD* gene. Unfortunately, a complementation test between *dpp* and *ded* is not possible, because *dpp* is dominant.

Future Perspectives

DPP encodes a ketoacyl reductase that is one major component of the fatty acid synthesis complex. The *dpp* mutation causes disproportionate trichomes, which have longer stalks and shorter branches as compared to wild type trichomes. Interestingly, the *dpp* trichome phenotype is temperature sensitive: below 22°C, the trichomes showed the *dpp* phenotype, whereas at temperatures above 24°C, the trichomes appeared normal. Additionally, the *dpp* mutation was monogenic, dominant, and homozygous lethal. A two-base (GC) deletion in the *dpp* gene causes a 30 amino acid-truncation from the C terminus of encoded ketoacyl reductase. Based on these results, several interesting questions come to mind. For example, why does this truncated ketoacyl reductase generate a dominant trichome phenotype? Is it a gain-of-function mutation or a loss-of-function mutation? Why and how is this truncated protein so sensitive to temperature? To answer these questions, biochemical assays *in vitro* need to be performed. For example, activity of the wild type and truncated DPP can be compared *in vitro*, at different temperatures.

Plants heterozygous for *dpp* have only defective trchomes. However, our results shows the F1 plants from the cross of the dpp mutant with the T-DNA insertion line containing a T-DNA in 5' UTR of *DPP* display pleitropic phenotypes including collapsed trichomes, crinkled leaves, fused floral organs, and waxless stems. Some of these phenotypes are similar to the phenotypes seen in *deadhead* (*ded*) mutants. In addition, the *ded* mutation has been roughly mapped to the south end of chromosome 1, which is the same location of *DPP*. Currently it is not known if *DPP* and *DED* are same gene. A simple complementation test between *dpp* and *ded* cannot be done, because *dpp* is a dominant mutation. To address this question, the *DPP* genes from multiple alleles of *ded* mutants

need to be sequenced. If all the *ded* alleles have mutations, then it is likely that *ded* and *dpp* are the same gene.

Published data show that mutations in the gene encoding an enoyl reductase, which is another major subunit of the fatty acid synthesis complex, caused defects in the Golgi apparatus. Leaf epidermal cells of the mutant display many clustered Golgi stacks. It would be interesting to examine the organization of the Golgi stacks in the dpp mutant. If the *dpp* mutant shows altered Golgi organization, then this result would support the idea that the Golgi apparatus plays an important role in cell expansion, and that fatty acid synthesis is crucial for proper membrane trafficking. To visualize the Golgi apparatus in live plant cells, the Golgi-labeled markers such as ST-YFP can be used for this study.

Table 4-1. Primers sequence used in this study

Primer name	Sequence(5'→3')	Use for*
dCAPS3F	GTAGTCGCCTTGAGAAAATCTTC**A**	*Nde*I at At1g68060
dCAPS3R	CCATTGCCTTTGTTAAAGTTTCA	
dCAPS6F	GGTCGCTTCGAGAACAACA**T**TA	*Mse*I at At1g67865
dCAPS6R	GGTGTGGTCAGGAGTCCTTTA	
dCAPS7F	GAGAGAATCACACGAATTCAAAAGAAA**C**C	*Mnl*I At1g68140
dCAPS7R	GGTGATAGCAGAAAGGCCAAAA	
dCAPS9F	GGGGTTCTGTCTACTGTGGTAACTCCA**T**	*aTag*I at AT1G67850
dCAPS9R	GGTATTGGATCTTATTTAGAAGCCTC	
dCAPS10F	CCACTCTTTAAATGGAAAATCTGGTCATCATC**T**A	*Xba*I at BAC F12A21
dCAPS10R	TGCTTGCAATTGTGATCATCTTG	
T30E16-57F	ACACTCTTTACTGGAAGATGCAA	RLD 138/Ler 81
T30E16-57R	AACACACCCATGCAAGTGAA	
F12P19-26F	CTGGAAATATCTGCGAAGTGGAA	RLD 119/Ler 93
F12P19-26 R	CATGAACTGTTTGTGCATCTCTG	
T1F15-42F	GCTGATAAGCGTATCATCACACA	RLD 153/Ler 111
T1F15-42R	GGTGCGCCATCAAATAATGT	
F5A8-15F	TGGAGTTAACATATTTTTAATTTATCC	RLD 143/Ler 128
F5A8-15R	GTGGTCAACATCACATTAAAAACA	
T22E19-6F	CCCAATCTAACGGATTTGAAT	RLD 92/Ler 86
T22E19-6R	GGGCTTTGTTTCTTGTGAAAT	
T26J14-42F	GTCTTTCAACTGGTTTCAAATTTGT	RLD 102/Ler 102
T26J14-42R	GTTCCATTTTGGTACTTAGTAATGGAC	
T6C23-20F	CGCTACTAAATTTGGTGGGGGTT	RLD 118/Ler 98
T6C23-20R	TGAGCCTAAAACTTTAACTTCTGC	
720S1	GCGACCTATAGAGGAGGCATTATTGCG	Identification of *DPP*
720S2	CCTTTTGTTCTGTCTCAAGTTACAGG	
730S1	GGCAACAGCAACCAAGTGCATGTCTC	Identification of *DPP*
730S2	CCTTGCTTACTAGCTTCCTCGAGC	
730cod1	CCTTGAAGAGACGCAAACCAT	Identification of *DPP*
730cod2	TTCTATCCACCTTCGTCCCTT	
DEd7	CGTCTTCTCTTCCCTCAGCTA	Identification of *DPP*
DEd8	CACTAGACTGGCTAACTCGGC	

* The primers here are used for the *DPP* mapping and identification. For mapping, dCAPS and SNP markers are listed, for example, two primers, dCAPS3F and dCAPS3R, are a primer pair for a dCAPS marker which is located at the gene At1g68060. When the PCR products from this primer pair are digested by *Nde*I a difference in the size of the digested DNAs between the ecotypes of RLD and Ler will be observed. The degenerated bases are bold and underlined. Similarly, T30E16-57F and T30E16-57R is a primer pair for a SNP marker. The PCR products from them display a difference in size. For the RLD ecotype, a 138-bp DNA is seen, whereas for the Ler ecotype the size is 81 bp.

Table 4-2. Segregation of trichome phenotypes in F2 of the *dpp* mutant crossed to wild-type plants

Genotype	*dpp*	Wt	Total	X^2 value*	P value*
dpp/+ RLD wild type	403	148	551	10.3662	>0.001
dpp/+ Col wild type	178	65	243	4.7407	>0.01
dpp/+ Ler wild type	322	135	457	2.8981	>0.05

* is the ratio of 2:1.

Table 4-3. Segregation of trichome phenotypes in F1 of the *dpp* mutant reciprocally crossed to wild type plants

Genotype	*dpp*	Wt	Total	X^2 value (1:1)	P value (1:1)
LD wild type/*dpp*	72	79	151	0.3245	>0.50
dpp/RLD wild type	75	106	181	5.3094	>0.01
Salk_143503/*dpp*	23	35	58	2.4828	>0.20
dpp/Salk_143503	44	114	158	31.0127	<0.001

Table 4-4. Single nucleotide polymorphism identified between the Ler and RLD ecotypes

Gene name	Position*	Ler	RLD
At1g67790	ATTCCGTATGACGATACAT**A**/**T**GACCGATTCTTT	A	T
At1g67760	ATTACTCAGCTCCATTAAT**T**/**G**TTCAACTTCATC	T	G
At1g67760	ATCAACCTTTTGTCTTTTA**G**/**A**CTGTCTTCACCT	G	A
At1g67670	ATAGGATTTGTCGAGACTT**G**/**T**TTTTTGTTTAT	G	T

* Red bold letters represent single nucleotide polymorphisms between the Ler and RLD ecotypes

Table 4-5. Segregation of phenotypes in the F1 of the *dpp* mutant crossed to the Salk lines

Gene name	Salk line	Position	*dpp*	Wt	Total	% *dpp*	º C
At1g67730	Salk_143503	300-UTR5	11	41	52	0.21	20
At1g67730	Salk_143503	300-UTR5	9	22	31	0.29	24
At1g67730	Salk_039982	300-UTR5	14	41	45	0.31	20
At1g67730	Salk_039982	300-UTR5	10	40	50	0.20	24
At1g67750	Salk_095735c	300-UTR5	6	13	19	0.32	20
At1g67750	Salk_017335c	300-UTR5	34	28	62	0.55	24
At1g67750	Salk_017336	300-UTR5	36	50	86	0.42	24
At1g67680	Salk_025786	Exon	11	11	22	0.50	24
At1g67770	Salk_129146	Exon	34	47	81	0.42	24
At1g67620	Salk_100543	Exon	26	32	58	0.49	24
At1g67630	Salk_017965	300-UTR3	20	40	60	0.33*	24

*The hybrid seeds were collected 9 days after pollination, whereas others were 15 days after pollination.

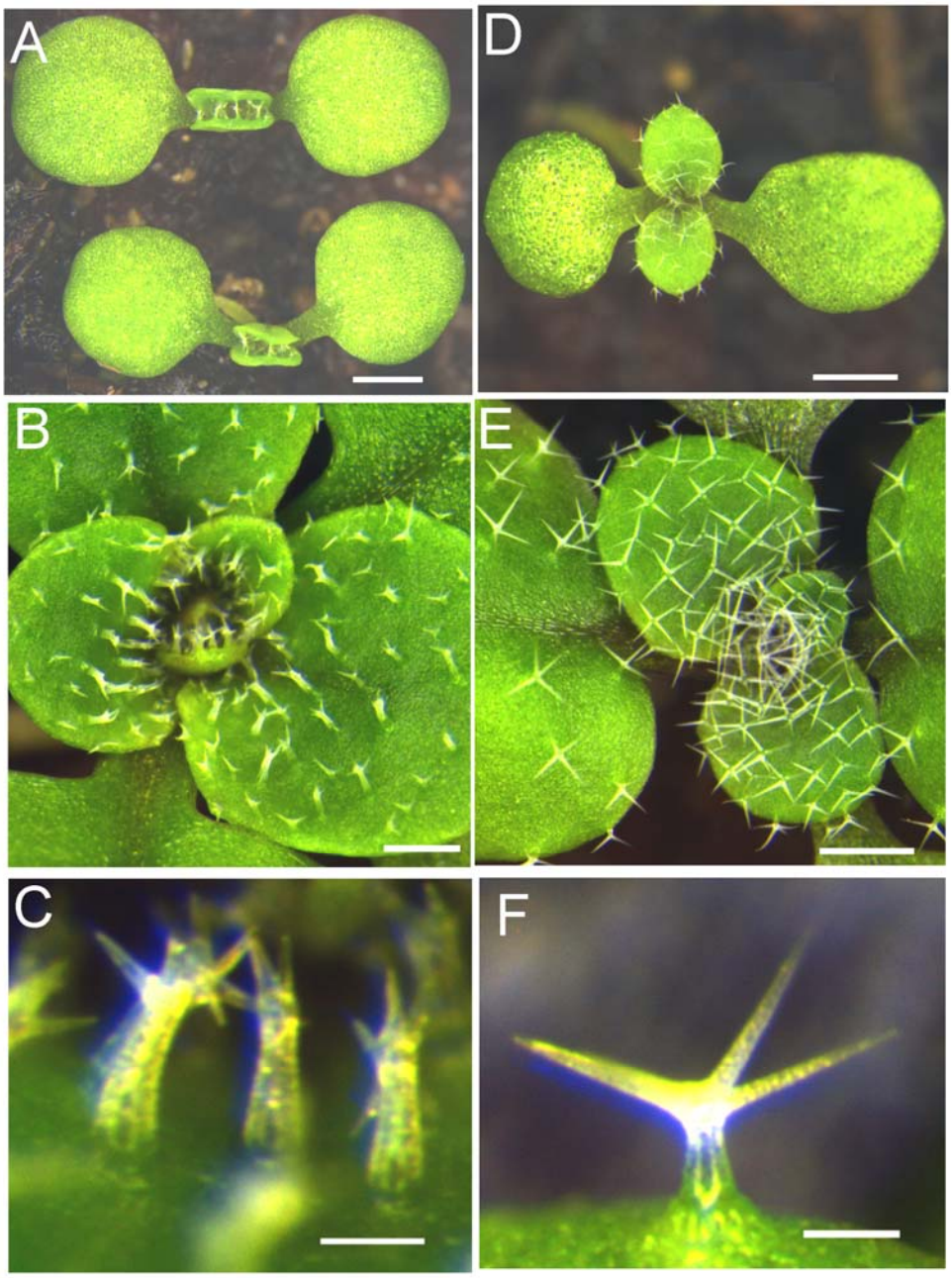

Figure 4-1. The *dpp* mutant trichomes in the RLD genetic background. (A), (B), and (C): *dpp* mutants; (D), (E), and (F): RLD wild type. Bar = 1000 μm in (A) and (D), 100μ in others.

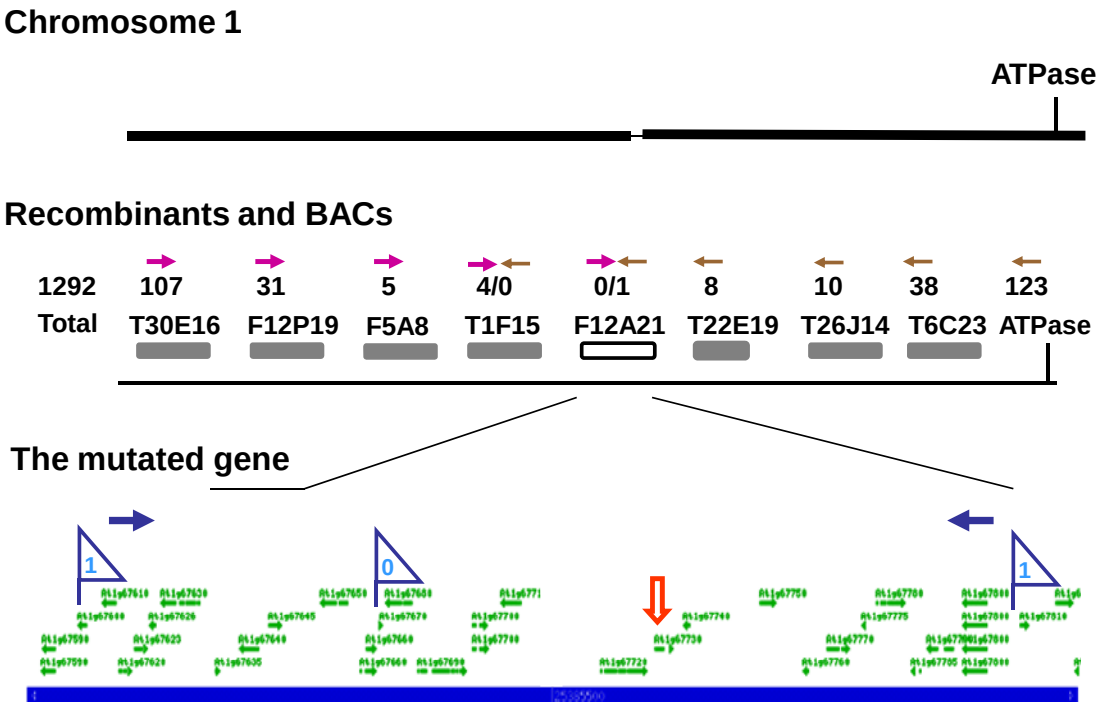

Figure 4-2. Positional cloning of *DPP*. The *dpp* mutation was mapped near SSLP marker ATPase on chromosome 1. Additional molecular markers were used to map the *dpp* mutation to BAC clone F12A21. The numbers of recombinants (out of 1292 chromatids screened) are given above BAC clones. The locations of all putative genes on BAC clone F12A21 are listed. The numbers inside the flags above specific genes are recombinant event numbers at that the specific location. *DPP* is indicated by the vertical arrow.

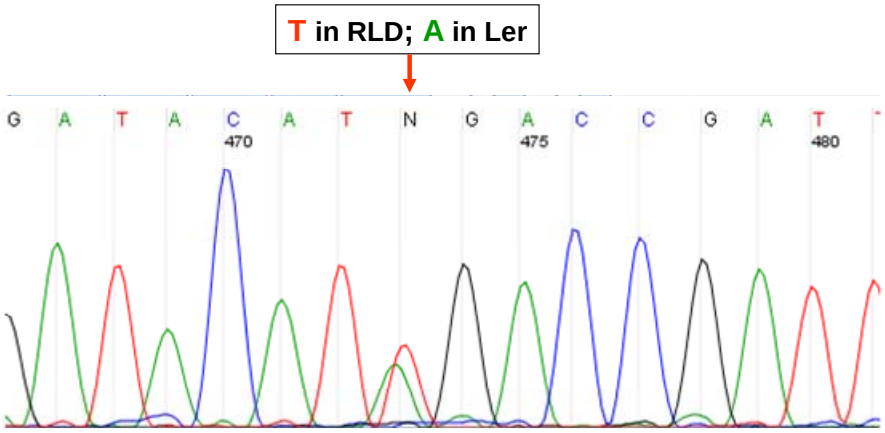

Figure 4-3. Single nucleotide polymorphism between RLD and Ler wild types. N is indicating a single nucleotide polymorphism in the gene At1g67790 between RLD and Ler wild types. N = T in the RLD wild type; N = A in the Ler wild type

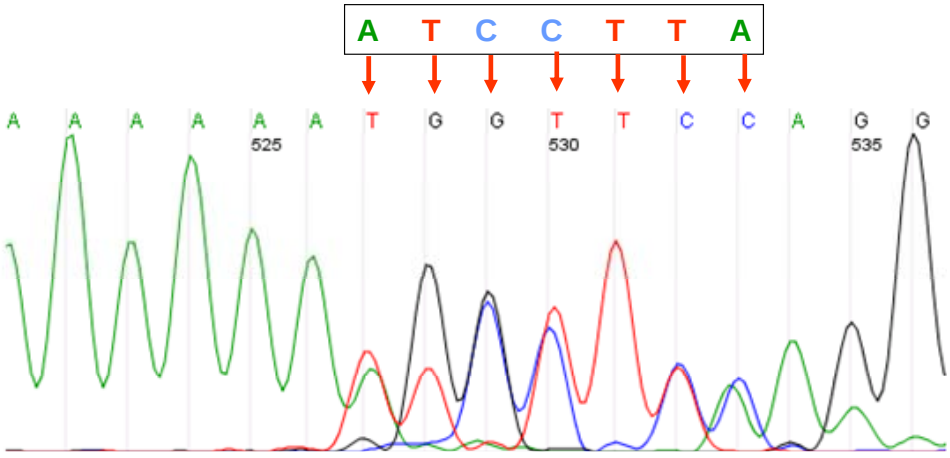

Figure 4-4. Equivocal sequencing result using the DNA template from plants heretozygous for the *dpp* mutation. The overlapping peaks at an exon in At1g67760 are showing in the rectangle, using DNA from *dpp* mutant plants.

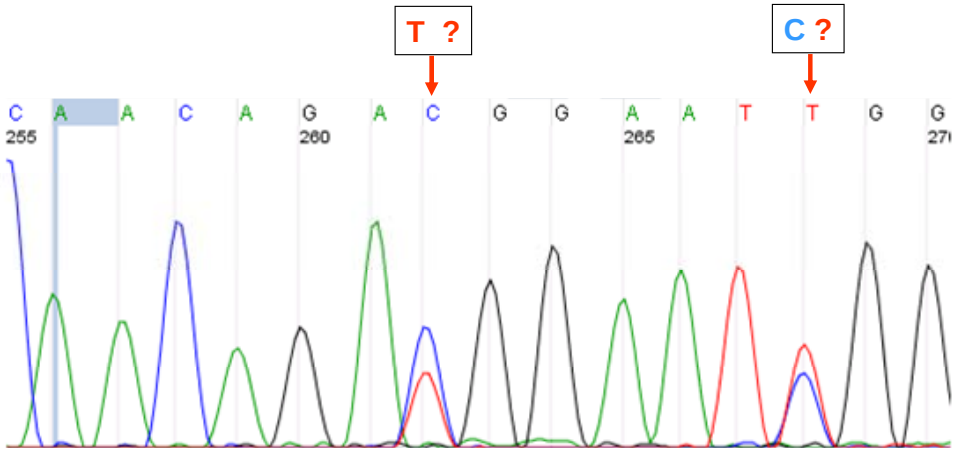

Figure 4-5. Sequencing result of At1g67730 using the *dpp* mutant DNA as a template. The indistinguishable bases are showed inside the rectangles, but they are distinguishable in the repeated experiment in Figure 4-11.

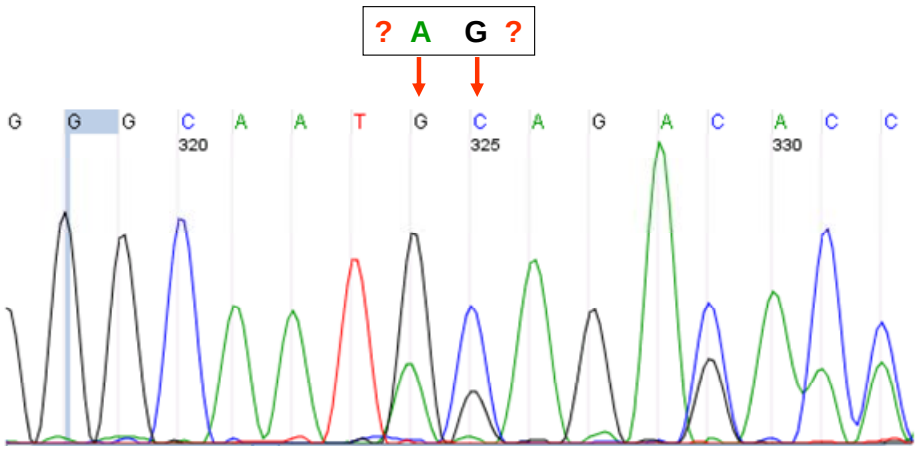

Figure 4-6. Sequencing result of At1g67730 using the *dpp* mutant DNA as a template. The bases of interest are showing indistinguishable inside the rectangles.

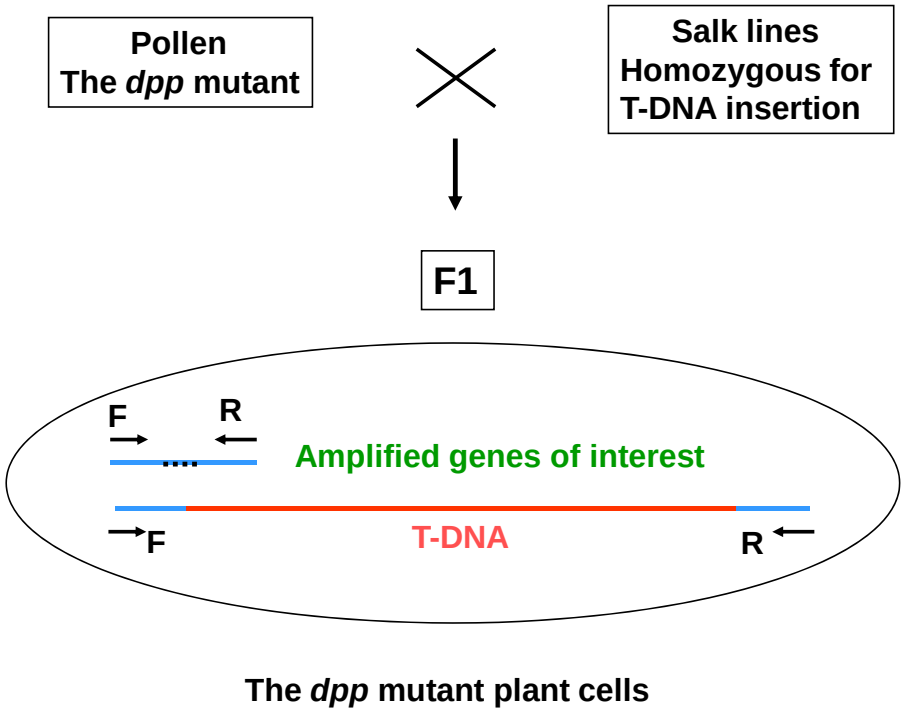

Figure 4-7. Schematic explanation of *DPP* identification. The cross of *dpp* mutants with T-DNA insertion lines for *DPP* identification. The F1 is generated by a cross with *dpp* mutants as the male parent and Salk lines homozygous for T-DNA insertion as the female parent. DNA is amplified by PCR with primers flanking the inserted T-DNA. No PCR product is amplified because of a large size of T-DNA between the regions, parts of which end sequences are identical with the designated primer pairs.

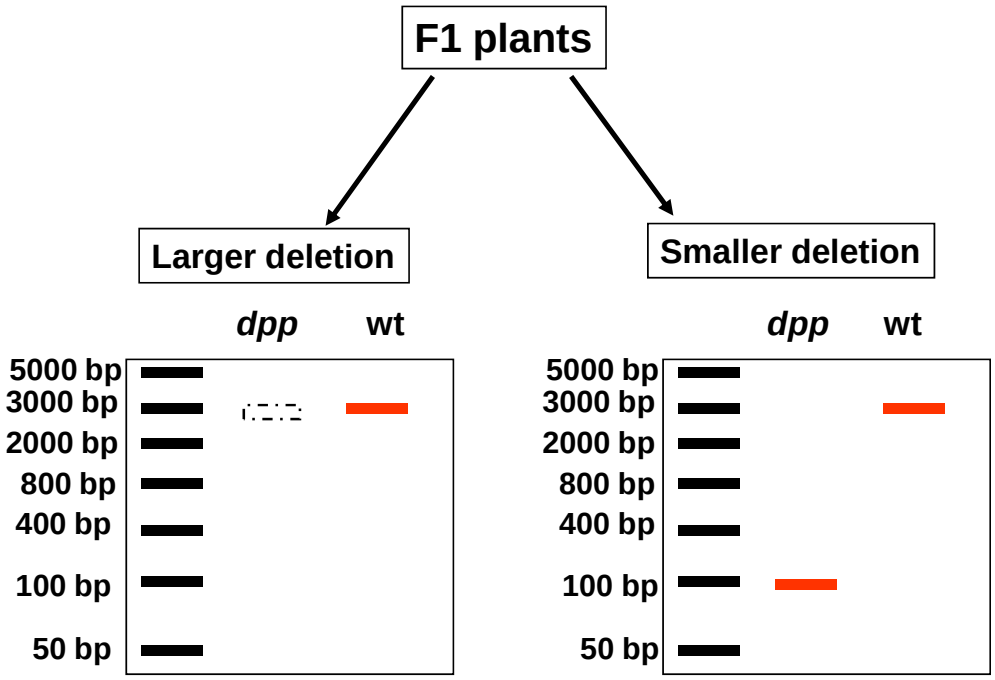

Figure 4-8. Schematic explanation of deletion identification in *dpp* mutants. F1 seedlings are segregated into the *dpp* and wild-type (wt) plants. DNA is extracted from these two kinds of plants, using for PCR as the template with primers indicated in Figure 4-7. The size of PCR products from *dpp* mutants and wt DNA are identified by running gels. The deletion of *dpp* mutations is roughly determined by band positions.

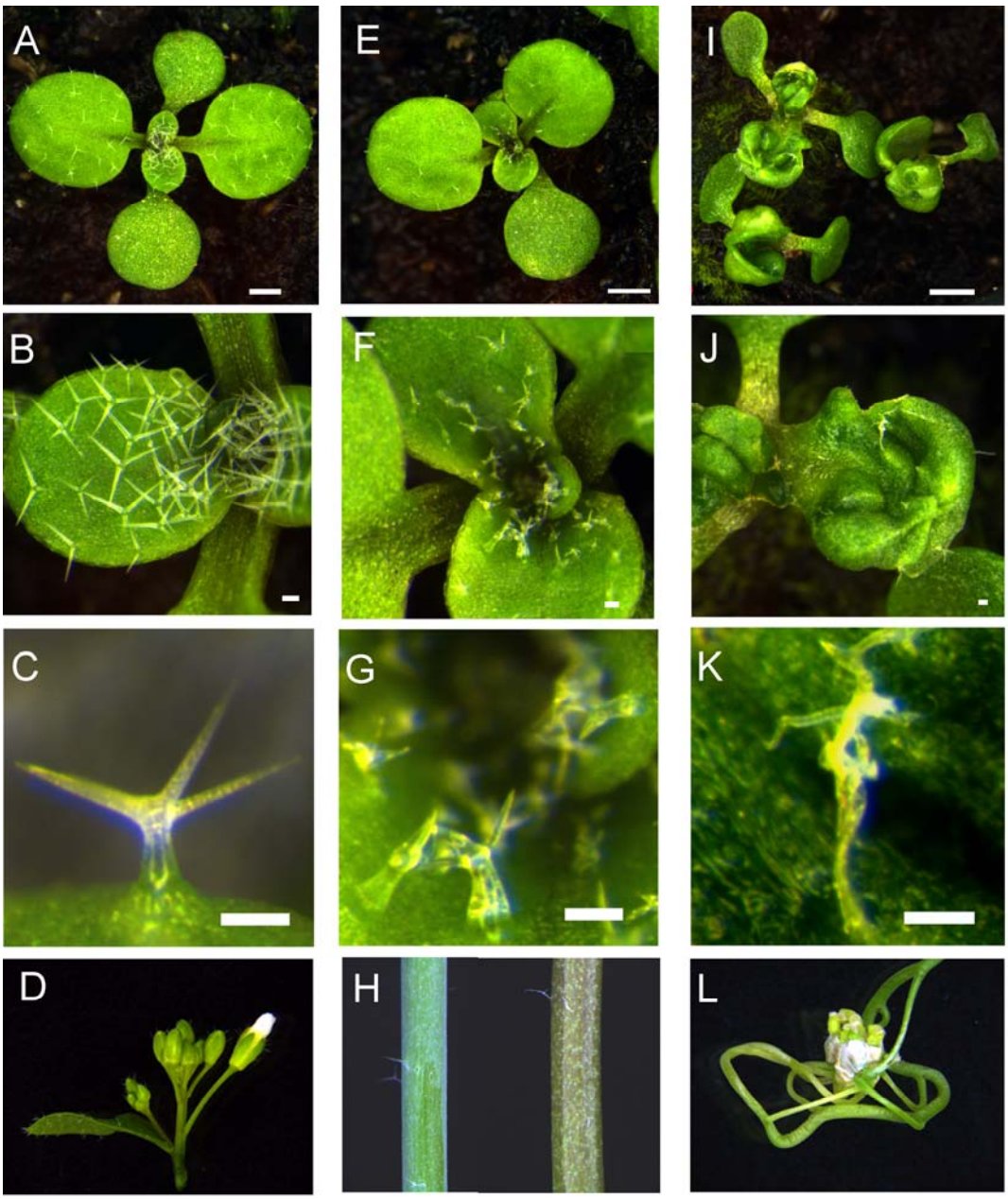

Figure 4-9. Novel phenotypes in the F1 of *dpp* mutants and T-DNA insertion lines. (A), (B), (C), and (D): RLD wild type; (E), (F), and (G): *dpp* mutants heterozygous for the *dpp* mutation and wild type. I, J, and K: F1 heterozygous for the *dpp* mutation and T-DNA insertion. (H) Showing the wax stem of the Col wild type (left) and the waxless stem of the F1 plant (right). (L) Showing fused organs of floral meristems. Bar = 1000 μm in (A), (E), and (I); 100 μm in others.

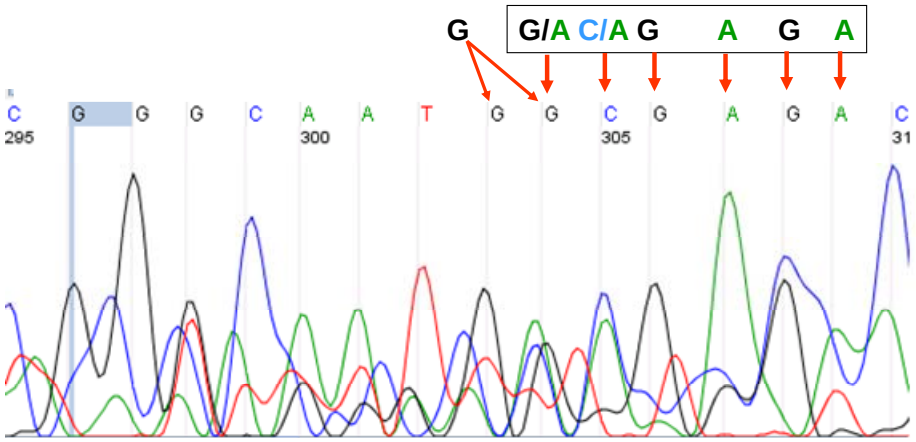

Figure 4-10. Equivocal sequencing result of At1g67730, using the DNA from *dpp* mutants as the template by the reward primer in the repeated experiment. The bases of interest are showing indistinguishable in the rectangle.

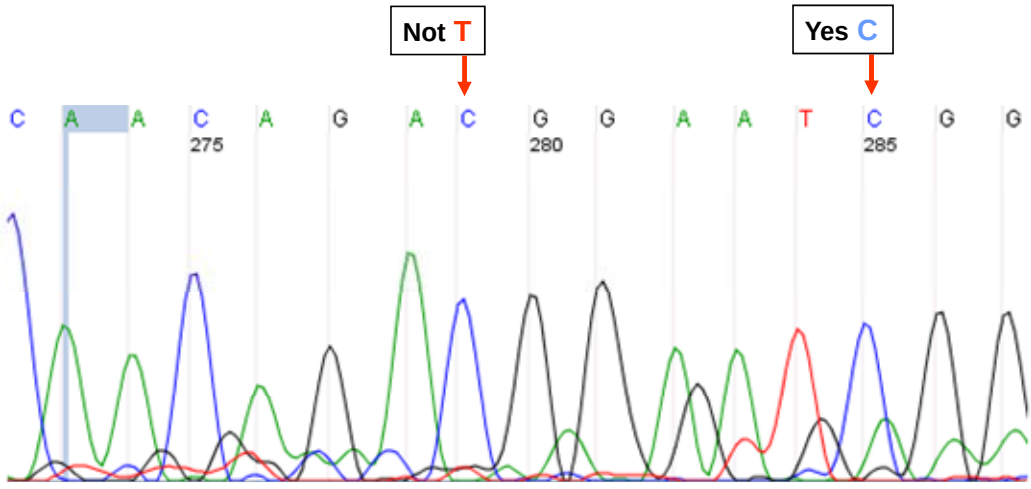

Figure 4-11. Unequivocal sequencing result of At1g67730, using the same DNA as in Figure 4-10 in the repeated experiment by the forward primer. The bases of interest, indicating two indistinguishable bases in Figure 4-5, are showing unequivocal.

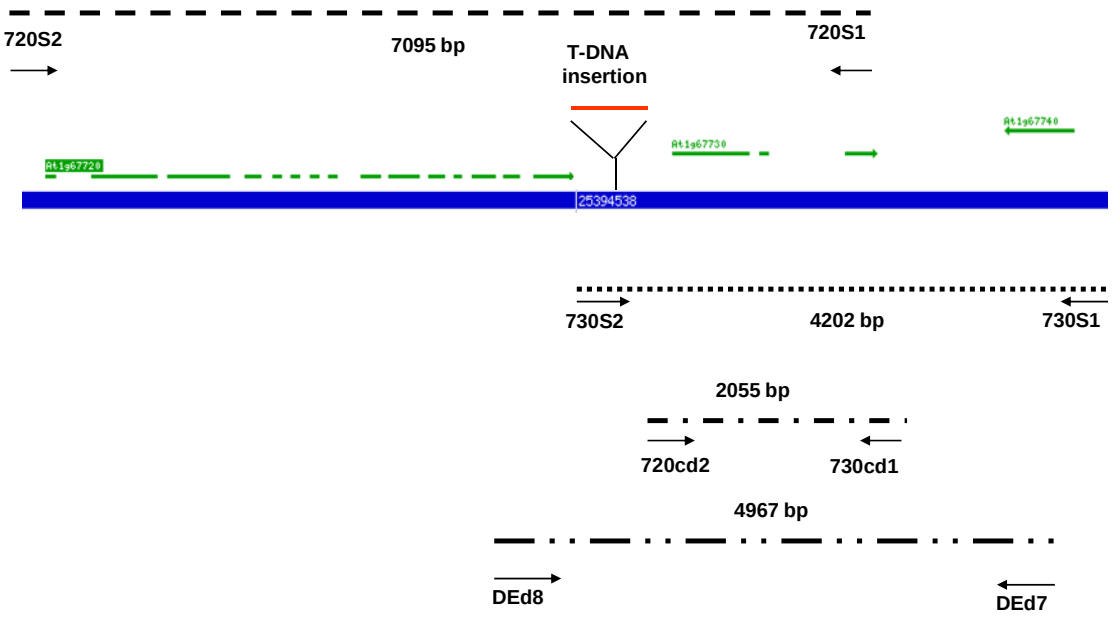

Figure 4-12. Identification of *DPP*. Gene structure of *DPP* and its neighboring genes are showing exons in green segmental lines. The T-DNA insertion is showing between the coding sequences of *DPP* and its neighbor genes. The specific primers used in the *DPP* identification are showing their positions.

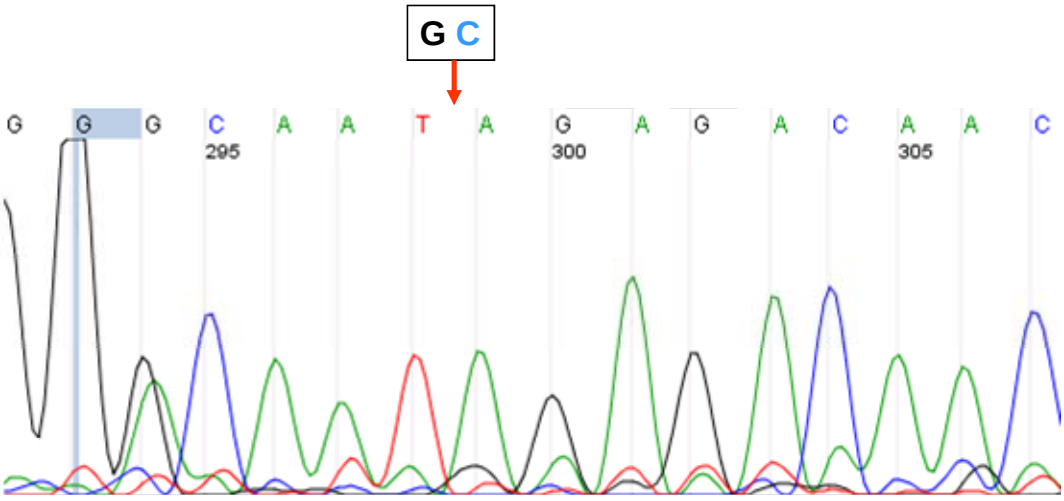

Figure 4-13. Unequivocal sequence result of At1g67730, using the DNA from *ded* plants of F1 in the combination of *dpp* mutants and Salk_143503 as the template. The deleted bases of interest are showing inside the rectangle.

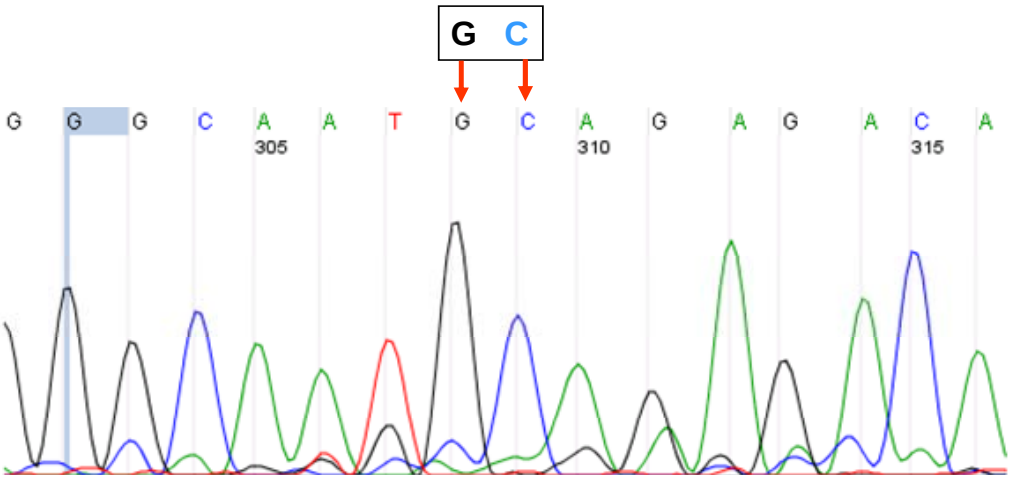

Figure 4-14. Unequivocal sequencing result of At1g67730, using the DNA from the wild-type plants of F1 in the combination of *dpp* mutants and Salk_143503 as the template. The bases of interest are showing inside the rectangle.

Figure 4-15. GC deletion in *dpp* cloned into pBluescript SK

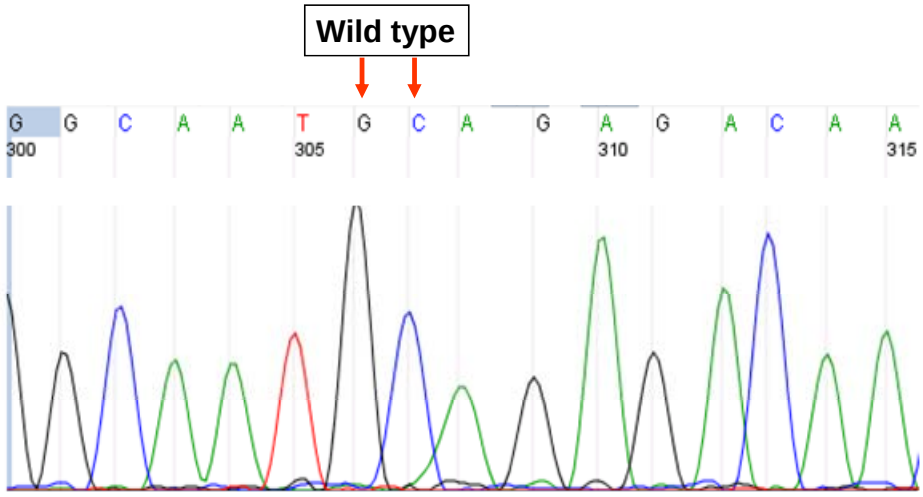

Figure 4-16 Wild-type *DPP* cloned into pBluescript SK

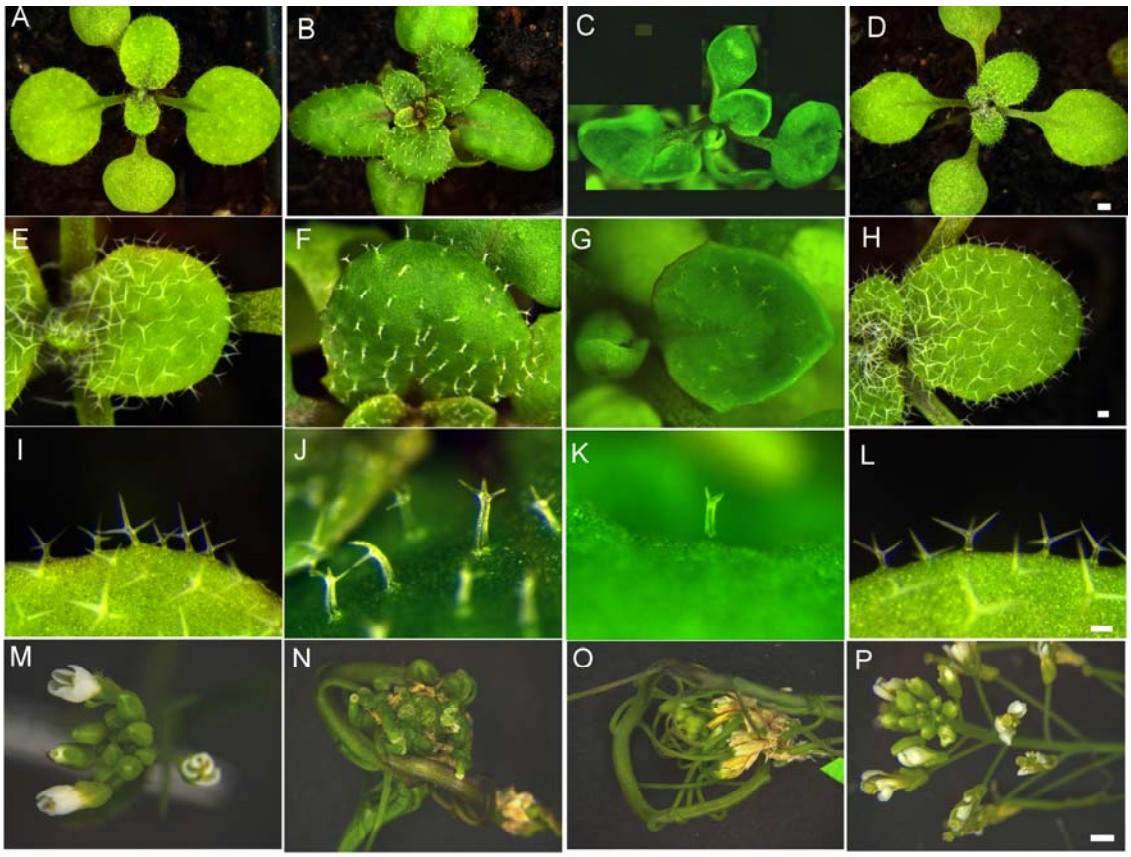

Figure 4-17. Transgenic plants with the mutated *DPP* in distinct genetic backgrounds. (A), (E), and (I): RLD wild type; (B), (F) (J), and (M): transgenic plants with the mutated *DPP* in the RLD wild-type ecotype; (C) (G) (K), and (O): transgenic plants with the mutated *DPP* in the Col wild-type ecotype; (D), (H) (L), and (P): Col wild type. (N): F1 between *dpp* mutants and Salk_143503. Bar = 500 µm in (A), (B), (C) and (D); 200 µm (E), (F) (G), and (H); 100 µm in (I), (J), (K), and (L); 1000 µm in (M), (N), (O), and (P).

CHAPTER 5
IRREGULAR TRICHOME BRANCH 4 IN ARABIDOPSIS ENCODES THE PLANT HOMOLOG OF THE 64 KDA SUBUNIT OF CLEAVAGE STIMULATION FACTOR AND REGULATES TRICHOME MORPHOGENESIS AND FLORAL DEVELOPMENT

Introduction

Polyadenylation includes two sequential reactions—endonucleolytic cleavage and adenylate-residue addition at specific poly(A) sites in 3' non-coding sequences of pre-mRNAs. During eukaryotic development, polyadenylation plays an important role in the regulation of gene expression through contributions to transcription (Zorio and Bentley, 2004), mRNA export to the cytoplasm (Vinciguerra and Stutz, 2004), mRNA stability, and translation efficiency (Wilusz et al., 2001). The specific cleavage at the 3'-end of pre-mRNAs is performed mainly by two complexes: cleavage and polyadenylation specificity factor (CPSF) and cleavage stimulation factor (CstF) (Zhao et al., 1999). In mammalian cells, the former is a heterotetramer consisting of the CPSF-160, CPSF-100, CPSF-73, and CPSF-30 subunits, which are necessary for both cleavage and polyadenylation (Murthy and Manley, 1992), while the latter is a heterotrimer that is composed of CstF-77, CstF-64, and CstF-50 subunits (Takagaki et al., 1990). A a recent model hypothesized that each component in the CstF complex is a homodimer (Bai et al., 2007). The CstF complex is required for cleavage, but is dispensable for the synthesis of the poly(A) tail. CPSF-73 is an endoribonuclease that cleaves pre-mRNAs at poly(A) sites (Mandel et al., 2006). CstF-77 functions as a bridge between CstF-64 and CstF-50 (Takagaki and Manley, 1994), and also interacts with the CPSF complex through CPSF-160 (Murthy and Manley, 1995). CPSF-160 specifically binds to the canonical AAUAAA element (Murthy and Manley, 1992). CstF-64 recognizes and binds to a conserved U- or G/U-rich downstream sequence element (DSE) in pre-mRNAs (Takagaki and Manley, 1997). The CstF complex cooperates with the CPSF complex to

facilitate stable binding of both complexes to a pre-mRNA, and enhances polyadenylation efficiency (Murthy and Manley, 1992).

CstF-64 is the limiting component for assembly of the active CstF complex (Takagaki et al., 1996). There is increasing evidence that shows that altered levels of CstF-64 expression has a significant impact on 3' mRNA processing, and thus regulates specific gene expression, which modulates eukaryotic development. For example, decreases in CstF-64 expression had a variety of effects on B-lymphoma cells (Takagaki and Manley, 1998). Decreased CstF-64 expression in chicken B cells caused lower IgM heavy chain mRNA accumulation as well as an isoform change due to the utilization of an alternative poly(A) site. Also the cell cycle prolonged, cells arrested in G0/G1, and eventually entered apoptosis. In contrast, increased CstF levels in differentiating mouse and human B-cells had the opposite effect; the cells transitioned from G0 to S phase and were induced to proliferate (Takagaki et al., 1996; Martincic et al., 1998). In mouse macrophages following lipopolysacchride stimulation, a 10-fold increase in CstF-64 expression significantly altered the expression of 51 genes (Shell et al., 2005). The change in gene expression was due to alternative polyadenylation through the choice of either a strong (or weak) poly(A) site, which removed (or retained) instability elements in the mature transcripts (Shell et al., 2005).

Five poly(A) sites, L1 to L5, in the adenovirus major late transcription unit (MLTU) are used for generation of distinct mRNAs through alternative polyadenylation (Larsson et al., 1992; Mann et al., 1993). During the course of adenovirus infection, the activity of CstF in HeLa cells varies (Mann et al., 1993). In the later phases of infection, the activity of CstF was substantially decreased. Additionally, the interaction of CstF with the L3 poly(A) site of the MLTU was found to be more stable than the interaction of CstF with the L1 poly(A) site and the L3 site was used

three times more frequently than the L1 site. These events are essentially a reverse of the events observed during the early phases of infection (Mann et al., 1993). CstF-64 expression was also reported to vary in other cell types. Mouse testicular cells contain at least 250-fold more CstF-64 mRNA than liver cells (Dass et al., 2001). Male germ line cells in meiosis, have no detectable CstF-64 mRNA (Wallace et al., 1999).

The *Arabidopsis* homologs of mammalian CstF have been cloned, and were named AtCstF-77, AtCstF-64 and AtCstF-50. Additionally, biochemical assays *in vitro* show that AtCstF-64 binds to mRNA 3' non-coding regions, and interacts with AtCstF-77 similarly to the mammalian CstF-64 (Yao et al., 2002). However, the role of AtCstF in the control of plant development has not been demonstrated. Here, we report the identification of a developmental role for AtCstF-64 in Arabidopsis. Our results show that AtCstF-64, encoded by the *ITB4* gene, is highly expressed in growing and proliferating cells, and it is required for normal trichome morphogenesis and floral development. Although the basic mechanism is widely conserved in all eukaryotic cells, results of our functional analysis of CstF-64 suggest that key differences exist in the specific mechanisms of mRNA 3'-end processing among yeast, plants and mammals,

Materials and Methods

Plant Materials and Growth Conditions

The *itb4-1* and *zwi-3* single mutants and the *itb4-1 zwi-3* double mutant are in the Columbia (Col) genetic background (Zhang et al., 2005b). A novel *itb4* mutant allele (*itb4-2*) is also in the Col genetic background. Seeds were sown on a soil-less potting medium, Fafard 2 Mix (Conrad Fafard Inc. Agawam, MA 01001, USA). Seedlings were grown at 24°C under constant light, which was provided by 40W cool white fluorescent tubes. Plants were watered with PGP nutrient solution (Pollock and Oppenheimer, 1999) every two weeks.

The *itb4-2* Mutant Isolation and *ITB4* Cloning

The F2 mapping population for cloning *ITB4* was generated as described by Zhang et al., (2005). A total of 2310 phenotypically *itb4 zwi-3* double mutant plants were selected from the F2 population. One of the cotyledons was removed from each selected plant for DNA extraction with the RED Extract-N-Amp plant PCR kit (Sigma-Aldrich, St. Louis, MO). The isolated DNA was used to map the *itb4-1* mutation relative to simple sequence length polymorphisms (SSLPs) (Bell and Ecker, 1994; Lukowitz et al., 2000). After the *itb4-1* mutation was mapped to a narrow region where the SSLP markers were not available, cleaved amplified polymorphic sequence (CAPS) markers were used (Konieczny and Ausubel, 1993). Landsberg *er* genomic information provided by Monsanto's Cereon SNP database (http://www.arabidopsis.org/Cereon/index.jsp), was used to design the SSLP and CAPS primers for fine scale mapping. Finally the *itb4* mutation was narrowed down to an approximately 41-kb region, where no additional markers were available. All of the putative genes in this region were examined for mutations by sequencing PCR products amplified from *itb4-1* mutant DNA. Putative mutations were re-checked through sequencing or enzymatic digestion of the PCR products from different template DNAs isolated from 20 individual double mutant plants from the F2 mapping population, the *zwi-3* single mutant and Col wild type. The primers used for these gene amplifications are listed Table 1.

To confirm that we had identified *ITB4*, the SALK T-DNA insertion line, SALK_131655, was ordered from Arabidopsis Biological Resource Center (The Ohio State University, Columbus, OH). The seeds were sown on plates containing MS medium with 1% sucrose and 50 μg/ml kanamycin. Kanamycin resistant seedlings were transferred into pots, and seeds of individual plants were collected separately and sown into different pots. The phenotypes of the resulting plants were characterized. The T-DNA insertion in SALK_131655 was confirmed by

PCR and sequencing using the *ITB4*-specific primers. Loss of detectable full-length *ITB4* transcript in this allele was verified by RT-PCR.

Transgene Construction

For *ITB4* overexpression, the ITB4 genomic region was expressed from either the constitutive 35S promoter, or the trichome and root-hair specific GL2 promoter (Szymanski et al., 1998). The resulting constructs were named *35S:ITB4* and *GL2:ITB4,* respectively. The genomic sequence was amplified by PCR from Col wild type genomic DNA. The PCR fragment was cloned into pENTR1A (Invitrogen, Carlsbad, CA) and transferred into either pAM-PAT-GW (a gift from B. Ulker, Max Planck Institute for Plant Breeding, Cologne, Germany) for expression from the 35S promoter or pCK86 (a gift from A. Schnittger, Max Planck Institute for Plant Breeding) for expression from the GL2 promoter through an LR recombination. To localize ITB4, *35S:ITB4-GFP* and *GL2:ITB4-GFP* were constructed. The PCR fragment was amplified using primer pairs that introduced an *Nco*I site at both ends of the PCR products. The digested PCR products were cloned into the *Nco*I site on the GFP fusion vector, pAVA319 (von Arnim et al., 1998). The resulting gene fusions were liberated by digestion with *Sma*I and *Xho*I, and transferred to either pAM-PAT-GW or pCK86, which were digested by *Pst*I, filled in using *Klenow,* and then digested with *Xho*I. To produce *Gal1:ITB4*, the full-length cDNA of *ITB4* was amplified by RT-PCR using total RNA from six-week-old Col wild-type plants. The PCR product was cloned into pYES-DEST52 (Invitrogen, Carlsbad, CA) through an LR recombination. To produce *35S:hCstF-64*, *35S:hτCstF-64*,*GL2:hCstF-64,* and *GL2:hτCstF-64*, the same 5'-leader sequence (TL) and 3'-terminator (Ter) as in the construct of *35S:ITB4-GFP* were used. The coding sequences of *hCstF-64* and *hτCstF-64* were amplified by PCR from the plasmids containing *hCsF-64* or *hτCstF-64* (gifts from C. C. Macdonald, Texas Tech University

Health Sciences Center, Lubbock, TX). The PCR products were cloned into the modified pNENR1A with TL and Ter elements using *Kpn*I and *Bgl*II. The resulting *TL-hCstF-64-Ter* and *TL-hτCstF-64-Ter* fusions were transferred into either pAM-PAT-GW or pCK86 through an LR recombination. All primers used for the constructs are listed in Table 1, and all PCR products were sequenced to confirm that no mutations were introduced. Sequencing was performed by the Interdisciplinary Center for Biotechnology Research (ICBR) at the University of Florida.

RNA Extraction and RT-PCR

Total RNA was extracted from six-week-old Col wild-type plants using the RNeasy Plant Mini Kit (Qiagen Inc. Valencia, CA) according to the manufacture's instructions. The full length *ITB4* cDNA was amplified using the cMaster RT plus PCR System (Eppendorf AG, Hamburg, Germany). First strand cDNA synthesis was primed using oligo $(dT)_{20}$. The cDNA was amplified using the *ITB4*-specific primers (see Table 5-1). The PCR products were sequenced by ICBR at the University of Florida.

Plant and Yeast Transformations

For ITB4 subcellular localization, the *35S:ITB4-GFP* construct was used to transiently transform onion epidermal cells by particle bombardment using the Biolistic PDS-1000/He Particle Delivery System (Bio-Rad, Richmond, CA). The transformation was carried out using the manufacturer's instructions. Briefly, 5 µL DNA (1 µg/µL) was precipitated onto 3 mg gold microcarriers (Bio-Rad) of 0.6 µm in diameter, by adding 50 µL 2.5 M $CaCl_2$ and 20 µL 0.1 M spermidine. After the precipitated DNA was washed once each with 140 µL 70% and 100% ethanol, it was resuspended in 50 µL 100% ethanol. Ten microliters of this DNA suspension solution was spread on one 1,100 psi rupture disk. The onion epidermal tissue was placed on solid MS medium for bombardment. Fluorescence was visualized after a 36-hour incubation at room temperature in darkness.

The *35S*:*ITB4*, *GL2*:*ITB4*, *35S*:*ITB4-GFP* and *GL2*:*ITB4-GFP* constructs were used to transform *itb4-1 zwi-3* double mutants and Col wild type plants. The *35S*:*hCstF-64*, *35S*: *hτCstF-64*, *GL2*:*hCstF-64* and *GL2*:*hτCstF-64* constructs were used to transform *itb4-1 zwi-3* double mutants. Transformation was accomplished using the floral dip method (Clough and Bent, 1998). The transgenic plants were selected using a 1000X dilution of Finale (5.78% glufosinate-ammonium) (Farnam Companies, Inc., Phoenix, AZ).

The Gal1:ITB4 construct was used to transform yeast using a Yeast Transformation Kit (Sigma-Aldrich, St. Louis, MO) according to the manufacture's instructions. The yeast strains transformed were rna14-1, rna15-1, and w303 wild type. These yeast strains were a generous gift from François Lacroute, Centre de Génétique Moléculaire, Yvette, France. The rna14-1 strain contains a mutation in RNA14 gene, a homolog of CstF-77 in mammals and AtCstF-77 in Arabidopsis; the rna15-1 strain contains the mutation in RNA15 gene, a homolog of CstF-64 in mammals and AtCstF-64 in Arabidopsis (http://www.uky.edu/~aghunt00/polyA2010.html).

Morphological Analysis

Arabidopsis trichomes were isolated from leaves and stained with Toluidine Blue as previously described (Zhang and Oppenheimer, 2004). About 50 plants of *itb4-2* and Col wild type were grown in constant light. After one week when the first flower opened on each plant, 50 flowers for each genotype were selected from different plants, and dissected under the microscope to determine the number of sepals, petals and stamens.

Microscopy

GFP images were obtained with a Zeiss Axiocam HRm camera mounted on a Zeiss Axioplan 2 Imaging microscope using Zeiss Filter set 10 (excitation: 450-490, dichroic: 510 LP, emission: 515-565). Zeiss Filter Set 02 (excitation: 365, dichroic: 395 LP, emission: 420 LP) was

used to collect fluorescent signal from DAPI stained tissue. A Zeiss Axiocam MRc5 camera mounted on a Zeiss Stemi SV11 dissecting microscope was used to obtain light micrographs. Environmental Scanning electron microscopy was carried out at the National High Magnetic Field Laboratory (Tallahassee, FL), in an Electroscan Model E-3 environmental scanning electron microscope. Tissue samples were mounted on moist paper towels and scanned at 20 kV under 1-2 torr pressure.

in situ Hybridization

Fixation, dehydration, and embedding of Arabidopsis inflorescences and young siliques were performed as previously described (Zhang et al., 2005a). RNA probes were made using the DIG RNA Labeling Kit (Roche Diagnostics, Indianapolis, IN) following the manufacturer's instructions. The gene-specific primer pairs and their antisense primer pairs were designed such that a T7 promoter was introduced (Table 5-1) and the transcription templates were prepared by PCR. The steps of in situ hybridization were essentially those described by the Meyerowitz's laboratory at http://www.its.caltech.edu/~plantlab/html/protocols.html, except for the following changes: the 50% Denhardt's Solution (in the hybridization solution) was replaced with 10% Blocking Reagent (Roche Diagnostics, GmbH, Mannheim, Germany), the hybridization temperature was 45° C, and the washing temperature was 50° C.

Results

ITB4 Encodes AtCstF-64

To further understand the role of ITB4 in trichome development, we cloned the *ITB4* gene using positional cloning methods. We generated an F2 mapping population through a cross of the *itb4-1 zwi-3* double mutant with Ler wild type. The *itb4-1 zwi-3* double mutant was used as a parent for the following reasons: first, the *itb4-1* mutant trichomes have three branches with a subtle change only in trichome branch length; second, the *zwi-3* mutant trichomes have two

branches and its mutation was known to be located on chromosome V, unlinked to *itb4-1*; finally, the *itb4-1 zwi-3* double mutant displayed an unequivocal trichome phenotype, i.e., unbranched trichomes. Therefore, we were able to unambiguously identify *itb4* plants in the F2 mapping population. A total of 2310 plants with unbranched trichomes were selected from the F2 population. Through the use of SSLP markers, we mapped the *itb4-1* mutation to a region between BAC clones F23N20 and F28P5 BAC. Using CAPS markers, *itb4-1* was further narrowed down to an approximately 41-kb region on the BAC clone F14O23 according to the TAIR database (Figure 5-1A). This region contains 10 putative genes. All open reading frames in this region were amplified by PCR using genomic DNA from *itb4-1* seedlings. The PCR products were sequenced, and a C to T transition at base 1896 (starting at the A in the ATG start codon) was found in gene *Atg71800*. The mutation, which was located in the last second exon of At1g71800, created a new TAA stop codon, causing an 88 amino acid truncation from the C-terminus of the putative ITB4 protein (Figure 5-1A).

To confirm that this mutation also exists in the *itb4-1 zwi-3* double mutants, we randomly selected 20 DNA samples from the F2 mapping population for amplification of the target sequence that contains the mutated base. Because the mutation creates an *Mse* I cut site in the amplified target sequence, the PCR products were digest with *Mse*I. Our results showed all the *itb4-1 zwi-3* double mutants indeed had the mutated base in the *ITB4* gene (Figure 5-1B).

To confirm that the phenotype observed in the *itb4-1* mutant is caused by the mutation in *At1g71800*, the wild type *At1g71800* gene was expressed in *itb4-1* zwi-3 double mutant plants. The construct used for transformation was a 2800-bp genomic fragment, which contained the 5'UTR (250 bp), the *At1g71800* coding sequence (2245 bp) and the 3' UTR (300 bp), and was expressed from either the 35S promoter or the GL2 promoter. Over 30 independent transgenic

plants for each construct displayed trichomes with two branches identical to the trichomes on *zwi-3* mutants (Figures 5-2C, 5-2D). Occasionally, three-branched trichomes were observed on some transgenic plants (Figure 5-2E). The rescue of the *itb4-1* mutant phenotype by the *At1g71800* coding sequence demonstrates that *ITB4* is *At1g71800*.

Loss-of-function Mutations in *ITB4* Cause Aberrant Development of Trichomes and Flowers

ITB4 contains three functional domains: the RNA recognition motif (RRM) that directly binds to mRNA; the Hinge domain that interacts with CstF-77 in mammals and Arabidopsis; and the PC4/sub1/res1 domain that interacts with polymerase processivity factors in mammals and yeast (Herr et al., 2006). The mutation in *itb4-1* causes a truncation of 88 amino acids at the C-terminus of ITB4. The truncated part includes the KIWI/KELP domain (Cormack et al., 1998), which is homologous to PC4 in mammals and Sub1 in yeast (Herr et al., 2006). The deletion of the KIWI/KELP domain in ITB4 causes only a slight alteration in trichome branch length and branch position. To further analyze the function of ITB4 in trichome morphogenesis, we used a reverse genetic approach to seek a complete loss-of-function mutation in the *ITB4* gene. By searching the SALK T-DNA Express Database (http://signal.salk.edu/cgi-bin/tdnaexpress), we identified eight lines that contained insertions in the *At1g71800* gene: Salk_131655, Salk_088885, Salk_088876, Salk_088877 Salk_150929, Salk_133589, Salk_038729, and Salk_150929. After selection for kanamycin resistance, the progeny from line Salk_131655 segregated plants showing a defective trichome phenotype. Additionally, the segregation ratio of wild type to mutant was nearly 3:1. *ITB4* in Salk_131655 is interrupted by a T-DNA insertion in its last exon (Figure 5-1A). Plants homozygous for the T-DNA insertion in this line were identified by PCR-based screening (Figure 5-1C). This mutant allele was named *itb4-2*. *ITB4*

expression was not detectable in the *itb4-2* mutant by RT-PCR (Figure 5-1D), indicating that *itb4-2* is likely to be a complete loss-of-function mutant allele of *ITB4*.

The mutant phenotype caused by the T-DNA insertion mutation in the *itb4-2* allele is considerably more severe than the *itb4*-1mutant. Because the latter exhibits shorter trichome branches and separate branch positions, it probably represents a partial loss-of-function mutation; however, the former shows dramatic defects in trichome morphogenesis and floral development.

The *itb4-2* plants displayed changes in both trichome shape and trichome cell fate. The branch length and branch positions of the *itb4-2* trichomes were clearly distinguished from wild type. In Col wild type trichomes, 96% trichomes have three branches (Table 5-2) and the lengths of the branches are almost equal. Additionally, the positions of the primary and secondary branch are adjacent or close to each other (Figure 5-3A). However, the branch number of the *itb4-2* trichomes covered a wide range from one branch (Figures 5-3D, 5-3F, Table 5-2) to five branches (Figure 5-3J, Table 5-2) and the percentage of three-branched trichomes is notably decreased. In contrast, the percentage of two-branched trichomes is prominently increased (Table 5-2). The branch lengths and positions of the trichomes on the *itb4-2* mutant show the same characteristics as the trichomes on the *itb4-1* mutant, i.e., unequal branch lengths and separated branch positions (Figures 5-3B, 5-3G-J) (Zhang et al., 2005b).

Interestingly, the *itb4-2* mutation produced trichome clusters, which appeared as "twins" on *itb4-2* plants. The twin frequency was 2.52% in the *itb4-2* mutant, but never observed in Col wild type (Table 5-2). The branch numbers of the twin trichomes varied (Figures 5-3C, 5-3F, 5-3K-N), and they all seem to be conjoined at the bottom of their stalks (Figures 5-3C, 5-3E, 5-3F, 5-3K-J). Separation of the twin trichomes was resistant to treatments with both EGTA and

pectinase (Figure 5-3E) (Zhang and Oppenheimer, 2004), which suggests that the trichomes share part of a cell wall.

The other major defect of the *ibt4-2* mutant is abnormal development of flowers. Beginning with stage 3 during floral development on wild type plants, the abaxial sepal primordia arise first, followed by the adaxial primordia. Entering stage 4, they elongate, curve inward and cover the dome-shaped meristem before petals arise (Figure 5-4A). The developing primordia rapidly enlarge from 30 μm at stage 3 to 70 μm at stage 4 (Smyth et al., 1990). Compared with wild type, the floral primordia on the *itb4-2* mutant displayed aberrant development. First, the sepals elongate slowly and do not cover the floral organ primordia after the petals arise (Figure 5-4B, large arrow). Second, the abaxial sepals preferentially grow (Figures 5-4B, 5-4F) and often fuse with adjacent sepals (Figure 4B, small arrow). Additionally, the numbers of sepals and petals is significantly increased (Figures 5-4B, 5-4C, 5-4F, 5-5); floral buds with seven sepals were often observed (Figure 5-4C). Throughout flower development, the defective sepals were unable to completely enclose the stamens and carpels as in wildtype (Figures 5-4D, 5- 4E). Third, the stigmatic papillae were aberrant (Figures 5-4H, 5-4I). On wild-type stigmas, the papillae stand straight and are regularly arranged, but the papillae on the *itb4-2* mutant displayed irregular shapes and clusters (Figures 5-4H, 5-4I). The anthers of the *itb4-2* mutant contained few pollen grains and the ones that did not form, were mostly unviable (Figures 5-4K, 5-4L). In spite of the extra floral organs, the overall floral bud size was smaller than wild type (Figures 5-4B, 5-4E).

The *itb4-2* mutant plants also showed a relatively minor alteration of rosette leaf color and shape. Col wild-type plants produce green rosette leaves with smooth edges (Figures 5-5A, 5-5C, 5-5E). However, *itb4-2* plants produced yellow-and-green mosaic rosette leaves with serrated

edges (Figures 5-5B, 5-5D). These defects are most prominent in the first leaf pair (Figure 5-6B), while subsequent leaves display a gradual transition toward normal leaf morphology during vegetative growth (Figures 5-6D, 5-6F).

ITB4 is Highly Expressed in Growing and Proliferating Cells

To gain insight into why *itb4* mutations caused the defects in specific cell types and organs, we examined the *ITB4* expression pattern by in situ hybridization. We found that *ITB4* is highly transcribed in developing trichome cells, embryos, meristems and floral primordia during plant vegetative growth and reproductive development (Figure 5-7). At the globular stage of embryo development in Col wild type, *ITB4* was highly expressed in the developing embryo, but not in cells of the suspensor (Figure 5-7A). At the heart stage, *ITB4* expression became stronger (Figure 5-7B), but in mature embryos, *ITB4* expression decreased (data not shown). During germination, *ITB4* was expressed in the apical meristem and provascular cells. The actively dividing cells in the meristem showed higher *ITB4* expression than the growing provascular cells (Figure 5-7C). Developing trichome cells displayed a higher *ITB4* expression level than other epidermal cells (Figure 5-7E). At stage 1 of trichome development, *ITB4* is strongly expressed. The nuclei of trichomes at this stage undergo endoreduplication from 2C to an average of about 8C with a concomitant increase in nuclear volume. This increase in nuclear size distinguishes cells committed to the trichome fate from other epidermal cells (Hulskamp et al., 1994). The strong expression of *ITB4* remains until stage 3 or 4, at which time the trichome size increases rapidly from about 20 μm to 400 μm. During flower development, *ITB4* is strongly expressed in floral meristems (Figure 5-7F). At later developmental stages, strong expression of *ITB4* can be observed in developing stamens and carpels, but weak expression is observed in developed sepals (Figure 5-7G).

Loss of ITB4 Function Alters the Expression Pattern of Perianth Organ Identity Genes

Complete loss-of-function of *ITB4* caused an increase in the number of sepals and petals, but no difference for stamen and carpel numbers. To understand how ITB4 influences perianth development, we examined the expression of the floral organ identity genes, *AP1*, *AP3* and *PI* in the *itb4-2* mutant and Col wild type flowers through in situ hybridization. At stage 3 of floral development, *AP1* expression domain is restricted to the outer two whorls because AG represses *AP1* expression in the inner two whorls of wild type flowers (Figure 5-8A) (Gustafson-Brown et al., 1994). However, in the *itb4-2* mutant, in addition to its strong expression in the outer two whorls at stage 3, *AP1* is ectopically expressed in the inner two whorls at stage 3 and even in stamens and carpels at stage 7 (Figure 5-8B). In wildtype, *AP3* is expressed from stage 3 in the presumptive second and third whorls. After floral stages 5 and 6, *AP3* is expressed throughout the developing petals and stamens, and at the adaxial base of sepals (Figure 5-8C) (Jack et al., 1992). In *itb4-2* mutant flowers, *AP3* expression appears precociously and ectopically in the inner two whorls at the stage 3 (Figure 5-8D). The PI expression pattern in *ibt4-2* mutants is indistinguishable from that in the wild type (Figures 5-8E, 5-8F).

ITB4 Localizes to Nuclei, but Does Not Functionally Complement Tts Homolog in Yeast

ITB4 was annotated as a cleavage stimulation factor by both the Arabidopsis Genome Initiative (http://arabidopsis .org/info/agi.html) and GSF-MIPS (http://mips.gsf.de/proj/plant/jsf/athal/searchjsp/index.jsp). The full length cDNA of *ITB4* was amplified by RT-PCR using Col wild type RNA as a template. The PCR product is identical with the computer-based prediction of both of the databases mentioned above. In silico translation of the *ITB4* coding sequence predicts a protein of 461 amino acids with an isoelectric point of 9.32. This protein sequence is identical to that reported by Yao et al. (2002) for AtCstF-64. Therefore, we renamed the ITB4/At1g71800 protein to AtCstF-64.

AtCstF-64 functions in the cleavage reaction for mRNA 3' end formation. It contains the same three functional domains as its homologs in yeast and mammals. It is generally believed that the CstF complex in plants functions in a similar way to the animal counterparts for mRNA 3'-end processing in nuclei (Yao et al., 2002; Herr et al., 2006). To support this idea, a GFP-tagged version of AtCstF-64, *35S:ITB4-GFP,* was transiently expressed in onion epidermal cells through biolistic transformation. The ITB4-GFP signal was found in nuclei (Fig. 5-9). This result is consistent with the nuclear location of RNA15 in yeast (Bonneaud et al., 1994) and CstF-64 in mammals (Schul et al., 1996). To test the functionality of ITB4-GFP *in vivo*, *35S*:*ITB4-GFP* and *GL2*:*ITB4-GFP* were used to transform *itb4-1 zwi-3* double mutant plants through *Agrobacterium*-mediated stable transformation. Both constructs rescued the unbranched trichome phenotype of the *itb4-1 zwi-3* double mutant, and transformants showed the two-branched trichome phenotype of the *zwi-3* mutant. However, the nuclear localized ITB4-GFP signal was weaker than that observed in onion cells (data not shown). The nuclear localization of the fusion protein supports a function for AtCstF-64 in pre-mRNA processing in Arabidopsis.

To determine if AtCstF-64 function is conserved, we examined the ability of AtCstF-64 to complement yeast CstF subunit mutants. *GAL1*:*ITB4* was used to transform three different yeast strains: *rna151-*, *rna14-1*, and *w303* (wild type). The *rna15-1* strain contains a mutation in *RNA15*, the counterpart of CstF-64 in mammals and AtCstF-64 in Arabidopsis; the *rna14-1* strain contains a mutation in *RNA14*, the counterpart of CstF-77 in mammals and AtCstF-77 in Arabidopsis. The mutations in both strains caused a temperature-sensitive phenotype. At the permissive temperature, 28º C, the *rna15-1* and *rna14-1* strains grow. However, at the restrictive temperature, 33º C, their growth stops. The transformed *rna15-1* or *rna14-1* strains that contained the *GAL1:ITB4* construct could not grow at 33º C, but the transformed wild type strain

grew normally (data not shown). These results indicate that AtCstF-64 does not functionally complement its counterpart in yeast.

To further examine the functional conservation of AtCstF-64, we attempted to rescue the *itb4* phenotype using CstF-64 homologs from mammals. *35S:hCstF-64*, *35S:hτCstF-64*, *GL2:hCstF-64* and *GL2:hτCstF-64* were used to stably transform *itb4-1 zwi-3* double mutant plants. The human counterpart of AtCstF-64, hCstF-64, exhibits 32% identity and 44% similarity to the Arabidopsis protein sequence. The human hτCstF-64 protein is a paralog of hCstF-64 that exhibits 74% protein sequence identity with hCstF-64 and is expressed in male germ cells to maintain normal spermatogenesis (Dass et al., 2001; Dass et al., 2002). None of the transgenic plants showed rescue or any other change in the *itb4-1 zwi-3* double mutant trichome phenotype (data not shown). These results indicate that the mammalian CstF-64 does not functionally complement its counterpart in Arabidopsis.

Discussion

Polyadenylation is a common event that occurs in the nuclei of all eukaryotic cells, during which a majority of mRNAs receive a string of A residues. Additionally, 25% mRNAs in Arabidopsis use alternative polyadenylation sites (Meyers et al., 2004). Alternative polyadenylation of a number of mRNAs has been shown to affect plant development (Cheng et al., 2003; Quesada et al., 2005). Although there is increasing data to suggest that alternative polyadenylation contributes to the control of gene expression in animals, its role in the regulation of development in plants is not well understood. The results presented in this paper are the first report that a plant homolog of a subunit of the CstF complex influences specific events during plant development.

ITB4 Plays a Crucial Role in Trichome Morphogenesis and Floral Development

The *itb4-1* mutation leads to a truncated AtCstF-64 protein that lacks the KIWI/KELP domain, and *itb4-1* plants display only a relatively mild trichome shape defect. The truncated AtCstF-64 protein retains the other important functional domains such as the RRM and Hinge. The function of the KIWI/KELP domain is not well understood in Arabidopsis. It has been proposed that the KIWI/KELP domain interacts with general transcription factors for activation of gene transcription (Cormack et al., 1998). Because AtCstF-64 is single copy gene in Arabidopsis and lack of the KIWI/KELP domain produces few phenotypic effects compared with the likely null *itb4-2* mutation, it is likely that the KIWI/KELP domain is nonessential for AtCstF-64 function. The relatively mild phenotype produced by the *itb4-1* mutation greatly contrasts with the phenotype of the *itb4-2* mutation, which led to profound changes in trichome, leaf, and flower development. These phenotypic defects suggest an important developmental role for AtCstF-64.

The occurrence of twin trichomes in the *itb4-2* mutant suggests that proper trichome cell fate specification requires AtCstF-64 function. Normally, once an epidermal cell acquires the trichome fate, division of that cell ceases. The twin trichomes seen in *itb4-2* mutants are reminiscent of the trichome clusters seen in *siamese* (*sim*) mutants, where incipient trichomes still divide due to a failure to properly enter the endoreduplication cycle (Walker et al., 2000). This phenotype suggests that in *itb4-2*, mRNAs encoding proteins involved in the control of endoreduplication may have altered in expression levels, and hence be direct or indirect targets of AtCstF-64.

Plants homozygous for *itb4-2* also displayed a significant increase in the number of sepals and petals, compared to wild type, although the organs were relatively normal in appearance. These results suggest that early developmental events are more sensitive to loss of At CstF-64

function than later differentiation events. This idea is supported by our finding that *ITB4* is most highly expressed in actively proliferating tissue and organ primordia. A similar developmental role for CstF-64 is seen during mammalian cell differentiation. High expression of CstF-64 is required for normal development of B-lymphocytes. Reduced expression of CstF-64 gave rise to aberrant differentiation and apoptotic cell death (Takagaki and Manley, 1998) Our results support the finding in mammals that the slowly growing or inactively dividing cells may be able to tolerate lower levels of CstF than the rapidly growing or actively dividing cells (Takagaki et al., 1996).

In contrast to the CstF-64 mutations in other organisms, the *itb4-2* homozygous plants are viable. Depletion of CstF-64 in chicken and mouse B lymphocytes caused apoptotic cell death (Takagaki and Manley, 1998). RNA15, the homolog of CstF-64 in yeast, is also essential for cell viability (Minvielle-Sebastia et al., 1991). These differences between plant and animal CstF-64 mutants suggest that plants are more tolerant of loss of CstF-64 function than other eukaryotes.

The recent identification of *ESP1* (At1g73840) in Arabidopsis suggests that there are at least two complexes that contain CstF-64 homologs in Arabidopsis (Herr et al., 2006). The enhanced silencing phenotype (*esp*) mutants affect gene silencing and are involved in RNA metabolism. ESP1 encodes an AtCstF-64 like protein that lacks the RNA-binding RRM domain. It has been postulated that the standard CstF complex contains AtCstF-64 that uses the RRM domain to bind pre-mRNAs. The other putative complex contains ESP1 and uses a separate RNA-binding protein to recognize pre-mRNAs (Herr et al., 2006). The two complexes function redundantly in mRNA 3' end formation, which is likely to be a reason why the *itb4-2* mutation is not lethal.

Loss of AtCstF-64 Function Influences the Expression of Multiple Genes that Control Floral Organ Development

In mammalian cells, altered levels of CstF-64 expression has been shown to influence the expression of at least 51 genes and induce alternative poly(A) site selection (Shell et al., 2005). This is also likely to also occur in plant cells. Our results showed that loss-of-function mutations in *ITB4* caused changes in trichome fate, shape, and floral structure. It is likely that these phenotypic defects are due to changes in the expression of the genes involved in control of trichome morphogenesis and floral development. There are at least 30 genes known to regulate trichome morphogenesis (Schellmann and Hulskamp, 2005). For example, STI, A*N, ZWI, FRC1-4* and *GL3* function as positive regulators that promote trichome branching (Hulskamp et al., 1994; Oppenheimer et al., 1997; Luo and Oppenheimer, 1999); loss of function mutations in these genes cause a decrease in the trichome branch number. Conversely, *TFCA, RFI*, *KAK*, *PYM*, and *SUZ4* function as a negative regulators that suppress trichome branching; mutations in these genes result in an increase in trichome branch number (Krishnakumar and Oppenheimer, 1999; Perazza et al., 1999; Kirik et al., 2002). Mutations in *ITB2* and *ITB3* affect trichome branch length (Zhang et al., 2005b), and mutations in TRY cause trichome clusters (Hulskamp et al., 1994). It is likely that the pre-mRNAs from the above-mentioned genes may be substrates of ITB4. Without ITB4 function, may not be correctly polyadenylated, and therefore, their expression levels are likely to be altered. Similar events may occur in the genes that regulate floral development. Regulators of floral organ identity genes may have altered expression leading to observed changes in floral architecture.

Differences Exist in the Mechanism of mRNA 3' End Formation among Plants, Yeast and Mammals

Formation of mRNA 3' ends is carried out by multiple *trans*-factors including CstF, CPSF, cleavage factors (CF) and the poly(A) polymerase (PAP). Homologs of subunits for each of

these factors have been identified in yeast, plants and mammals (Zhao et al., 1999; Yao et al., 2002; Elliott et al., 2003; Herr et al., 2006). It has been widely accepted that mRNA 3' end formation is similar in all eukaryotic cells, based on the high level of protein sequence identity of these factors, and the cooperative RNA-protein and protein-protein interactions within the processing machinery (Yao et al., 2002; Elliott et al., 2003; Delaney et al., 2006; Herr et al., 2006; Xu et al., 2006).

The results of our *in vivo* functional assays indicated that the homologs of CstF-64 in yeast, plants and mammals are not functionally equivalent. It is possible that this is due to the differences in the sequences of the poly(A) signals in pre-mRNAs in yeasts, plants and mammals (Mogen et al., 1990; Mogen et al., 1992; Li and Hunt, 1997; Zhao et al., 1999; Loke et al., 2005; Herr et al., 2006; Ji et al., 2007). The common minimal poly(A) signal is composed of an A-rich sequence, a U-rich element, and a PyA cleavage site in all eukaryotes. Nonetheless, the requirement for specific sequence elements differs greatly between yeast, plants, and animals (Zhao et al., 1999).

In mammals, a single copy of the AAUAAA element is highly conserved and absolutely necessary for precise 3' end formation. The AAUAAA element is located about 15–30 nucleotides upstream of the poly(A) site; and the DSE is located within 50 nucleotides (Zhao et al., 1999). CPSF-160 and CstF-64 specifically recognize and bind to the AAUAAA element and DSE in pre-mRNAs, respectively (Murthy and Manley, 1992; Takagaki and Manley, 1997), and cleavage occurs preferentially at CA (Zhao et al., 1999). However, the plant poly(A) signal lacks a consensus element as in mammals. It has a wide distribution of multiple AAUAAA-like sequences, and the GU-rich elements are located upstream of the poly(A) site, not downstream as in mammals, and cleavage occurs preferentially at PyA(Wu et al., 1995; Li and Hunt, 1997;

Zhao et al., 1999). Previous work has shown that plant cells do not properly recognize animal polyadenylation signals (Hunt, 1987). It is therefore likely, that human CstF-64 does not recognize plant polyadenylation signals. This may explain why the human CstF-64 was not able to functionally complement the *itb4-2* mutant in Arabidopsis. The yeast poly(A) signal seems to be more similar to that in plants. In yeast, usually redundant A-rich and U-rich elements are located upstream of the cleavage site, and no unambiguous DSEs have been identified. As in plants, the preferential cleavage site is PyA. However, yeast and plants do not share a consensus element in their poly(A) signal sequences (Zhao et al., 1999). This may explain our result that ITB4 could not complement the yeast CstF-64 mutant.

In summary, we have shown that *ITB4* encodes AtCstF-64, which is highly expressed in growing and proliferating cells, and is required for normal trichome morphogenesis and floral development. Loss of ITB4 results in aberrant floral architecture due, in part, to the altered expression of floral organ identity genes. The finding that ITB4 is not functionally equivalent to its yeast counterpart, and that the mammalian CstF-64 could not functionally complement the *itb4-2* mutant, supports the idea that there exists key differences between polyadenylation in yeast, plants, and animals even though the basic mechanism is conserved in all eukaryotic cells (Zhao et al., 1999; Yao et al., 2002; Elliott et al., 2003; Delaney et al., 2006; Herr et al., 2006; Ji et al., 2007). Given the importance of 3' end processing for a host of cellular processes including gene regulation and cell proliferation (Danckwardt et al., 2008), understanding these differences is needed to unravel the role of CstF in development.

Future Perspectives

Polyadenylation is a common event that occurs in all eukaryotic nuclei, but alternative polyadenylation events that affect plant development have rarely been reported. Our results show that absence of the plant homolog of CstF-64 encoded by *ITB4* causes pleiotropic effects in plant

development such as severe defects in trichomes and floral organs. *ITB4* is highly expressed in these rapidly expanding and proliferating cells. ITB4 protein was localized to nuclei. The *itb4* mutants had altered gene expression of important floral developmental regulators. These results provide a link between Cst-64 and plant development. However, the function of ITB4 is still far away from being fully understood. Multiple questions need to be answered. The most important is which genes are affected by either the aberrant alternative polyadenylation or the failure of poly(A) addition in the *itb4* mutants. To answer these questions, the following approach can be used. Through microarray experiments using mRNA isolated from *itb4-2* mutants and wild type, genes whose expression is altered in the mutant can be identified. The poly(A) site of these genes can be examined by using 3' rapid amplification of cDNA ends (3' RACE).

Although polyadenylation has been considered as a conserved mechanism in all eukaryotic cells, and the 3' end formation machinery is found in mammalian, yeast and plant cells, our results suggest that there may be important differences in 3' end processing between these groups. We were unable to rescue a yeast CstF-64 mutant using the Arabidopsis coding sequence, and the mammalian CstF-64 could not functionally complement *itb4* mutants. However, alternative explanations exist. First, the mammalian CstF-64 gene may not be properly expressed in plants. To check this, we could use western blotting of proteins extracted from transformants using an antibody to the mammalian CstF-64 protein. Likewise, we have to rule out lack of expression before we conclude that ITB4 cannot rescue the yeast mutant.

Table 5-1. Primers used in this study

Primer name	Sequence (5'→3')	Used for
itb4m F	TGGCAAAAGAATAAACGAGGG	*itb4-1* mutation identification
itb4m R	ATTCAGGGCATTCTAAGCGA	
ITB4g F	CTCCTATCGACGACGAATACGAAAG	ITB4 expression construct
ITB4g R	AGGGGCCACAGGATTAAAACCA	
ITB4cDNA F	CTCCTATCGACGACGAATACGAAAG	ITB4 cDNA amplification
ITB4cDNA R	CTATGAAGGCTGCATCATGTGGTCTTGC	
ITB4GFP F	ATGGCTTCAT CATCATCCCA ACGACGC	ITB4-GFP expression construct
ITB4GFP R	TGAAGGCTGCATCATGTGGTCCTTGCTTG	
CstF64 F	ATGGCGGGTTTGACTGTGAGAGACCC	CstF64 expression construct
CstF64 R	TACAGGTGCTCCAGTGGATTTCTGTATTTGTTCC	
τCstF64 F	ATGTCGAGTTTGGCGGTGAGAGACCC	τCstF64 expression construct
τCstF64 R	GGAGGAGGGAAACCCTAATCCAAGTGTGGG	
ITB4i1 F	ATGGCTTCATCATCATCCCAAC	ITB4 in situ hybridization
ITB4i1 R *	GTGCCTTTGTCATTCTCAGCAA	
ITB4ic F *	ATGGCTTCATCATCATCCCAAC	ITB4 in situ hybridization
ITB4ic R	GTGCCTTTGTCATTCTCAGCAA	
ITB4i2 F	CGCCAAATATTGTTCAGGCCC	ITB4 in situ hybridization
ITB4i2 R	TTGGTAATGCTTGGTGGGG	
ITB4i3 F	AAGCAGATTGGAGGGCCAGTAGATT	ITB4 in situ hybridization
ITB4i3 R	TTTGCGTAAACTGCGAACCGA	
AP1i F	GGGAAGGGGTAGGGTTCAATTGAAGA	AP1 in situ hybridization
AP1i R	GACAACAAGAGCAACTTCAGCATCAC	
AP1ic F	GGGAAGGGGTAGGGTTCAATTGAAGA	AP1 in situ hybridization
AP1ic R	GACAACAAGAGCAACTTCAGCATCAC	
AP3i F	CGAGAGGGAAGATCCAGATCAAGA	AP3 in situ hybridization
AP3i R	GCTAGAGAACATGATAATCGAAACCC	
PIi F	GGAGGAATGGATTGGTGAAGAAGGCT	PI in situ hybridization
PIi R	GCCAGATAACTTCTGGTATTGGTCCA	

* Primers used for in situ hybridization included the T7 promoter sequence, 5'taatacgactcactataggg3' at the 5' end, for example: ITB4i1 R, 5'taatacgactcactatagggGTGCCTTTGTCATTCTCAGCAA3' for the antisense RNA probe, and ITB4ic F, 5'taatacgactcactatagggATGGCTTCATCATCATCCCAAC3' for the control sense RNA probe.

Table 5-2. Alteration of trichome cell shape in the *itb4-2* mutant

Strain	Trichome branches % [a]					Total number [b]	%Twin cluster [c]
	0	2	3	4	5		
Col wt	0	0.1	96.0	3.9	0	1120	0
itb4-2	3.4	18.0	70.3	7.8	0.5	1540	2.52

[a] Numbers represent percentages of the total number of trichomes with the indicated number of branches.
[b] Total number of trichomes counted on at least ten leaves.
[c] Numbers represent percentages of the total number of trichomes that were present as twins.

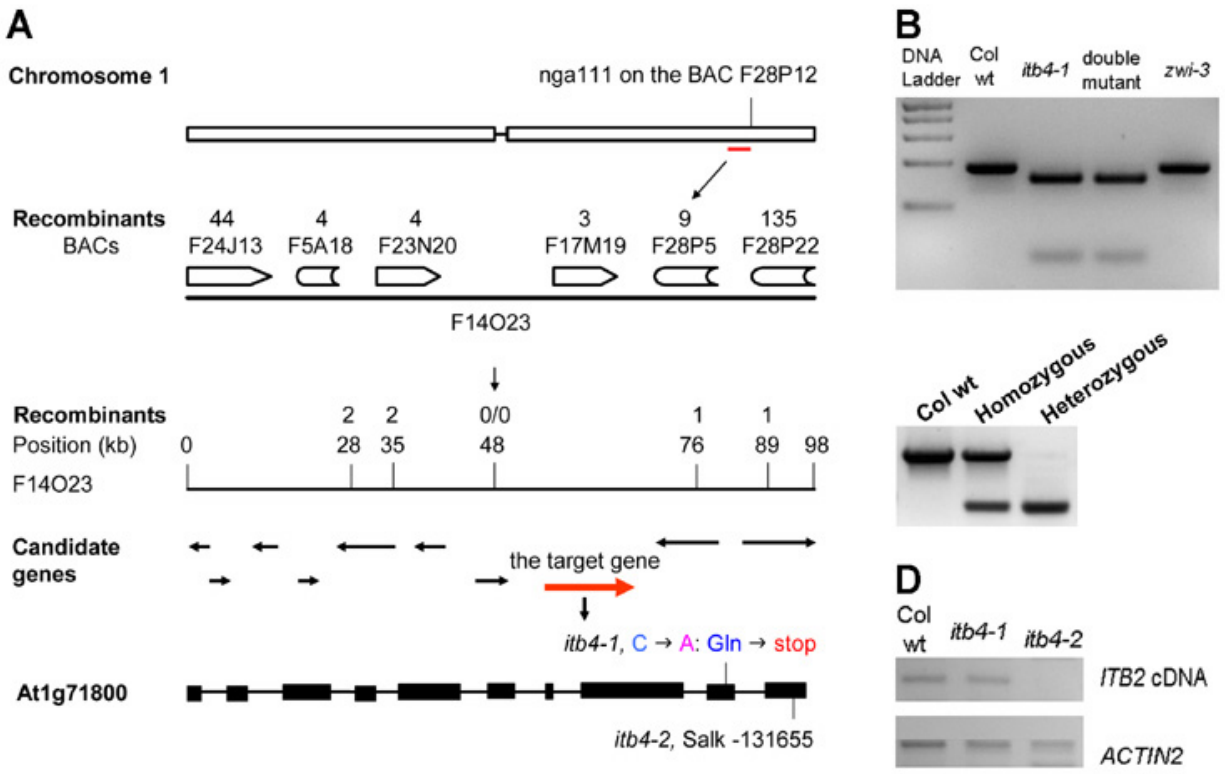

Figure 5-1. Positional cloning of *ITB4*. (A) Positional cloning strategy to identify *ITB4* gene. (B) Confirmation of the C to T transition in the *itb4-1* allele by digestion of PCR products with *Mse*I. The C to T transition creates an *Mse*I site in the *itb4-1* allele. PCR products amplified using *ITB4* specific primers (see Table 1) were digested with *Mse*I and subjected to electrophoresis through an agarose gel. (C) Identification of the *itb4-2* mutant homozygous for the T-DNA insertion. Genomic DNA from wildtype, heterozygous or homozygous *itb4-2* mutants was amplified using *ITB4* and T-DNA specific primers (see Table 1), and the products were subjected to electrophoresis through an agarose gel. (D) Results of RT-PCR using *ITB4* specific primers showing similar levels of *ITB4* transcript in *itb4-1* and wild type plants, and no detectable transcript in *itb4-2* mutants.

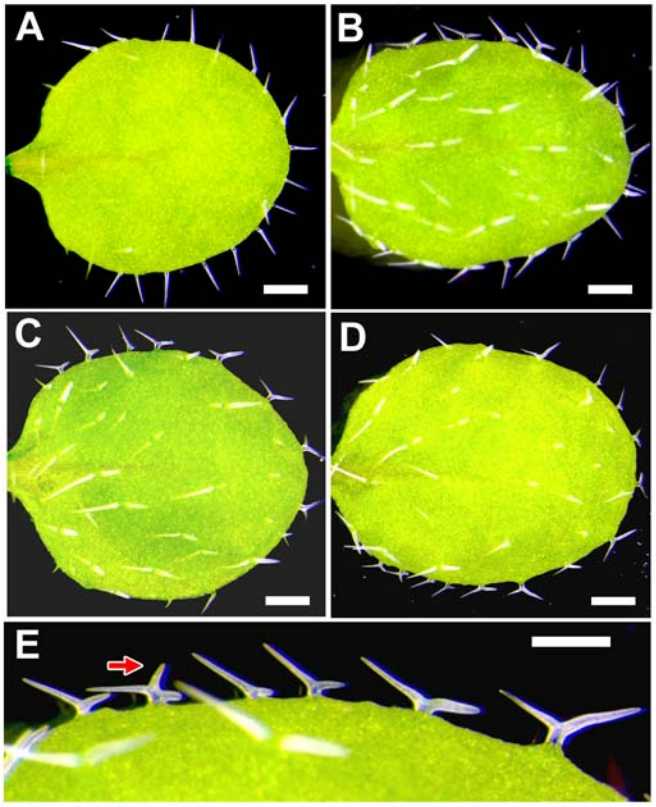

Figure 5-2**.** Rescue of the *itb4-1 zwi-3* double mutant phenotype by At1g71800. (A) Light micrograph showing unbranched trichomes on the *itb4-1 zwi-3* double mutant. (B) Light micrograph showing the two-branched trichomes on the *zwi-3* single mutant. (C) Light micrograph of an *itb4-1 zwi-3* double mutant transformed with the *GL2:ITB4* construct. The transgenic double mutant shows the same phenotype as the *zwi-3* single mutant, demonstrating rescue of the unbranched trichome phenotype. (D) Light micrograph of an *itb4-1 zwi-3* double mutant transformed with the *35S:ITB4* showing two-branched trichomes. (E) Magnified image from panel D showing a three-branched trichome. Scale bar = 200 µm.

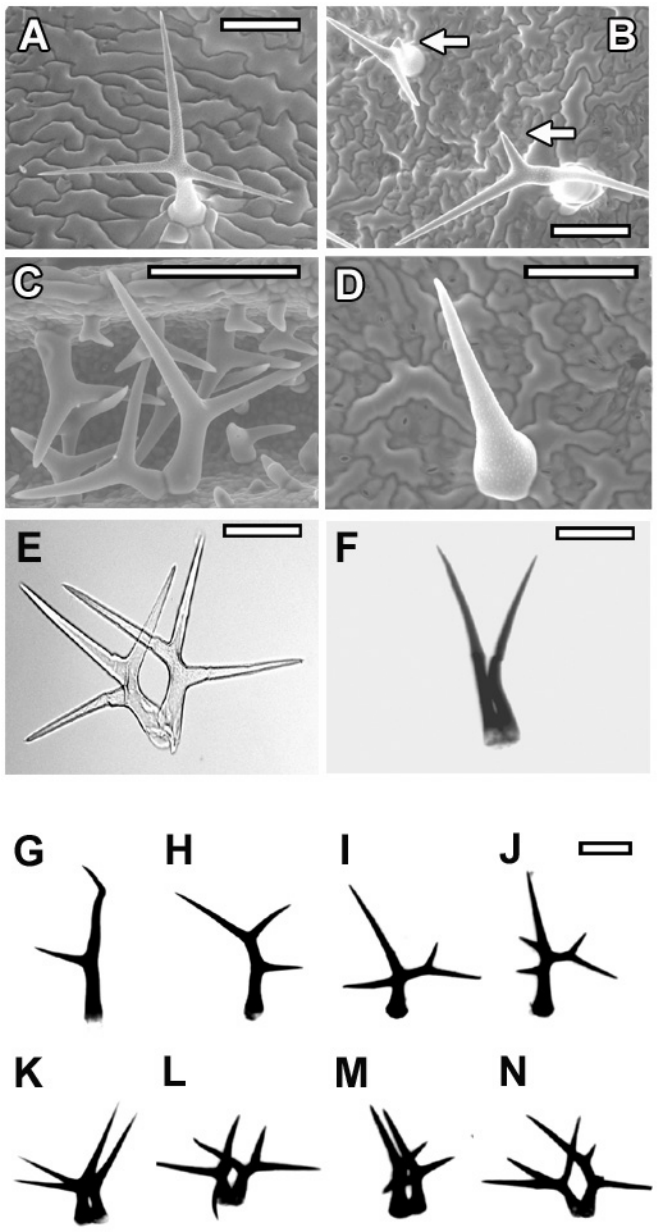

Figure 5-3. The *itb4-2* mutants display the trichome shape defects. (A) – (D) Scanning electron micrographs. (E) – (H) Light micrographs of isolated trichomes. (A) Symmetrical Col wild type trichomes with equal branch length. (B) Irregular trichomes on an *itb4-2* mutant showing unequal branch length and multiple branch points. (C) Developing twin trichome on an *itb4-2* mutant showing a trichome cluster. (D) Developing unbranched trichome on an *itb4-2*.mutant. (E) Twin trichome still attached following treatment with EGTA and pectinase. (F) Twin unbranched trichome on an *itb4-2* mutant. (G) - (J) Irregular trichomes on *itb4-2* mutants showing different numbers of branches and separated branch positions. (K) - (N) Twin trichomes with different numbers of branches.Scale bar = 100 µm in (A) – (F), and 50 µm in (G) - (N).

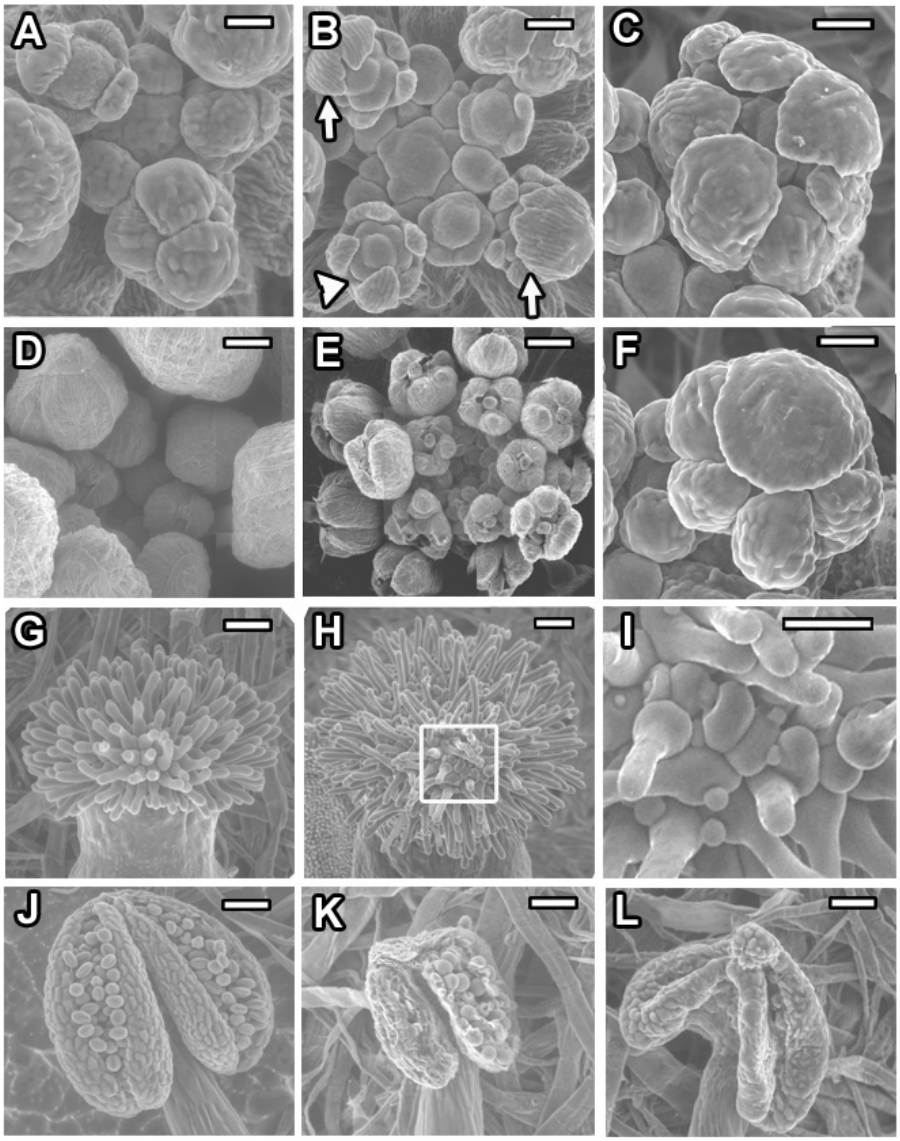

Figure 5-4. Floral defects of *itb4-2* mutants. (A), (D), (G), and (J) SEMs of Col wild type flowers. (B), (C), (E), (F), (H), (I), (K), and (L) SEMs of flowers from *itb4-2* mutants. (A) Wildtype developing flower buds showing four sepal primordia. (D) Older wildtype buds showing the sepal completely enclosing the floral organs. (G) Wildtype stigma with normal papillae. (J) Wildtype anther containing normal pollen. (B) Developing *itb4-2* flower buds showing the developing petal primordia (large arrow). Small Arrow indicates fused sepal primordia. (C) *itb4-2* flower bud with extra sepals. (E) Developing *itb4-2* flower buds showing the exposed stigmas. (F) Preferentially growing sepal on an *itb4-2* flower bud (H) and (I) Abnormal *itb4-2* stigma showing malformed papillae. (K) Abnormal *itb4-2* anther with abortive pollen. (L) Abnormal *itb4-2* anther lacking pollen. Scale bar = 100 μm.

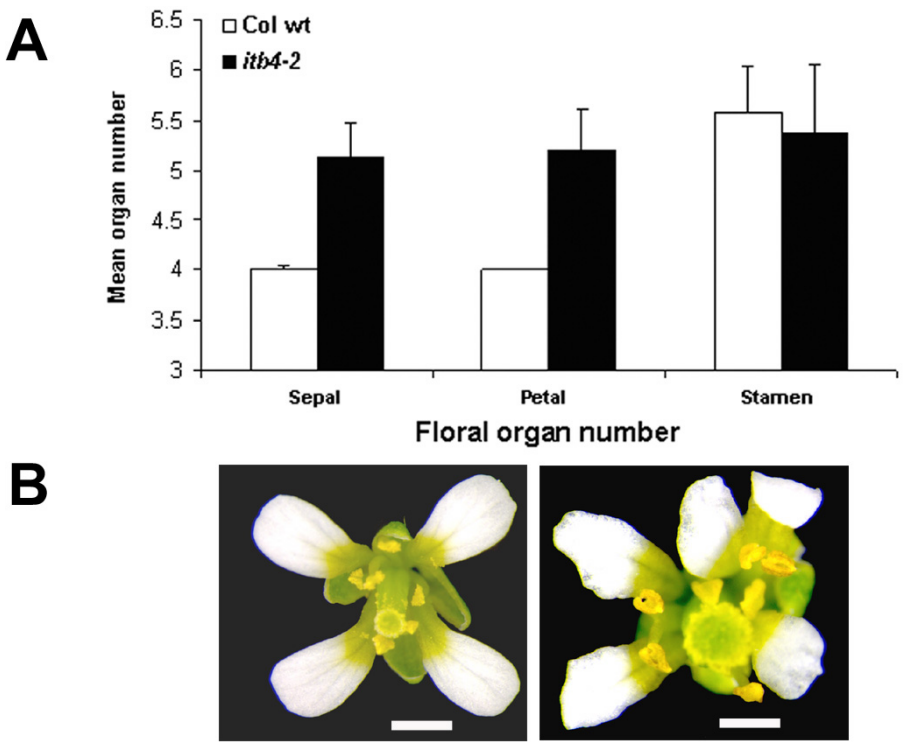

Figure 5-5. Increased number of floral organs *itb4-2* mutants. (A) Floral organ numbers for Col wild type and *itb4-2* mutant flowers. (B) Representative flowers from wild type, left, and an *itb4-2* mutant, right. Scale bar = 1 mm.

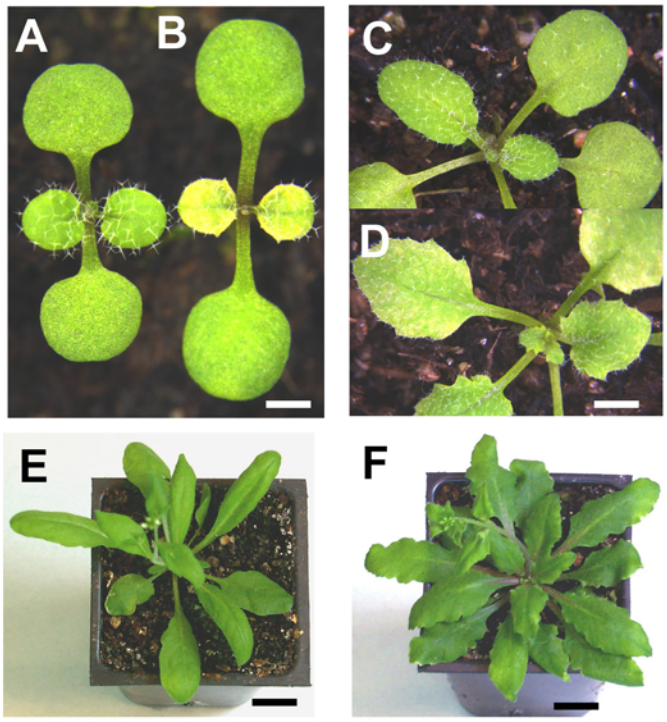

Figure 5-6. Leaf shape and color defects in *itb4-2* mutants. (A), (C), and (E) Col wild type plants. (B), (D), and (F) *itb4-2* mutant plants. (A) Wild type plant showing normal first leaf pair. (B) *itb4-2* mutant showing yellow first leaf pair. (C) Wild type seedling showing smooth leaf edge. (D) *itb4-2* mutant seedling showing serrated leaf edge and less yellow leaf color. (E) Wild type mature plant. (F) *itb4-2* mutant plant showing normal color leaves. Scale bar in (A) and (B) = 0.1 mm; Scale bar in (C) and (D) = 5 mm; Scale bar in (E) and (F) = 10 mm;

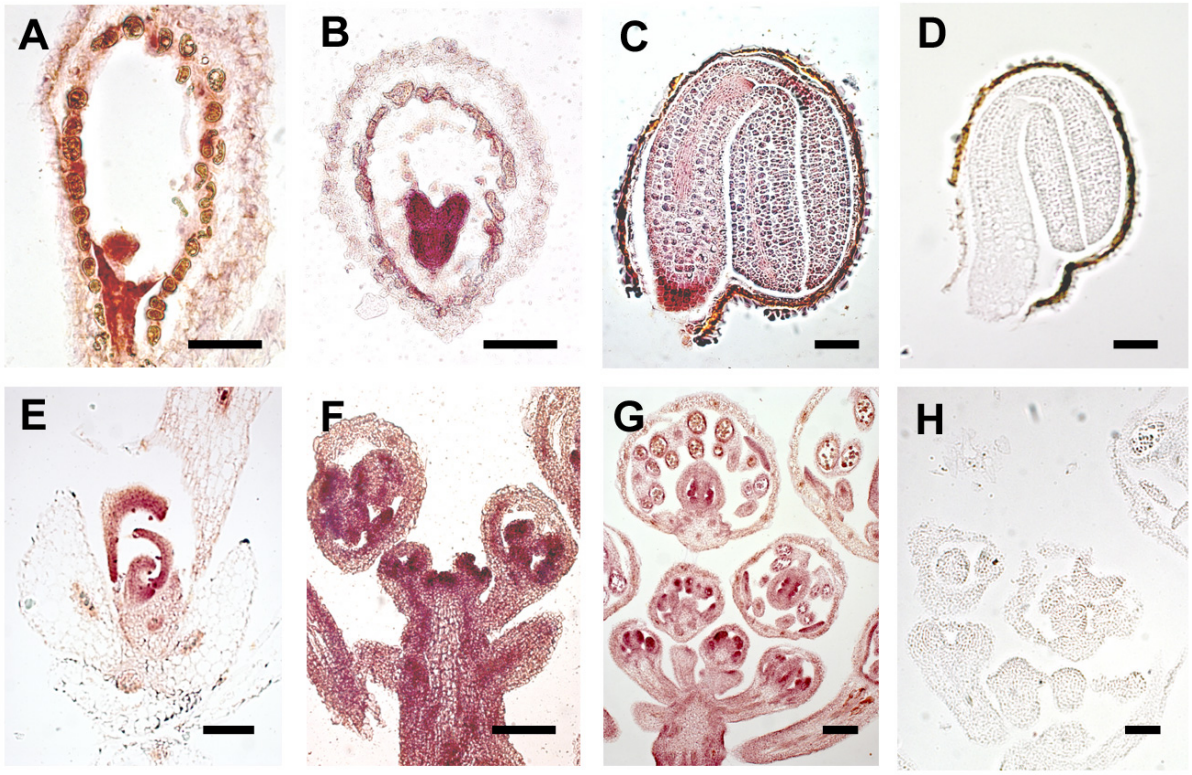

Figure 5-7. *ITB2* expression pattern in Col wild type. (A) Globular stage embryo showing strong expression. (B) Heart stage embryo showing strong expression. (C) Germinating seed showing strong expression in the root cap and shoot apical meristem. (D) Germinating seed hybridized with the negative control sense RNA probe. (E) Longitudinal section of a six-week-old seedling showing strong expression in the developing leaves and trichomes. (F) Longitudinal section of the floral meristem showing strong expression in the floral meristem and developing flower buds. (G) Floral organ primordia showing strong expression in the developing stamens and carpals and weak expression in the developed sepals. (H) Floral organ primordia hybridized with the negative control sense RNA probe. Scale bar = 10 µm in (A) and (B), 50 µm (B) and (C), 100 µm in (E) – (H).

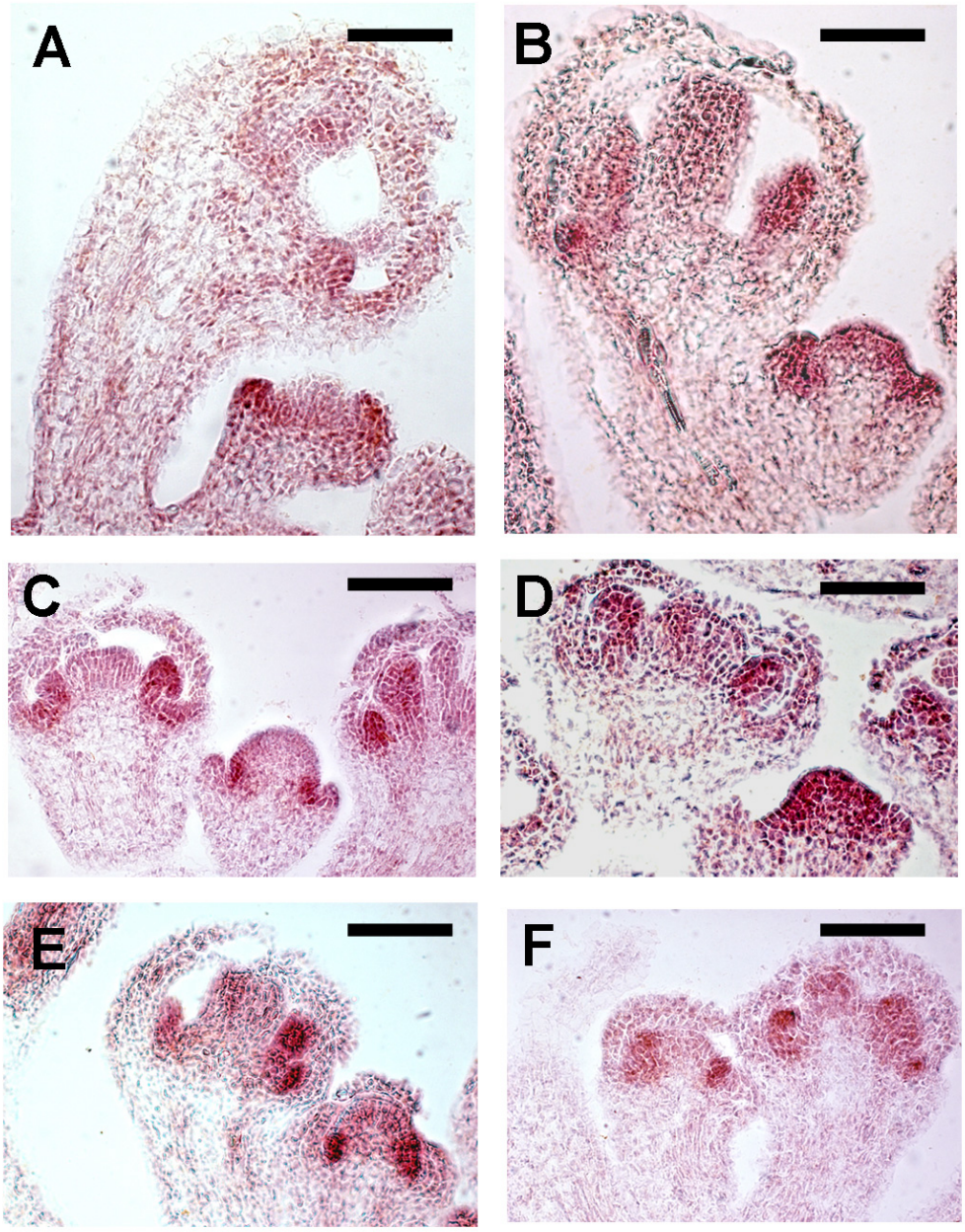

Figure 5-8. Altered expression patterns of floral organ identity genes in *itb4-2* mutants. (A), (C) and (E) Longitudinal sections of Col wild type flower primordia. (B), (D), and (F) Longitudinal sections of flower primordia of the *itb4-2* mutant. (A) and (B) *AP1* antisense probe. (C) and (D) *AP3* antisense probe. (E) and (F) *PI* antisense probe. Scale bar = 50 µm.

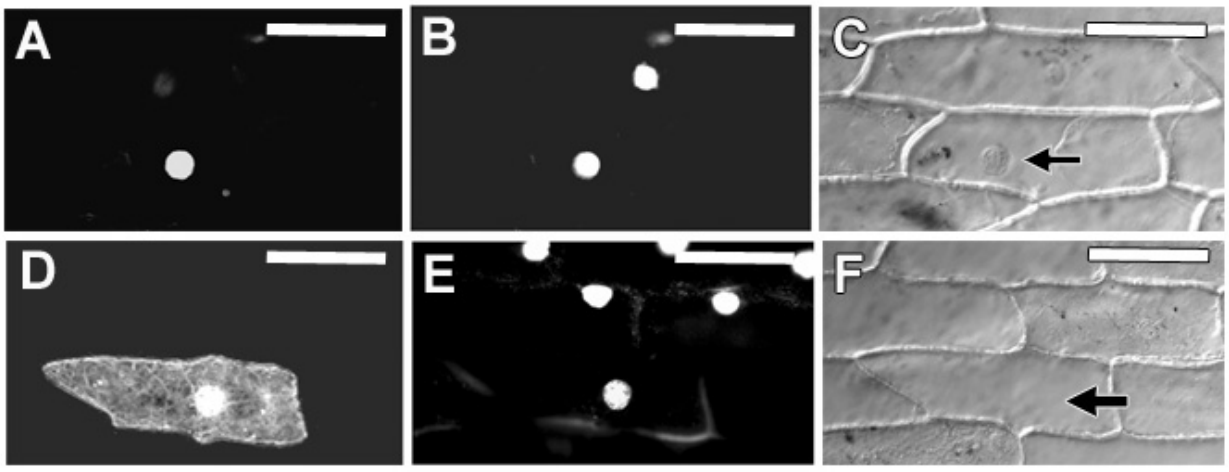

Figure 5-9. ITB4 is localized to the nucleus. Onion epidermal cells were transiently transformed with either *35S:ITB4-GFP* (A) – (C), or *35S:GFP*. (D) – (F). (A) GFP localization confined to the nucleus. (B) Same cell as in (A), but stained with DAPI to show position of the nucleus. (C) DIC image of the same cell as in (A) showing the position of the nucleus (arrow). (D) GFP localization in both the cytoplasm and the nucleus. (E) The same cell as in (D) stained with DAPI to show the position of the nucleus. (F) DIC image of the same cell as in (D) showing the position of the nucleus (arrow). Scale bar = 100 μm

LIST OF REFERENCES

Abe, T., and Hashimoto, T. (2005). Altered microtubule dynamics by expression of modified alpha-tubulin protein causes right-handed helical growth in transgenic Arabidopsis plants. Plant J **43,** 191-204.

Alder-Baerens, N., Lisman, Q., Luong, L., Pomorski, T., and Holthuis, J.C. (2006). Loss of P4 ATPases Drs2p and Dnf3p disrupts aminophospholipid transport and asymmetry in yeast post-Golgi secretory vesicles. Mol Biol Cell **17,** 1632-1642.

Alonso, J.M., and Stepanova, A.N. (2003). T-DNA mutagenesis in Arabidopsis. Methods Mol Biol **236,** 177-188.

Anthony, R.G., Henriques, R., Helfer, A., Meszaros, T., Rios, G., Testerink, C., Munnik, T., Deak, M., Koncz, C., and Bogre, L. (2004). A protein kinase target of a PDK1 signalling pathway is involved in root hair growth in Arabidopsis. EMBO J **23,** 572-581.

Arioli, T., Peng, L., Betzner, A.S., Burn, J., Wittke, W., Herth, W., Camilleri, C., Hofte, H., Plazinski, J., Birch, R., Cork, A., Glover, J., Redmond, J., and Williamson, R.E. (1998). Molecular analysis of cellulose biosynthesis in Arabidopsis. Science **279,** 717-720.

Atilgan, E., and Sun, S.X. (2007). Shape transitions in lipid membranes and protein mediated vesicle fusion and fission. J Chem Phys **126,** 095102.

Axelsen, K.B., and Palmgren, M.G. (2001). Inventory of the superfamily of P-type ion pumps in Arabidopsis. Plant Physiol **126,** 696-706.

Bacic, A. (2006). Breaking an impasse in pectin biosynthesis. Proc Natl Acad Sci U S A **103,** 5639-5640.

Bacic, A., Du, H., Stone, B.A., and Clarke, A.E. (1996). Arabinogalactan proteins: a family of cell-surface and extracellular matrix plant proteoglycans. Essays Biochem **31,** 91-101.

Bagnat, M., and Simons, K. (2002). Lipid rafts in protein sorting and cell polarity in budding yeast Saccharomyces cerevisiae. Biol Chem **383,** 1475-1480.

Bagnat, M., Keranen, S., Shevchenko, A., and Simons, K. (2000). Lipid rafts function in biosynthetic delivery of proteins to the cell surface in yeast. Proc Natl Acad Sci U S A **97,** 3254-3259.

Baluska, F., Salaj, J., Mathur, J., Braun, M., Jasper, F., Samaj, J., Chua, N.H., Barlow, P.W., and Volkmann, D. (2000). Root hair formation: F-actin-dependent tip growth is initiated by local assembly of profilin-supported F-actin meshworks accumulated within expansin-enriched bulges. Dev Biol **227,** 618-632.

Baluska, F., Hlavacka, A., Samaj, J., Palme, K., Robinson, D.G., Matoh, T., McCurdy, D.W., Menzel, D., and Volkmann, D. (2002). F-actin-dependent endocytosis of cell

wall pectins in meristematic root cells. Insights from brefeldin A-induced compartments. Plant Physiol **130,** 422-431.

Baskin, T.I. (2001). On the alignment of cellulose microfibrils by cortical microtubules: a review and a model. Protoplasma **215,** 150-171.

Baskin, T.I. (2005). Anisotropic expansion of the plant cell wall. Annu Rev Cell Dev Biol **21,** 203-222.

Baskin, T.I., Wilson, J.E., Cork, A., and Williamson, R.E. (1994). Morphology and microtubule organization in Arabidopsis roots exposed to oryzalin or taxol. Plant Cell Physiol **35,** 935-942.

Basu, D., Le, J., El-Essal Sel, D., Huang, S., Zhang, C., Mallery, E.L., Koliantz, G., Staiger, C.J., and Szymanski, D.B. (2005). DISTORTED3/SCAR2 is a putative arabidopsis WAVE complex subunit that activates the Arp2/3 complex and is required for epidermal morphogenesis. Plant Cell **17,** 502-524.

Beaudoin, F., Gable, K., Sayanova, O., Dunn, T., and Napier, J.A. (2002). A Saccharomyces cerevisiae gene required for heterologous fatty acid elongase activity encodes a microsomal beta-keto-reductase. J Biol Chem **277,** 11481-11488.

Bell, C.J., and Ecker, J.R. (1994). Assignment of 30 microsatellite loci to the linkage map of Arabidopsis. Genomics **19,** 137-144.

Bertling, E., Hotulainen, P., Mattila, P.K., Matilainen, T., Salminen, M., and Lappalainen, P. (2004). Cyclase-associated protein 1 (CAP1) promotes cofilin-induced actin dynamics in mammalian nonmuscle cells. Mol Biol Cell **15,** 2324-2334.

Bhat, R.A., and Panstruga, R. (2005). Lipid rafts in plants. Planta **223,** 5-19.

Birchmeier, W., Lanz, J.H., Winterhalter, K.H., and Conrad, M.J. (1979). ATP-induced endocytosis in human erythrocyte ghosts. Characterization of the process and isolation of the endocytosed vesicles. J Biol Chem **254,** 9298-9304.

Bird, D., Beisson, F., Brigham, A., Shin, J., Greer, S., Jetter, R., Kunst, L., Wu, X., Yephremov, A., and Samuels, L. (2007). Characterization of Arabidopsis ABCG11/WBC11, an ATP binding cassette (ABC) transporter that is required for cuticular lipid secretion. Plant J **52,** 485-498.

Boevink, P., Oparka, K., Santa Cruz, S., Martin, B., Betteridge, A., and Hawes, C. (1998). Stacks on tracks: the plant Golgi apparatus traffics on an actin/ER network. Plant J **15,** 441-447.

Boman, A.L. (2001). GGA proteins: new players in the sorting game. J Cell Sci **114,** 3413-3418.

Bonifacino, J.S., and Glick, B.S. (2004). The mechanisms of vesicle budding and fusion. Cell **116,** 153-166.

Bonin, C.P., Potter, I., Vanzin, G.F., and Reiter, W.D. (1997). The MUR1 gene of Arabidopsis thaliana encodes an isoform of GDP-D-mannose-4,6-dehydratase, catalyzing the first step in the de novo synthesis of GDP-L-fucose. Proc Natl Acad Sci U S A **94,** 2085-2090.

Bosch, M., Cheung, A.Y., and Hepler, P.K. (2005). Pectin methylesterase, a regulator of pollen tube growth. Plant Physiol **138,** 1334-1346.

Bouton, S., Leboeuf, E., Mouille, G., Leydecker, M.T., Talbotec, J., Granier, F., Lahaye, M., Hofte, H., and Truong, H.N. (2002). QUASIMODO1 encodes a putative membrane-bound glycosyltransferase required for normal pectin synthesis and cell adhesion in Arabidopsis. Plant Cell **14,** 2577-2590.

Brandizzi, F., Saint-Jore, C., Moore, I., and Hawes, C. (2003). The relationship between endomembranes and the plant cytoskeleton. Cell Biol Int **27,** 177-179.

Brummell, D.A., Harpster, M.H., Civello, P.M., Palys, J.M., Bennett, A.B., and Dunsmuir, P. (1999). Modification of expansin protein abundance in tomato fruit alters softening and cell wall polymer metabolism during ripening. Plant Cell **11,** 2203-2216.

Burk, D.H., and Ye, Z.H. (2002). Alteration of oriented deposition of cellulose microfibrils by mutation of a katanin-like microtubule-severing protein. Plant Cell **14,** 2145-2160.

Burn, J.E., Hocart, C.H., Birch, R.J., Cork, A.C., and Williamson, R.E. (2002). Functional analysis of the cellulose synthase genes CesA1, CesA2, and CesA3 in Arabidopsis. Plant Physiol **129,** 797-807.

Cameron, L.A., Giardini, P.A., Soo, F.S., and Theriot, J.A. (2000). Secrets of actin-based motility revealed by a bacterial pathogen. Nat Rev Mol Cell Biol **1,** 110-119.

Carland, F.M., Fujioka, S., Takatsuto, S., Yoshida, S., and Nelson, T. (2002). The identification of CVP1 reveals a role for sterols in vascular patterning. Plant Cell **14,** 2045-2058.

Catoire, L., Pierron, M., Morvan, C., du Penhoat, C.H., and Goldberg, R. (1998). Investigation of the action patterns of pectinmethylesterase isoforms through kinetic analyses and NMR spectroscopy. Implications In cell wall expansion. J Biol Chem **273,** 33150-33156.

Chaudhry, F., Guerin, C., von Witsch, M., Blanchoin, L., and Staiger, C.J. (2007). Identification of Arabidopsis cyclase-associated protein 1 as the first nucleotide exchange factor for plant actin. Mol Biol Cell **18,** 3002-3014.

Chen, C.Y., Wong, E.I., Vidali, L., Estavillo, A., Hepler, P.K., Wu, H.M., and Cheung, A.Y. (2002). The regulation of actin organization by actin-depolymerizing factor in elongating pollen tubes. Plant Cell **14,** 2175-2190.

Chen, T., Teng, N., Wu, X., Wang, Y., Tang, W., Samaj, J., Baluska, F., and Lin, J. (2007). Disruption of actin filaments by latrunculin B affects cell wall construction in Picea meyeri pollen tube by disturbing vesicle trafficking. Plant Cell Physiol **48,** 19-30.

Chen, Y.A., and Scheller, R.H. (2001). SNARE-mediated membrane fusion. Nat Rev Mol Cell Biol **2,** 98-106.

Cheng, J., Park, T.S., Fischl, A.S., and Ye, X.S. (2001). Cell cycle progression and cell polarity require sphingolipid biosynthesis in Aspergillus nidulans. Mol Cell Biol **21,** 6198-6209.

Cheng, Y., Kato, N., Wang, W., Li, J., and Chen, X. (2003). Two RNA binding proteins, HEN4 and HUA1, act in the processing of AGAMOUS pre-mRNA in Arabidopsis thaliana. Dev Cell **4,** 53-66.

Cheung, A.Y., and Wu, H.M. (2004). Overexpression of an Arabidopsis formin stimulates supernumerary actin cable formation from pollen tube cell membrane. Plant Cell **16,** 257-269.

Cheung, A.Y., Chen, C.Y., Glaven, R.H., de Graaf, B.H., Vidali, L., Hepler, P.K., and Wu, H.M. (2002). Rab2 GTPase regulates vesicle trafficking between the endoplasmic reticulum and the Golgi bodies and is important to pollen tube growth. Plant Cell **14,** 945-962.

Cho, H.T., and Cosgrove, D.J. (2000). Altered expression of expansin modulates leaf growth and pedicel abscission in Arabidopsis thaliana. Proc Natl Acad Sci U S A **97,** 9783-9788.

Classen, B., Mau, S.L., and Bacic, A. (2005). The arabinogalactan-proteins from pressed juice of Echinacea purpurea belong to the hybrid class of hydroxyproline-rich glycoproteins. Planta Med **71,** 59-66.

Clough, S.J., and Bent, A.F. (1998). Floral dip: a simplified method for Agrobacterium-mediated transformation of Arabidopsis thaliana. Plant J **16,** 735-743.

Co, C., Wong, D.T., Gierke, S., Chang, V., and Taunton, J. (2007). Mechanism of actin network attachment to moving membranes: barbed end capture by N-WASP WH2 domains. Cell **128,** 901-913.

Cole, R.A., and Fowler, J.E. (2006). Polarized growth: maintaining focus on the tip. Curr Opin Plant Biol **9,** 579-588.

Cosgrove, D.J. (2000a). Loosening of plant cell walls by expansins. Nature **407,** 321-326.

Cosgrove, D.J. (2000b). Expansive growth of plant cell walls. Plant Physiol Biochem **38,** 109-124.

Cosgrove, D.J., Li, L.C., Cho, H.T., Hoffmann-Benning, S., Moore, R.C., and Blecker, D. (2002). The growing world of expansins. Plant Cell Physiol **43,** 1436-1444.

Costaglioli, P., Joubes, J., Garcia, C., Stef, M., Arveiler, B., Lessire, R., and Garbay, B. (2005). Profiling candidate genes involved in wax biosynthesis in Arabidopsis thaliana by microarray analysis. Biochim Biophys Acta **1734,** 247-258.

Danielsen, E.M., and Hansen, G.H. (2006). Lipid raft organization and function in brush borders of epithelial cells. Mol Membr Biol **23,** 71-79.

Darley, C.P., Forrester, A.M., and McQueen-Mason, S.J. (2001). The molecular basis of plant cell wall extension. Plant Mol Biol **47,** 179-195.

Dass, B., McDaniel, L., Schultz, R.A., Attaya, E., and MacDonald, C.C. (2002). The gene CSTF2T, encoding the human variant CstF-64 polyadenylation protein tauCstF-64, lacks introns and may be associated with male sterility. Genomics **80,** 509-514.

Dass, B., McMahon, K.W., Jenkins, N.A., Gilbert, D.J., Copeland, N.G., and MacDonald, C.C. (2001). The gene for a variant form of the polyadenylation protein CstF-64 is on chromosome 19 and is expressed in pachytene spermatocytes in mice. J Biol Chem **276,** 8044-8050.

de Graaf, B.H., Cheung, A.Y., Andreyeva, T., Levasseur, K., Kieliszewski, M., and Wu, H.M. (2005). Rab11 GTPase-regulated membrane trafficking is crucial for tip-focused pollen tube growth in tobacco. Plant Cell **17,** 2564-2579.

Decottignies, A., Grant, A.M., Nichols, J.W., de Wet, H., McIntosh, D.B., and Goffeau, A. (1998). ATPase and multidrug transport activities of the overexpressed yeast ABC protein Yor1p. J Biol Chem **273,** 12612-12622.

Delaney, K.J., Xu, R., Zhang, J., Li, Q.Q., Yun, K.Y., Falcone, D.L., and Hunt, A.G. (2006). Calmodulin interacts with and regulates the RNA-binding activity of an Arabidopsis polyadenylation factor subunit. Plant Physiol **140,** 1507-1521.

Denes, J.M., Baron, A., Renard, C.M., Pean, C., and Drilleau, J.F. (2000). Different action patterns for apple pectin methylesterase at pH 7.0 and 4.5. Carbohydr Res **327,** 385-393.

Dhonukshe, P., Laxalt, A.M., Goedhart, J., Gadella, T.W., and Munnik, T. (2003). Phospholipase d activation correlates with microtubule reorganization in living plant cells. Plant Cell **15,** 2666-2679.

Dhugga, K.S. (2005). Plant Golgi cell wall synthesis: from genes to enzyme activities. Proc Natl Acad Sci U S A **102,** 1815-1816.

Dickinson, R.B., and Purich, D.L. (2002). Clamped-filament elongation model for actin-based motors. Biophys J **82,** 605-617.

Dickinson, R.B., Caro, L., and Purich, D.L. (2004). Force generation by cytoskeletal filament end-tracking proteins. Biophys J **87,** 2838-2854.

Didry, D., Carlier, M.F., and Pantaloni, D. (1998). Synergy between actin depolymerizing factor/cofilin and profilin in increasing actin filament turnover. J Biol Chem **273,** 25602-25611.

Ding, L., and Zhu, J.K. (1997). A role for arabinogalactan-proteins in root epidermal cell expansion. Planta **203,** 289-294.

Ding, X., Cory, G., and Song, W.Y. (2004). A high-throughput system to verify candidate interactors from yeast two-hybrid screening using rolling circle amplification. Anal Biochem **331,** 195-197.

Djerbi, S., Lindskog, M., Arvestad, L., Sterky, F., and Teeri, T.T. (2005). The genome sequence of black cottonwood (Populus trichocarpa) reveals 18 conserved cellulose synthase (CesA) genes. Planta **221,** 739-746.

Donaldson, J.G., and Jackson, C.L. (2000). Regulators and effectors of the ARF GTPases. Curr Opin Cell Biol **12,** 475-482.

Donaldson, J.G., Honda, A., and Weigert, R. (2005). Multiple activities for Arf1 at the Golgi complex. Biochim Biophys Acta **1744,** 364-373.

Edwards, K., Johnstone, C., and Thompson, C. (1991). A simple and rapid method for the preparation of plant genomic DNA for PCR analysis. Nucleic Acids Res **19,** 1349.

Elliott, B.J., Dattaroy, T., Meeks-Midkiff, L.R., Forbes, K.P., and Hunt, A.G. (2003). An interaction between an Arabidopsis poly(A) polymerase and a homologue of the 100 kDa subunit of CPSF. Plant Mol Biol **51,** 373-384.

Engqvist-Goldstein, A.E., Zhang, C.X., Carreno, S., Barroso, C., Heuser, J.E., and Drubin, D.G. (2004). RNAi-mediated Hip1R silencing results in stable association between the endocytic machinery and the actin assembly machinery. Mol Biol Cell **15,** 1666-1679.

Fagard, M., Desnos, T., Desprez, T., Goubet, F., Refregier, G., Mouille, G., McCann, M., Rayon, C., Vernhettes, S., and Hofte, H. (2000). PROCUSTE1 encodes a cellulose synthase required for normal cell elongation specifically in roots and dark-grown hypocotyls of Arabidopsis. Plant Cell **12,** 2409-2424.

Fiebig, A., Mayfield, J.A., Miley, N.L., Chau, S., Fischer, R.L., and Preuss, D. (2000). Alterations in CER6, a gene identical to CUT1, differentially affect long-chain lipid content on the surface of pollen and stems. Plant Cell **12,** 2001-2008.

Fischer, U., Men, S., and Grebe, M. (2004). Lipid function in plant cell polarity. Curr Opin Plant Biol **7,** 670-676.

Friml, J., Benfey, P., Benkova, E., Bennett, M., Berleth, T., Geldner, N., Grebe, M., Heisler, M., Hejatko, J., Jurgens, G., Laux, T., Lindsey, K., Lukowitz, W., Luschnig, C., Offringa, R., Scheres, B., Swarup, R., Torres-Ruiz, R., Weijers, D., and Zazimalova,

E. (2006). Apical-basal polarity: why plant cells don't stand on their heads. Trends Plant Sci **11,** 12-14.

Fu, Y., Li, H., and Yang, Z. (2002). The ROP2 GTPase controls the formation of cortical fine F-actin and the early phase of directional cell expansion during Arabidopsis organogenesis. Plant Cell **14,** 777-794.

Fu, Y., Gu, Y., Zheng, Z., Wasteneys, G., and Yang, Z. (2005). Arabidopsis interdigitating cell growth requires two antagonistic pathways with opposing action on cell morphogenesis. Cell **120,** 687-700.

Gall, W.E., Geething, N.C., Hua, Z., Ingram, M.F., Liu, K., Chen, S.I., and Graham, T.R. (2002). Drs2p-dependent formation of exocytic clathrin-coated vesicles in vivo. Curr Biol **12,** 1623-1627.

Gardiner, J.C., Harper, J.D., Weerakoon, N.D., Collings, D.A., Ritchie, S., Gilroy, S., Cyr, R.J., and Marc, J. (2001). A 90-kD phospholipase D from tobacco binds to microtubules and the plasma membrane. Plant Cell **13,** 2143-2158.

Geldner, N., Anders, N., Wolters, H., Keicher, J., Kornberger, W., Muller, P., Delbarre, A., Ueda, T., Nakano, A., and Jurgens, G. (2003). The Arabidopsis GNOM ARF-GEF mediates endosomal recycling, auxin transport, and auxin-dependent plant growth. Cell **112,** 219-230.

Gibbon, B.C., Kovar, D.R., and Staiger, C.J. (1999). Latrunculin B has different effects on pollen germination and tube growth. Plant Cell **11,** 2349-2363.

Giddings THJ, Staehelin LA. (1991). Microtubule-mediated control of microfibril deposition: a re-examination of the hypothesis. In The Cytoskeletal Basis of Plant growth and Form. Ed CW, Lloyd, pp 85-99, New York: Academie.

Gillmor, C.S., Lukowitz, W., Brininstool, G., Sedbrook, J.C., Hamann, T., Poindexter, P., and Somerville, C. (2005). Glycosylphosphatidylinositol-anchored proteins are required for cell wall synthesis and morphogenesis in Arabidopsis. Plant Cell **17,** 1128-1140.

Goley, E.D., and Welch, M.D. (2006). The ARP2/3 complex: an actin nucleator comes of age. Nat Rev Mol Cell Biol **7,** 713-726.

Gomes, E., Jakobsen, M.K., Axelsen, K.B., Geisler, M., and Palmgren, M.G. (2000). Chilling tolerance in Arabidopsis involves ALA1, a member of a new family of putative aminophospholipid translocases. Plant Cell **12,** 2441-2454.

Grebe, M., Friml, J., Swarup, R., Ljung, K., Sandberg, G., Terlou, M., Palme, K., Bennett, M.J., and Scheres, B. (2002). Cell polarity signaling in Arabidopsis involves a BFA-sensitive auxin influx pathway. Curr Biol **12,** 329-334.

Green, P.B. (1962). Mechanism for Plant Cellular Morphogenesis. Science **138,** 1404-1405.

Grennan, A.K. (2007). Lipid rafts in plants. Plant Physiol **143,** 1083-1085.

Gungabissoon, R.A., Khan, S., Hussey, P.J., and Maciver, S.K. (2001). Interaction of elongation factor 1alpha from Zea mays (ZmEF-1alpha) with F-actin and interplay with the maize actin severing protein, ZmADF3. Cell Motil Cytoskeleton **49,** 104-111.

Hasenstein, K.H., Blancaflor, E.B., and Lee, J.S. (1999). The microtubule cytoskeleton does not integrate auxin transport and gravitropism in maize roots. Physiol Plant **105,** 729-738.

Hawes, C. (2005). Cell biology of the plant Golgi apparatus. New Phytol **165,** 29-44.

Hawes, C., and Satiat-Jeunemaitre, B. (2005a). The plant Golgi apparatus--going with the flow. Biochim Biophys Acta **1744,** 93-107.

Hawes, C., and Satiat-Jeunemaitre, B. (2005b). The plant Golgi apparatus--going with the flow. Biochim Biophys Acta **1744,** 466-480.

Hepler, P.K., Vidali, L., and Cheung, A.Y. (2001). Polarized cell growth in higher plants. Annu Rev Cell Dev Biol **17,** 159-187.

Herr, A.J., Molnar, A., Jones, A., and Baulcombe, D.C. (2006). Defective RNA processing enhances RNA silencing and influences flowering of Arabidopsis. Proc Natl Acad Sci U S A **103,** 14994-15001.

Holthuis, J.C., and Levine, T.P. (2005). Lipid traffic: floppy drives and a superhighway. Nat Rev Mol Cell Biol **6,** 209-220.

Huang, T.Y., DerMardirossian, C., and Bokoch, G.M. (2006). Cofilin phosphatases and regulation of actin dynamics. Curr Opin Cell Biol **18,** 26-31.

Hulskamp, M., Misra, S., and Jurgens, G. (1994). Genetic dissection of trichome cell development in Arabidopsis. Cell **76,** 555-566.

Hulskamp, M., Folkers, U., and Grini, P.E. (1998). Cell morphogenesis in Arabidopsis. Bioessays **20,** 20-29.

Hussey, P.J., Allwood, E.G., and Smertenko, A.P. (2002). Actin-binding proteins in the Arabidopsis genome database: properties of functionally distinct plant actin-depolymerizing factors/cofilins. Philos Trans R Soc Lond B Biol Sci **357,** 791-798.

Hussey, P.J., Ketelaar, T., and Deeks, M.J. (2006). Control of the actin cytoskeleton in plant cell growth. Annu Rev Plant Biol **57,** 109-125.

Iwai, H., Masaoka, N., Ishii, T., and Satoh, S. (2002). A pectin glucuronyltransferase gene is essential for intercellular attachment in the plant meristem. Proc Natl Acad Sci U S A **99,** 16319-16324.

Jaillais, Y., and Gaude, T. (2008). Plant Cell Polarity: Sterols Enter into Action after Cytokinesis. Dev Cell **14,** 318-320.

Ji, G., Zheng, J., Shen, Y., Wu, X., Jiang, R., Lin, Y., Loke, J.C., Davis, K.M., Reese, G.J., and Li, Q.Q. (2007). Predictive modeling of plant messenger RNA polyadenylation sites. BMC Bioinformatics **8,** 43.

Jiang, L., Yang, S.L., Xie, L.F., Puah, C.S., Zhang, X.Q., Yang, W.C., Sundaresan, V., and Ye, D. (2005). VANGUARD1 encodes a pectin methylesterase that enhances pollen tube growth in the Arabidopsis style and transmitting tract. Plant Cell **17,** 584-596.

Johansen, J.N., Vernhettes, S., and Hofte, H. (2006). The ins and outs of plant cell walls. Curr Opin Plant Biol **9,** 616-620.

Jouhet, J., Marechal, E., and Block, M.A. (2007). Glycerolipid transfer for the building of membranes in plant cells. Prog Lipid Res **46,** 37-55.

Kaksonen, M., Toret, C.P., and Drubin, D.G. (2006). Harnessing actin dynamics for clathrin-mediated endocytosis. Nat Rev Mol Cell Biol **7,** 404-414.

Kandasamy, M.K., Burgos-Rivera, B., McKinney, E.C., Ruzicka, D.R., and Meagher, R.B. (2007). Class-specific interaction of profilin and ADF isovariants with actin in the regulation of plant development. Plant Cell **19,** 3111-3126.

Kean, L.S., Grant, A.M., Angeletti, C., Mahe, Y., Kuchler, K., Fuller, R.S., and Nichols, J.W. (1997). Plasma membrane translocation of fluorescent-labeled phosphatidylethanolamine is controlled by transcription regulators, PDR1 and PDR3. J Cell Biol **138,** 255-270.

Keegstra, K., and Walton, J. (2006). Plant science. Beta-glucans--brewer's bane, dietician's delight. Science **311,** 1872-1873.

Kessels, M.M., and Qualmann, B. (2005). Extending the court for cortactin: from the cortex to the Golgi. Nat Cell Biol **7,** 448-449.

Kohlwein, S.D., Eder, S., Oh, C.S., Martin, C.E., Gable, K., Bacikova, D., and Dunn, T. (2001). Tsc13p is required for fatty acid elongation and localizes to a novel structure at the nuclear-vacuolar interface in Saccharomyces cerevisiae. Mol Cell Biol **21,** 109-125.

Konieczny, A., and Ausubel, F.M. (1993). A procedure for mapping Arabidopsis mutations using co-dominant ecotype-specific PCR-based markers. Plant J **4,** 403-410.

Kovar, D.R. (2006). Molecular details of formin-mediated actin assembly. Curr Opin Cell Biol **18,** 11-17.

Kramer, E.M., and Bennett, M.J. (2006). Auxin transport: a field in flux. Trends Plant Sci **11,** 382-386.

Kunst, L., and Samuels, A.L. (2003). Biosynthesis and secretion of plant cuticular wax. Prog Lipid Res **42,** 51-80.

Kurata, T., Kawabata-Awai, C., Sakuradani, E., Shimizu, S., Okada, K., and Wada, T. (2003). The YORE-YORE gene regulates multiple aspects of epidermal cell differentiation in Arabidopsis. Plant J **36,** 55-66.

Kurdyukov, S., Faust, A., Nawrath, C., Bar, S., Voisin, D., Efremova, N., Franke, R., Schreiber, L., Saedler, H., Metraux, J.P., and Yephremov, A. (2006). The epidermis-specific extracellular BODYGUARD controls cuticle development and morphogenesis in Arabidopsis. Plant Cell **18,** 321-339.

Kusano, H., Testerink, C., Vermeer, J.E., Tsuge, T., Shimada, H., Oka, A., Munnik, T., and Aoyama, T. (2008). The Arabidopsis Phosphatidylinositol Phosphate 5-Kinase PIP5K3 Is a Key Regulator of Root Hair Tip Growth. Plant Cell.

Lalanne, E., Honys, D., Johnson, A., Borner, G.H., Lilley, K.S., Dupree, P., Grossniklaus, U., and Twell, D. (2004). SETH1 and SETH2, two components of the glycosylphosphatidylinositol anchor biosynthetic pathway, are required for pollen germination and tube growth in Arabidopsis. Plant Cell **16,** 229-240.

Lao, N.T., Long, D., Kiang, S., Coupland, G., Shoue, D.A., Carpita, N.C., and Kavanagh, T.A. (2003). Mutation of a family 8 glycosyltransferase gene alters cell wall carbohydrate composition and causes a humidity-sensitive semi-sterile dwarf phenotype in Arabidopsis. Plant Mol Biol **53,** 687-701.

Larsson, S., Svensson, C., and Akusjarvi, G. (1992). Control of adenovirus major late gene expression at multiple levels. J Mol Biol **225,** 287-298.

Latijnhouwers, M., Hawes, C., and Carvalho, C. (2005). Holding it all together? Candidate proteins for the plant Golgi matrix. Curr Opin Plant Biol **8,** 632-639.

Laxalt, A.M., and Munnik, T. (2002). Phospholipid signalling in plant defence. Curr Opin Plant Biol **5,** 332-338.

Lee, S.Y., Yang, J.S., Hong, W., Premont, R.T., and Hsu, V.W. (2005). ARFGAP1 plays a central role in coupling COPI cargo sorting with vesicle formation. J Cell Biol **168,** 281-290.

Lerouxel, O., Cavalier, D.M., Liepman, A.H., and Keegstra, K. (2006). Biosynthesis of plant cell wall polysaccharides - a complex process. Curr Opin Plant Biol **9,** 621-630.

Li, G., and Xue, H.W. (2007). Arabidopsis PLDzeta2 regulates vesicle trafficking and is required for auxin response. Plant Cell **19,** 281-295.

Li, J., Yang, H., Peer, W.A., Richter, G., Blakeslee, J., Bandyopadhyay, A., Titapiwantakun, B., Undurraga, S., Khodakovskaya, M., Richards, E.L., Krizek, B.,

Murphy, A.S., Gilroy, S., and Gaxiola, R. (2005). Arabidopsis H+-PPase AVP1 regulates auxin-mediated organ development. Science **310,** 121-125.

Li, Q., and Hunt, A.G. (1997). The Polyadenylation of RNA in Plants. Plant Physiol **115,** 321-325.

Li, S., Du, L., Yuen, G., and Harris, S.D. (2006). Distinct ceramide synthases regulate polarized growth in the filamentous fungus Aspergillus nidulans. Mol Biol Cell **17,** 1218-1227.

Liu, K., Hua, Z., Nepute, J.A., and Graham, T.R. (2007). Yeast P4-ATPases Drs2p and Dnf1p are essential cargos of the NPFXD/Sla1p endocytic pathway. Mol Biol Cell **18,** 487-500.

Loke, J.C., Stahlberg, E.A., Strenski, D.G., Haas, B.J., Wood, P.C., and Li, Q.Q. (2005). Compilation of mRNA polyadenylation signals in Arabidopsis revealed a new signal element and potential secondary structures. Plant Physiol **138,** 1457-1468.

Lolle, S.J., Cheung, A.Y., and Sussex, I.M. (1992). Fiddlehead: an Arabidopsis mutant constitutively expressing an organ fusion program that involves interactions between epidermal cells. Dev Biol **152,** 383-392.

Lolle, S.J., Hsu, W., and Pruitt, R.E. (1998). Genetic analysis of organ fusion in Arabidopsis thaliana. Genetics **149,** 607-619.

Lu, L., Lee, Y.R., Pan, R., Maloof, J.N., and Liu, B. (2005). An internal motor kinesin is associated with the Golgi apparatus and plays a role in trichome morphogenesis in Arabidopsis. Mol Biol Cell **16,** 811-823.

Lukowitz, W., Gillmor, C.S., and Scheible, W.R. (2000). Positional cloning in Arabidopsis. Why it feels good to have a genome initiative working for you. Plant Physiol **123,** 795-805.

Luo, B., Xue, X.Y., Hu, W.L., Wang, L.J., and Chen, X.Y. (2007). An ABC Transporter Gene of Arabidopsis thaliana, AtWBC11, is Involved in Cuticle Development and Prevention of Organ Fusion. Plant Cell Physiol **48,** 1790-1802.

Luo, D., and Oppenheimer, D.G. (1999). Genetic control of trichome branch number in Arabidopsis: the roles of the FURCA loci. Development **126,** 5547-5557.

Madson, M., Dunand, C., Li, X., Verma, R., Vanzin, G.F., Caplan, J., Shoue, D.A., Carpita, N.C., and Reiter, W.D. (2003). The MUR3 gene of Arabidopsis encodes a xyloglucan galactosyltransferase that is evolutionarily related to animal exostosins. Plant Cell **15,** 1662-1670.

Mann, K.P., Weiss, E.A., and Nevins, J.R. (1993). Alternative poly(A) site utilization during adenovirus infection coincides with a decrease in the activity of a poly(A) site processing factor. Mol Cell Biol **13,** 2411-2419.

Marc, J., Sharkey, D.E., Durso, N.A., Zhang, M., and Cyr, R.J. (1996). Isolation of a 90-kD Microtubule-Associated Protein from Tobacco Membranes. Plant Cell **8,** 2127-2138.

Marks, B., Stowell, M.H., Vallis, Y., Mills, I.G., Gibson, A., Hopkins, C.R., and McMahon, H.T. (2001). GTPase activity of dynamin and resulting conformation change are essential for endocytosis. Nature **410,** 231-235.

Marks, M.D. (1997). Molecular Genetic Analysis of Trichome Development in Arabidopsis. Annu Rev Plant Physiol Plant Mol Biol **48,** 137-163.

Markvoort, A.J., Smeijers, A.F., Pieterse, K., van Santen, R.A., and Hilbers, P.A. (2007). Lipid-based mechanisms for vesicle fission. J Phys Chem B **111,** 5719-5725.

Martincic, K., Campbell, R., Edwalds-Gilbert, G., Souan, L., Lotze, M.T., and Milcarek, C. (1998). Increase in the 64-kDa subunit of the polyadenylation/cleavage stimulatory factor during the G0 to S phase transition. Proc Natl Acad Sci U S A **95,** 11095-11100.

Mathur, J., and Hulskamp, M. (2002). Microtubules and microfilaments in cell morphogenesis in higher plants. Curr Biol **12,** R669-676.

Mathur, J., Mathur, N., and Hulskamp, M. (2002). Simultaneous visualization of peroxisomes and cytoskeletal elements reveals actin and not microtubule-based peroxisome motility in plants. Plant Physiol **128,** 1031-1045.

Mathur, J., Spielhofer, P., Kost, B., and Chua, N. (1999). The actin cytoskeleton is required to elaborate and maintain spatial patterning during trichome cell morphogenesis in Arabidopsis thaliana. Development **126,** 5559-5568.

Mathur, J., Mathur, N., Kernebeck, B., and Hulskamp, M. (2003). Mutations in actin-related proteins 2 and 3 affect cell shape development in Arabidopsis. Plant Cell **15,** 1632-1645.

McQueen-Mason, S., Durachko, D.M., and Cosgrove, D.J. (1992). Two endogenous proteins that induce cell wall extension in plants. Plant Cell **4,** 1425-1433.

Meijer, H.J., and Munnik, T. (2003). Phospholipid-based signaling in plants. Annu Rev Plant Biol **54,** 265-306.

Merrifield, C.J., Perrais, D., and Zenisek, D. (2005). Coupling between clathrin-coated-pit invagination, cortactin recruitment, and membrane scission observed in live cells. Cell **121,** 593-606.

Merrifield, C.J., Feldman, M.E., Wan, L., and Almers, W. (2002). Imaging actin and dynamin recruitment during invagination of single clathrin-coated pits. Nat Cell Biol **4,** 691-698.

Millar, A.A., and Kunst, L. (1997). Very-long-chain fatty acid biosynthesis is controlled through the expression and specificity of the condensing enzyme. Plant J **12,** 121-131.

Millar, A.A., Clemens, S., Zachgo, S., Giblin, E.M., Taylor, D.C., and Kunst, L. (1999). CUT1, an Arabidopsis gene required for cuticular wax biosynthesis and pollen fertility, encodes a very-long-chain fatty acid condensing enzyme. Plant Cell **11,** 825-838.

Mogen, B.D., MacDonald, M.H., Graybosch, R., and Hunt, A.G. (1990). Upstream sequences other than AAUAAA are required for efficient messenger RNA 3'-end formation in plants. Plant Cell **2,** 1261-1272.

Mogen, B.D., MacDonald, M.H., Leggewie, G., and Hunt, A.G. (1992). Several distinct types of sequence elements are required for efficient mRNA 3' end formation in a pea rbcS gene. Mol Cell Biol **12,** 5406-5414.

Mohri, K., Ono, K., Yu, R., Yamashiro, S., and Ono, S. (2006). Enhancement of actin-depolymerizing factor/cofilin-dependent actin disassembly by actin-interacting protein 1 is required for organized actin filament assembly in the Caenorhabditis elegans body wall muscle. Mol Biol Cell **17,** 2190-2199.

Moreau, P., Bessoule, J.J., Mongrand, S., Testet, E., Vincent, P., and Cassagne, C. (1998). Lipid trafficking in plant cells. Prog Lipid Res **37,** 371-391.

Muller, A., Guan, C., Galweiler, L., Tanzler, P., Huijser, P., Marchant, A., Parry, G., Bennett, M., Wisman, E., and Palme, K. (1998). AtPIN2 defines a locus of Arabidopsis for root gravitropism control. EMBO J **17,** 6903-6911.

Muller, P., Pomorski, T., and Herrmann, A. (1994). Incorporation of phospholipid analogues into the plasma membrane affects ATP-induced vesiculation of human erythrocyte ghosts. Biochem Biophys Res Commun **199,** 881-887.

Mullins, R.D., Kelleher, J.F., Xu, J., and Pollard, T.D. (1998). Arp2/3 complex from Acanthamoeba binds profilin and cross-links actin filaments. Mol Biol Cell **9,** 841-852.

Murphy, A.S., Bandyopadhyay, A., Holstein, S.E., and Peer, W.A. (2005). Endocytotic cycling of PM proteins. Annu Rev Plant Biol **56,** 221-251.

Murthy, K.G., and Manley, J.L. (1992). Characterization of the multisubunit cleavage-polyadenylation specificity factor from calf thymus. J Biol Chem **267,** 14804-14811.

Natarajan, P., Wang, J., Hua, Z., and Graham, T.R. (2004). Drs2p-coupled aminophospholipid translocase activity in yeast Golgi membranes and relationship to in vivo function. Proc Natl Acad Sci U S A **101,** 10614-10619.

Nebenfuhr, A., Gallagher, L.A., Dunahay, T.G., Frohlick, J.A., Mazurkiewicz, A.M., Meehl, J.B., and Staehelin, L.A. (1999). Stop-and-go movements of plant Golgi stacks are mediated by the acto-myosin system. Plant Physiol **121,** 1127-1142.

Neumann, U., Brandizzi, F., and Hawes, C. (2003). Protein transport in plant cells: in and out of the Golgi. Ann Bot (Lond) **92,** 167-180.

Nibau, C., Wu, H.M., and Cheung, A.Y. (2006). RAC/ROP GTPases: 'hubs' for signal integration and diversification in plants. Trends Plant Sci **11,** 309-315.

Nishitani, K., and Tominaga, R. (1992). Endo-xyloglucan transferase, a novel class of glycosyltransferase that catalyzes transfer of a segment of xyloglucan molecule to another xyloglucan molecule. J Biol Chem **267,** 21058-21064.

O'Neill, M.A., Ishii, T., Albersheim, P., and Darvill, A.G. (2004). Rhamnogalacturonan II: structure and function of a borate cross-linked cell wall pectic polysaccharide. Annu Rev Plant Biol **55,** 109-139.

Ohashi, Y., Oka, A., Rodrigues-Pousada, R., Possenti, M., Ruberti, I., Morelli, G., and Aoyama, T. (2003). Modulation of phospholipid signaling by GLABRA2 in root-hair pattern formation. Science **300,** 1427-1430.

Ojangu, E.L., Jarve, K., Paves, H., and Truve, E. (2007). Arabidopsis thaliana myosin XIK is involved in root hair as well as trichome morphogenesis on stems and leaves. Protoplasma **230,** 193-202.

Okada, K., Blanchoin, L., Abe, H., Chen, H., Pollard, T.D., and Bamburg, J.R. (2002). Xenopus actin-interacting protein 1 (XAip1) enhances cofilin fragmentation of filaments by capping filament ends. J Biol Chem **277,** 43011-43016.

Oxley, D., and Bacic, A. (1999). Structure of the glycosylphosphatidylinositol anchor of an arabinogalactan protein from Pyrus communis suspension-cultured cells. Proc Natl Acad Sci U S A **96,** 14246-14251.

Panikashvili, D., Savaldi-Goldstein, S., Mandel, T., Yifhar, T., Franke, R.B., Hofer, R., Schreiber, L., Chory, J., and Aharoni, A. (2007). The Arabidopsis DESPERADO/AtWBC11 Transporter Is Required for Cutin and Wax Secretion. Plant Physiol **145,** 1345-1360.

Paredez, A.R., Somerville, C.R., and Ehrhardt, D.W. (2006). Visualization of cellulose synthase demonstrates functional association with microtubules. Science **312,** 1491-1495.

Pena, M.J., Ryden, P., Madson, M., Smith, A.C., and Carpita, N.C. (2004). The galactose residues of xyloglucan are essential to maintain mechanical strength of the primary cell walls in Arabidopsis during growth. Plant Physiol **134,** 443-451.

Perez-Victoria, F.J., Gamarro, F., Ouellette, M., and Castanys, S. (2003). Functional cloning of the miltefosine transporter. A novel P-type phospholipid translocase from Leishmania involved in drug resistance. J Biol Chem **278,** 49965-49971.

Pighin, J.A., Zheng, H., Balakshin, L.J., Goodman, I.P., Western, T.L., Jetter, R., Kunst, L., and Samuels, A.L. (2004). Plant cuticular lipid export requires an ABC transporter. Science **306,** 702-704.

Pollard, T.D., and Borisy, G.G. (2003). Cellular motility driven by assembly and disassembly of actin filaments. Cell **112,** 453-465.

Pollock, M.A., and Oppenheimer, D.G. (1999). Inexpensive alternative to M&S medium for selection of Arabidopsis plants in culture. Biotechniques **26,** 254-257.

Pomorski, T., and Menon, A.K. (2006). Lipid flippases and their biological functions. Cell Mol Life Sci **63,** 2908-2921.

Pomorski, T., Holthuis, J.C., Herrmann, A., and van Meer, G. (2004). Tracking down lipid flippases and their biological functions. J Cell Sci **117,** 805-813.

Pomorski, T., Lombardi, R., Riezman, H., Devaux, P.F., van Meer, G., and Holthuis, J.C. (2003). Drs2p-related P-type ATPases Dnf1p and Dnf2p are required for phospholipid translocation across the yeast plasma membrane and serve a role in endocytosis. Mol Biol Cell **14,** 1240-1254.

Poon, P.P., Cassel, D., Spang, A., Rotman, M., Pick, E., Singer, R.A., and Johnston, G.C. (1999). Retrograde transport from the yeast Golgi is mediated by two ARF GAP proteins with overlapping function. EMBO J **18,** 555-564.

Poulsen, R.L., Rosa, L.L., Stephen, C., McDowell, J.O., Dirk, L., Alexander, S., Thomas, P., Jeffrey F. Harper, F.J., and Michael, G.P. (2008). The Arabidopsis P_4-ATPase ALA3 Localizes to the Golgi and Requires a β-Subunit to Function in Lipid Translocation and Secretory Vesicle Formation. Plant Cell **Preview**, March 14.

Preuss, M.L., Serna, J., Falbel, T.G., Bednarek, S.Y., and Nielsen, E. (2004). The Arabidopsis Rab GTPase RabA4b localizes to the tips of growing root hair cells. Plant Cell **16,** 1589-1603.

Pruitt, R.E., Vielle-Calzada, J.P., Ploense, S.E., Grossniklaus, U., and Lolle, S.J. (2000). FIDDLEHEAD, a gene required to suppress epidermal cell interactions in Arabidopsis, encodes a putative lipid biosynthetic enzyme. Proc Natl Acad Sci U S A **97,** 1311-1316.

Quesada, V., Dean, C., and Simpson, G.G. (2005). Regulated RNA processing in the control of Arabidopsis flowering. Int J Dev Biol **49,** 773-780.

Rajendran, L., and Simons, K. (2005). Lipid rafts and membrane dynamics. J Cell Sci **118,** 1099-1102.

Rein, U., Andag, U., Duden, R., Schmitt, H.D., and Spang, A. (2002). ARF-GAP-mediated interaction between the ER-Golgi v-SNAREs and the COPI coat. J Cell Biol **157,** 395-404.

Reiter, W.D. (2002). Biosynthesis and properties of the plant cell wall. Curr Opin Plant Biol **5,** 536-542.

Reiter, W.D., Chapple, C.C., and Somerville, C.R. (1993). Altered Growth and Cell Walls in a Fucose-Deficient Mutant of Arabidopsis. Science **261,** 1032-1035.

Ridley, B.L., O'Neill, M.A., and Mohnen, D. (2001). Pectins: structure, biosynthesis, and oligogalacturonide-related signaling. Phytochemistry **57,** 929-967.

Ripmaster, T.L., Vaughn, G.P., and Woolford, J.L., Jr. (1993). DRS1 to DRS7, novel genes required for ribosome assembly and function in Saccharomyces cerevisiae. Mol Cell Biol **13,** 7901-7912.

Robineau, S., Chabre, M., and Antonny, B. (2000). Binding site of brefeldin A at the interface between the small G protein ADP-ribosylation factor 1 (ARF1) and the nucleotide-exchange factor Sec7 domain. Proc Natl Acad Sci U S A **97,** 9913-9918.

Robinson, M., Poon, P.P., Schindler, C., Murray, L.E., Kama, R., Gabriely, G., Singer, R.A., Spang, A., Johnston, G.C., and Gerst, J.E. (2006). The Gcs1 Arf-GAP mediates Snc1,2 v-SNARE retrieval to the Golgi in yeast. Mol Biol Cell **17,** 1845-1858.

Rose, J.K., Braam, J., Fry, S.C., and Nishitani, K. (2002). The XTH family of enzymes involved in xyloglucan endotransglucosylation and endohydrolysis: current perspectives and a new unifying nomenclature. Plant Cell Physiol **43,** 1421-1435.

Roudier, F., Fernandez, A.G., Fujita, M., Himmelspach, R., Borner, G.H., Schindelman, G., Song, S., Baskin, T.I., Dupree, P., Wasteneys, G.O., and Benfey, P.N. (2005). COBRA, an Arabidopsis extracellular glycosyl-phosphatidyl inositol-anchored protein, specifically controls highly anisotropic expansion through its involvement in cellulose microfibril orientation. Plant Cell **17,** 1749-1763.

Roux, A., Uyhazi, K., Frost, A., and De Camilli, P. (2006). GTP-dependent twisting of dynamin implicates constriction and tension in membrane fission. Nature **441,** 528-531.

Samaj, J., Read, N.D., Volkmann, D., Menzel, D., and Baluska, F. (2005). The endocytic network in plants. Trends Cell Biol **15,** 425-433.

Samaj, J., Muller, J., Beck, M., Bohm, N., and Menzel, D. (2006). Vesicular trafficking, cytoskeleton and signalling in root hairs and pollen tubes. Trends Plant Sci **11,** 594-600.

Samaj, J., Baluska, F., Voigt, B., Schlicht, M., Volkmann, D., and Menzel, D. (2004). Endocytosis, actin cytoskeleton, and signaling. Plant Physiol **135,** 1150-1161.

Sanderfoot, A. (2007). Increases in the number of SNARE genes parallels the rise of multicellularity among the green plants. Plant Physiol **144,** 6-17.

Sanderfoot, A.A., and Raikhel, N.V. (1999). The specificity of vesicle trafficking: coat proteins and SNAREs. Plant Cell **11,** 629-642.

Sanderfoot, A.A., Assaad, F.F., and Raikhel, N.V. (2000). The Arabidopsis genome. An abundance of soluble N-ethylmaleimide-sensitive factor adaptor protein receptors. Plant Physiol **124,** 1558-1569.

Schellmann, S., and Hulskamp, M. (2005). Epidermal differentiation: trichomes in Arabidopsis as a model system. Int J Dev Biol **49,** 579-584.

Schindelman, G., Morikami, A., Jung, J., Baskin, T.I., Carpita, N.C., Derbyshire, P., McCann, M.C., and Benfey, P.N. (2001). COBRA encodes a putative GPI-anchored protein, which is polarly localized and necessary for oriented cell expansion in Arabidopsis. Genes Dev **15,** 1115-1127.

Schrick, K., Mayer, U., Horrichs, A., Kuhnt, C., Bellini, C., Dangl, J., Schmidt, J., and Jurgens, G. (2000). FACKEL is a sterol C-14 reductase required for organized cell division and expansion in Arabidopsis embryogenesis. Genes Dev **14,** 1471-1484.

Schumacher, K., Vafeados, D., McCarthy, M., Sze, H., Wilkins, T., and Chory, J. (1999). The Arabidopsis det3 mutant reveals a central role for the vacuolar H(+)-ATPase in plant growth and development. Genes Dev **13,** 3259-3270.

Sedbrook, J.C., Carroll, K.L., Hung, K.F., Masson, P.H., and Somerville, C.R. (2002). The Arabidopsis SKU5 gene encodes an extracellular glycosyl phosphatidylinositol-anchored glycoprotein involved in directional root growth. Plant Cell **14,** 1635-1648.

Segev, N. (2001). Ypt and Rab GTPases: insight into functions through novel interactions. Curr Opin Cell Biol **13,** 500-511.

Sherrier, D.J., Prime, T.A., and Dupree, P. (1999). Glycosylphosphatidylinositol-anchored cell-surface proteins from Arabidopsis. Electrophoresis **20,** 2027-2035.

Shi, H., Kim, Y., Guo, Y., Stevenson, B., and Zhu, J.K. (2003). The Arabidopsis SOS5 locus encodes a putative cell surface adhesion protein and is required for normal cell expansion. Plant Cell **15,** 19-32.

Simons, K., and Ikonen, E. (1997). Functional rafts in cell membranes. Nature **387,** 569-572.

Simons, K., and Toomre, D. (2000). Lipid rafts and signal transduction. Nat Rev Mol Cell Biol **1,** 31-39.

Smith, L.G., and Oppenheimer, D.G. (2005). Spatial control of cell expansion by the plant cytoskeleton. Annu Rev Cell Dev Biol **21,** 271-295.

Snowman, B.N., Kovar, D.R., Shevchenko, G., Franklin-Tong, V.E., and Staiger, C.J. (2002). Signal-mediated depolymerization of actin in pollen during the self-incompatibility response. Plant Cell **14,** 2613-2626.

Sollner, T.H., and Rothman, J.E. (1996). Molecular machinery mediating vesicle budding, docking and fusion. Experientia **52,** 1021-1025.

Somerville, C. (2006). Cellulose synthesis in higher plants. Annu Rev Cell Dev Biol **22,** 53-78.

Song, X.F., Yang, C.Y., Liu, J., and Yang, W.C. (2006). RPA, a class II ARFGAP protein, activates ARF1 and U5 and plays a role in root hair development in Arabidopsis. Plant Physiol **141,** 966-976.

Souter, M., Topping, J., Pullen, M., Friml, J., Palme, K., Hackett, R., Grierson, D., and Lindsey, K. (2002). hydra Mutants of Arabidopsis are defective in sterol profiles and auxin and ethylene signaling. Plant Cell **14,** 1017-1031.

Spang, A. (2002). ARF1 regulatory factors and COPI vesicle formation. Curr Opin Cell Biol **14,** 423-427.

Staiger, C.J., and Blanchoin, L. (2006). Actin dynamics: old friends with new stories. Curr Opin Plant Biol **9,** 554-562.

Stepka, M., Ciampolini, F., Charzynska, M., and Cresti, M. (2000). Localization of pectins in the pollen tube wall of Ornithogalum virens L. Does the pattern of pectin distribution depend on the growth rate of the pollen tube? Planta **210,** 630-635.

Sterling, J.D., Atmodjo, M.A., Inwood, S.E., Kumar Kolli, V.S., Quigley, H.F., Hahn, M.G., and Mohnen, D. (2006). Functional identification of an Arabidopsis pectin biosynthetic homogalacturonan galacturonosyltransferase. Proc Natl Acad Sci U S A **103,** 5236-5241.

Steudle, E., and Zimmermann, U. (1977). Effect of Turgor Pressure and Cell Size on the Wall Elasticity of Plant Cells. Plant Physiol **59,** 285-289.

Sturaro, M., Hartings, H., Schmelzer, E., Velasco, R., Salamini, F., and Motto, M. (2005). Cloning and characterization of GLOSSY1, a maize gene involved in cuticle membrane and wax production. Plant Physiol **138,** 478-489.

Sugimoto, K., Himmelspach, R., Williamson, R.E., and Wasteneys, G.O. (2003). Mutation or drug-dependent microtubule disruption causes radial swelling without altering parallel cellulose microfibril deposition in Arabidopsis root cells. Plant Cell **15,** 1414-1429.

Suh, M.C., Samuels, A.L., Jetter, R., Kunst, L., Pollard, M., Ohlrogge, J., and Beisson, F. (2005). Cuticular lipid composition, surface structure, and gene expression in Arabidopsis stem epidermis. Plant Physiol **139,** 1649-1665.

Svitkina, T.M., and Borisy, G.G. (1999). Arp2/3 complex and actin depolymerizing factor/cofilin in dendritic organization and treadmilling of actin filament array in lamellipodia. J Cell Biol **145,** 1009-1026.

Swarup, R., Friml, J., Marchant, A., Ljung, K., Sandberg, G., Palme, K., and Bennett, M. (2001). Localization of the auxin permease AUX1 suggests two functionally distinct hormone transport pathways operate in the Arabidopsis root apex. Genes Dev **15,** 2648-2653.

Szymanski, D.B. (2005). Breaking the WAVE complex: the point of Arabidopsis trichomes. Curr Opin Plant Biol **8,** 103-112.

Szymanski, D.B., Marks, M.D., and Wick, S.M. (1999). Organized F-actin is essential for normal trichome morphogenesis in Arabidopsis. Plant Cell **11,** 2331-2347.

Takagaki, Y., and Manley, J.L. (1997). RNA recognition by the human polyadenylation factor CstF. Mol Cell Biol **17,** 3907-3914.

Takagaki, Y., Seipelt, R.L., Peterson, M.L., and Manley, J.L. (1996). The polyadenylation factor CstF-64 regulates alternative processing of IgM heavy chain pre-mRNA during B cell differentiation. Cell **87,** 941-952.

Takeda, S., Gapper, C., Kaya, H., Bell, E., Kuchitsu, K., and Dolan, L. (2008). Local positive feedback regulation determines cell shape in root hair cells. Science **319,** 1241-1244.

Takeuchi, M., Ueda, T., Yahara, N., and Nakano, A. (2002). Arf1 GTPase plays roles in the protein traffic between the endoplasmic reticulum and the Golgi apparatus in tobacco and Arabidopsis cultured cells. Plant J **31,** 499-515.

Tang, X., Halleck, M.S., Schlegel, R.A., and Williamson, P. (1996). A subfamily of P-type ATPases with aminophospholipid transporting activity. Science **272,** 1495-1497.

Thitamadee, S., Tuchihara, K., and Hashimoto, T. (2002). Microtubule basis for left-handed helical growth in Arabidopsis. Nature **417,** 193-196.

Thole, J.M., Vermeer, J.E., Zhang, Y., Gadella, T.W., Jr., and Nielsen, E. (2008). ROOT HAIR DEFECTIVE4 Encodes a Phosphatidylinositol-4-Phosphate Phosphatase Required for Proper Root Hair Development in Arabidopsis thaliana. Plant Cell.

Thompson DW. (1917). On growth and form. Cambridge, UK: Cambrige Univ. Press.

Ueda, T., Anai, T., Tsukaya, H., Hirata, A., and Uchimiya, H. (1996). Characterization and subcellular localization of a small GTP-binding protein (Ara-4) from Arabidopsis: conditional expression under control of the promoter of the gene for heat-shock protein HSP81-1. Mol Gen Genet **250,** 533-539.

Uhrig, J.F., and Hulskamp, M. (2006). Plant GTPases: regulation of morphogenesis by ROPs and ROS. Curr Biol **16,** R211-213.

Uhrig, J.F., Mutondo, M., Zimmermann, I., Deeks, M.J., Machesky, L.M., Thomas, P., Uhrig, S., Rambke, C., Hussey, P.J., and Hulskamp, M. (2007). The role of Arabidopsis SCAR genes in ARP2-ARP3-dependent cell morphogenesis. Development **134,** 967-977.

Ujhazy, P., Ortiz, D., Misra, S., Li, S., Moseley, J., Jones, H., and Arias, I.M. (2001). Familial intrahepatic cholestasis 1: studies of localization and function. Hepatology **34,** 768-775.

Vissenberg, K., Fry, S.C., and Verbelen, J.P. (2001). Root hair initiation is coupled to a highly localized increase of xyloglucan endotransglycosylase action in Arabidopsis roots. Plant Physiol **127,** 1125-1135.

Voigt, B., Timmers, A.C., Samaj, J., Hlavacka, A., Ueda, T., Preuss, M., Nielsen, E., Mathur, J., Emans, N., Stenmark, H., Nakano, A., Baluska, F., and Menzel, D. (2005). Actin-based motility of endosomes is linked to the polar tip growth of root hairs. Eur J Cell Biol **84,** 609-621.

von Arnim, A.G., Deng, X.W., and Stacey, M.G. (1998). Cloning vectors for the expression of green fluorescent protein fusion proteins in transgenic plants. Gene **221,** 35-43.

Wagner, T.A., and Kohorn, B.D. (2001). Wall-associated kinases are expressed throughout plant development and are required for cell expansion. Plant Cell **13,** 303-318.

Wang, H.Y., Yu, Y., Chen, Z.L., and Xia, G.X. (2005a). Functional characterization of Gossypium hirsutum profilin 1 gene (GhPFN1) in tobacco suspension cells. Characterization of in vivo functions of a cotton profilin gene. Planta **222,** 594-603.

Wang, L., Beserra, C., and Garbers, D.L. (2004). A novel aminophospholipid transporter exclusively expressed in spermatozoa is required for membrane lipid asymmetry and normal fertilization. Dev Biol **267,** 203-215.

Wang, Q., Kong, L., Hao, H., Wang, X., Lin, J., Samaj, J., and Baluska, F. (2005b). Effects of brefeldin A on pollen germination and tube growth. Antagonistic effects on endocytosis and secretion. Plant Physiol **139,** 1692-1703.

Wang, X., Wang, C., Sang, Y., Qin, C., and Welti, R. (2002). Networking of phospholipases in plant signal transduction. Physiol Plant **115,** 331-335.

Wasteneys, G.O. (2004). Progress in understanding the role of microtubules in plant cells. Curr Opin Plant Biol **7,** 651-660.

Watanabe, M., Tanaka, H., Watanabe, D., Machida, C., and Machida, Y. (2004). The ACR4 receptor-like kinase is required for surface formation of epidermis-related tissues in Arabidopsis thaliana. Plant J **39,** 298-308.

Wellesen, K., Durst, F., Pinot, F., Benveniste, I., Nettesheim, K., Wisman, E., Steiner-Lange, S., Saedler, H., and Yephremov, A. (2001). Functional analysis of the LACERATA gene of Arabidopsis provides evidence for different roles of fatty acid omega -hydroxylation in development. Proc Natl Acad Sci U S A **98,** 9694-9699.

Wen, F., Zhu, Y., and Hawes, M.C. (1999). Effect of pectin methylesterase gene expression on pea root development. Plant Cell **11,** 1129-1140.

Whittington, A.T., Vugrek, O., Wei, K.J., Hasenbein, N.G., Sugimoto, K., Rashbrooke, M.C., and Wasteneys, G.O. (2001). MOR1 is essential for organizing cortical microtubules in plants. Nature **411,** 610-613.

Willats, W.G., and Knox, J.P. (1996). A role for arabinogalactan-proteins in plant cell expansion: evidence from studies on the interaction of beta-glucosyl Yariv reagent with seedlings of Arabidopsis thaliana. Plant J **9,** 919-925.

Willats, W.G., McCartney, L., Mackie, W., and Knox, J.P. (2001). Pectin: cell biology and prospects for functional analysis. Plant Mol Biol **47,** 9-27.

Willemsen, V., Friml, J., Grebe, M., van den Toorn, A., Palme, K., and Scheres, B. (2003). Cell polarity and PIN protein positioning in Arabidopsis require STEROL METHYLTRANSFERASE1 function. Plant Cell **15,** 612-625.

Williamson, R.E., Burn, J.E., Birch, R., Baskin, T.I., Arioli, T., Betzner, A.S., and Cork, A. (2001). Morphology of rsw1, a cellulose-deficient mutant of Arabidopsis thaliana. Protoplasma **215,** 116-127.

Wu, L., Ueda, T., and Messing, J. (1995). The formation of mRNA 3'-ends in plants. Plant J **8,** 323-329.

Xu, J., and Scheres, B. (2005a). Cell polarity: ROPing the ends together. Curr Opin Plant Biol **8,** 613-618.

Xu, J., and Scheres, B. (2005b). Dissection of Arabidopsis ADP-RIBOSYLATION FACTOR 1 function in epidermal cell polarity. Plant Cell **17,** 525-536.

Xu, R., Zhao, H., Dinkins, R.D., Cheng, X., Carberry, G., and Li, Q.Q. (2006). The 73 kD subunit of the cleavage and polyadenylation specificity factor (CPSF) complex affects reproductive development in Arabidopsis. Plant Mol Biol **61,** 799-815.

Xu, X., Dietrich, C.R., Delledonne, M., Xia, Y., Wen, T.J., Robertson, D.S., Nikolau, B.J., and Schnable, P.S. (1997). Sequence analysis of the cloned glossy8 gene of maize suggests that it may code for a beta-ketoacyl reductase required for the biosynthesis of cuticular waxes. Plant Physiol **115,** 501-510.

Yang, J.S., Zhang, L., Lee, S.Y., Gad, H., Luini, A., and Hsu, V.W. (2006). Key components of the fission machinery are interchangeable. Nat Cell Biol **8,** 1376-1382.

Yang, J.S., Lee, S.Y., Gao, M., Bourgoin, S., Randazzo, P.A., Premont, R.T., and Hsu, V.W. (2002). ARFGAP1 promotes the formation of COPI vesicles, suggesting function as a component of the coat. J Cell Biol **159,** 69-78.

Yang, J.S., Lee, S.Y., Spano, S., Gad, H., Zhang, L., Nie, Z., Bonazzi, M., Corda, D., Luini, A., and Hsu, V.W. (2005). A role for BARS at the fission step of COPI vesicle formation from Golgi membrane. EMBO J **24,** 4133-4143.

Yang, Z., and Fu, Y. (2007). ROP/RAC GTPase signaling. Curr Opin Plant Biol **10,** 490-494.

Yao, Y., Song, L., Katz, Y., and Galili, G. (2002). Cloning and characterization of Arabidopsis homologues of the animal CstF complex that regulates 3' mRNA cleavage and polyadenylation. J Exp Bot **53,** 2277-2278.

Yarar, D., Waterman-Storer, C.M., and Schmid, S.L. (2005). A dynamic actin cytoskeleton functions at multiple stages of clathrin-mediated endocytosis. Mol Biol Cell **16,** 964-975.

Yephremov, A., Wisman, E., Huijser, P., Huijser, C., Wellesen, K., and Saedler, H. (1999). Characterization of the FIDDLEHEAD gene of Arabidopsis reveals a link between adhesion response and cell differentiation in the epidermis. Plant Cell **11,** 2187-2201.

Yokota, E., Motoki, T., Issei, M., Yasunori, T., Staiger, J.C., Kazuhiro O., and Teruo, S. (2005). Plant villin, lily P-135-ABP, possesses G-actin binding activity and accelerates the polymerization and depolymerization of actin in a Ca^{2+}-sensitive manner**.** Plant Cell Physiol **46**, 1690-1703.

Yuan, M., Shaw, P.J., Warn, R.M., and Lloyd, C.W. (1994). Dynamic reorientation of cortical microtubules, from transverse to longitudinal, in living plant cells. Proc Natl Acad Sci U S A **91,** 6050-6053.

Zachowski, A., and Gaudry-Talarmain, Y.M. (1990). Phospholipid transverse diffusion in synaptosomes: evidence for the involvement of the aminophospholipid translocase. J Neurochem **55,** 1352-1356.

Zeile, W.L., Zhang, F., Dickinson, R.B., and Purich, D.L. (2005). Listeria's right-handed helical rocket-tail trajectories: mechanistic implications for force generation in actin-based motility. Cell Motil Cytoskeleton **60,** 121-128.

Zerial, M., and McBride, H. (2001). Rab proteins as membrane organizers. Nat Rev Mol Cell Biol **2,** 107-117.

Zhang, X., and Oppenheimer, D.G. (2004). A simple and efficient method for isolating trichomes for downstream analyses. Plant Cell Physiol **45,** 221-224.

Zhang, X., Grey, P.H., Krishnakumar, S., and Oppenheimer, D.G. (2005a). The IRREGULAR TRICHOME BRANCH loci regulate trichome elongation in Arabidopsis. Plant Cell Physiol **46,** 1549-1560.

Zhang, X., Dyachok, J., Krishnakumar, S., Smith, L.G., and Oppenheimer, D.G. (2005b). IRREGULAR TRICHOME BRANCH1 in Arabidopsis encodes a plant homolog of the actin-related protein2/3 complex activator Scar/WAVE that regulates actin and microtubule organization. Plant Cell **17,** 2314-2326.

Zhao, J., Hyman, L., and Moore, C. (1999). Formation of mRNA 3' ends in eukaryotes: mechanism, regulation, and interrelationships with other steps in mRNA synthesis. Microbiol Mol Biol Rev **63,** 405-445.

Zhao, Z.D., Tan, L., Showalter, A.M., Lamport, D.T., and Kieliszewski, M.J. (2002). Tomato LeAGP-1 arabinogalactan-protein purified from transgenic tobacco corroborates the Hyp contiguity hypothesis. Plant J **31,** 431-444.

Zheng, H., Rowland, O., and Kunst, L. (2005). Disruptions of the Arabidopsis Enoyl-CoA reductase gene reveal an essential role for very-long-chain fatty acid synthesis in cell expansion during plant morphogenesis. Plant Cell **17,** 1467-1481.

Zhuang, X., Xu, Y., Chong, K., Lan, L., Xue, Y., and Xu, Z. (2005). OsAGAP, an ARF-GAP from rice, regulates root development mediated by auxin in Arabidopsis. Plant Cell Environ **28,** 147-156.

Zhuang, X., Jiang, J., Li, J., Ma, Q., Xu, Y., Xue, Y., Xu, Z., and Chong, K. (2006). Over-expression of OsAGAP, an ARF-GAP, interferes with auxin influx, vesicle trafficking and root development. Plant J **48,** 581-591.

BIOGRAPHICAL SKETCH

Xiaoguo Zhang was born in Hubei province, China. After completing his college education at Huazhong Agricultural University, he attended China Agricultural University for his master's degree in crop genetics and breeding. After his graduation, he worked at Wuhan University. He started his Ph.D. program in plant molecular and cellular biology in 2005 at University of Florida.